ON THE CRITICAL SPEEDS[1] OF A SHAFT

TOSHIO YAMAMOTO

Department of Mechanical Engineering

(Received October 31, 1954)

CONTENTS

Nomenclature

The following nomenclature is used in this paper:
o-xyz = fixed rectangular coordinate system,
G = gravitational center of the rotating disc,
(x_G, y_G, z_G) = coordinates of the point G,
M = geometrical center of the shaft and the disc,
(x, y, z) = coordinates of the point M,
W = weight of the disc,
m = mass of the disc,
I = moment of inertia of the disc about the symmetrical axis of the disc,
I_p = polar moment of inertia of the disc,
g = gravitational acceleration,
$k = \sqrt{I/m}$ = radius of gyration of the disc,
M_t = moment acting on the disc,
F = force acting on the disc,
α, γ, δ = spring constants of the shaft,
$e = \overline{MG}$ = eccentricity of the disc,
τ = small deviational angle between the plane of the disc and the plane A which is orthogonal to the tangent of the deflection curve of shaft at the point M,
θ_1, φ_1, ψ_1 = Eulerian angles denoting the angular position of the disc,
θ, φ, ψ = Eulerian angles denoting the angular position of the plane A,
θ = angle between the tangent of the deflection curve of shaft at the point M and the bearing center line oz,
θ_x, θ_y = components of θ in x- and y-directions, respectively,
ω = angular velocity of the rotating disc,
p = natural frequency of the vibratory system,
l = length of the shaft,
$a : b$ = ratio representing the position of the disc on the shaft,
$2\Delta\alpha$, $2\Delta\gamma$, $2\Delta\delta$ = differences between maximum and minimum values of α, γ

and δ, respectively,
T = kinetic energy of the system,
V = potential energy of the system,
β = phase angle between e and τ,
ω_c = major critical speed,
ω_b = critical speed of backward synchronous precession,
ω_{b_2} = lower critical speed of backward synchronous precession,
ω_{b_1} = higher critical speed of backward synchronous precession,
$a_1 = a/l$,
$b_1 = b/l$,
$\Gamma = k^2/l^2$,
d = diameter of steel balls in ball bearing,
D = outer diamenter of the inner ring of ball bearing,
ω_1 = precessional angular velocity of vibrations of balls,
$\alpha_1 = \omega_1/\omega$,
ω_a = critical speed of vibrations of $[\omega_1]$,
e_0 = eccrentricity of inner ring due to the difference of diameter of ball, or, the magnitude of backlash,
e_1 = eccentricity of the disc center M due to e_0, or, the magnitude of radial clearance in the upper bearing,
e_2 = the magnitude of radial clearance in the lower bearing,
S = geometrical center of the disc,
τ_1 = inclination angle due to e_0,
$o\text{-}x_1y_1$ = rotating rectangular coordinate system with angular velocity ω_1,
$\beta_1 = 2\alpha_1 - 1 = \dfrac{1}{\omega}(2\omega_1 - \omega)$,
ω_d = critical speed of vibrations of $[2\omega_1 - \omega]$,
c = damping coefficient,
$2n = c/m$,
$r = a_0/e_0$,
a_0 = amplitude of vibration of whirl,
$v = \omega^2/p^2$,
$\nu^2 = 4n^2/p^2$,
$E = e/e_0$,
μ, μ_1, μ_2 = the coefficient of friction in bearings.

General Introduction

For the past eighty years the problems of rotating shafts have been considered by scientific workers with a variety of aims and procedures. In 1869 Rankin carried out the first theoretical treatment of rotating shafts, following which numerous researches were made by Dunkerley, Stodola, Föpple and others. The problem of critical speed of rotating shaft has been studied by Stodola,[2] Schwerin,[3] Timoshenko[4] and Den Hartog,[5] using the simple theory of statics. As the problem of dynamics, *i.e.*, the lateral vibrations, Jeffcott,[6] Lees,[7][8] Sezawa,[9] Udoguchi[10] and Watari[11] have treated the whirling of shaft. Most of these studies have been discussed under the assumption that the angular velocity of rotation is constant, but Watari[11] has discussed the effects of variation of angular velocity and Shimoyama and the author[28] have studied the case of retardation of shaft. Furthermore

the gyroscopic action is usually present in the system of rotating shaft carrying a disc. The effects of gyroscopic action have been discussed by Stodola,[2] Karas,[12][13][14] Prohl[15] and others. In this paper we will introduce the differential equations of motion of disc without the restriction of constant angular velocity of rotating shaft and then we will show in our experiment that we can solve the problem of the shaft having an approximately constant angular velocity. Furthermore, we will take into consideration the deviational angle τ (see Fig. 6).

In addition to the whirl of shafts having the same angular velocity, there are many kinds of vibrations. With regard to synchronous backward precession, one of these vibrations, Stodola[2] has pointed out that it appeared in shafts of the turbine. We will prove our point that the flexibility of bearing pedestals causes it. Timoshenko,[4] Smith,[16] Foote[17] and Miller[18] discussed the problem of flexible bearing pedestal but they did not touch upon this point.

Secondary critical speeds have been treated by Stodola,[2] Oki,[19] Föpple,[20] Lorenze,[21] Karas,[12][13] Nakanishi,[22] Taylor,[23] and others. We will study the lower critical speeds caused by irregularities in ball bearings.

Newkirk,[26] Kimball[27] and Sawaragi[25] have studied self-excited vibrations of rotating shaft. In our experiments, most of the vibrations which appeared at rotating speeds lower or higher than the major critical speed do not belong to self-excited vibration, but are caused by irregularities in ball bearings.

There are then valid practical reasons for treating with irregularities in bearings. In this paper we treat mainly with the vibrations due to bearing and bearing pedestal irregularities.

Chapter I. General Matters

1. Preliminaries

Even in such a simple apparatus as shown in Figs. 1 and 2, various sorts of vibrations take place in the rotating shaft carrying one disc. In our numerous experiments, some of these vibrations always appeared and others occurred occasionally. While in this paper we will clear up the nature of these vibrations, we will first treat with general matters concerning apparatus and experiments.

2. Experimental apparatus and methods of experiments

The greater part of our experiments is performed on the vertical shaft mounting one disc. Remaining and supplementary experiments are carried out on the shaft having two discs. The experimental apparatus is shown in Figs. 1 and 2. The disc D is driven by a V-belt, power supplied by a 5-H.P. D.C. motor with speed variations of from 0 to 6,000 r.p.m., shunt controlled. In Figs. 1 and 2, V is a V-pulley. In order to secure the safty and to remove the disturbance from the belt, the spring coupling S consisting of a helical spring is inserted between the pulley and the shaft.[29] The guard ring G (omitted in Fig. 1) is equipped to check the increase of deflections of the shaft. To analyse the motion of the rotating disc, it is desirable to record simultaneously both the rotational motion and the whirling motion. The whirl is measured by observing the rectangular components of the motion relating to the fixed rectangular coordinate system. For this purpose the projections of motion to the rectangular coordinates OA and OB and the angular speed of rotation of the shaft are simultaneously recorded by our equipment. As shown in Fig. 1, the light from lamp S_2, passing through the condensing lens

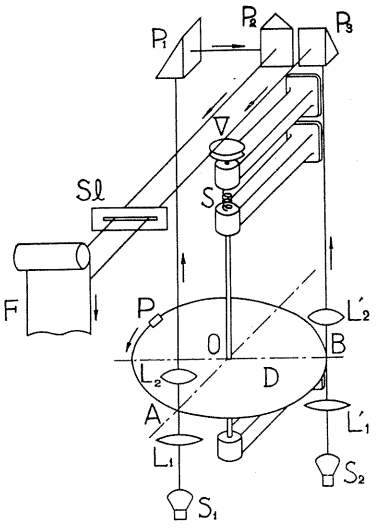

FIG. 1. Experimental apparatus and optical system.

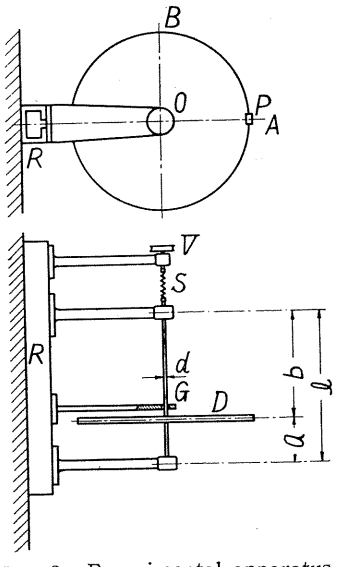

FIG. 2. Experimental apparatus.

L_1' placed before the disc, goes to point B on the disc edge and is bent 90 degrees by the prism P_3 and focused on a rotating film F by lens L_2' of 10~20 magnifications. At the same time another light from S_1, passing through point A and reflected by P_1 and P_2 is focused by lens L_2. In order to not only bend the light from S_1 90 degrees but also to rotate the vibration plane by 90 degrees, two prisms P_1 and P_2 must be used. Thus the images of the disc edge are made on the screen F in two directions, enlarged by lenses L_2' and L_2. The slit Sl is placed before screen F in order to obtain sharp images. A scale of 1.0 mm is put on the slit for measuring the amplitudes of vibrations of the shaft. The optical box of the electromagnetic oscillograph is used as the screen. A small piece of paper is attached to the disc edge. The light is intercepted by this paper at each revolution of the shaft and thus the record of rotation is obtained. The time record of 1/100 seconds is obtained as the synchronous motor is driven by a tuning-fork having 100 ≂ frequency. In experiments on the vertical shaft, the direction of OA (which

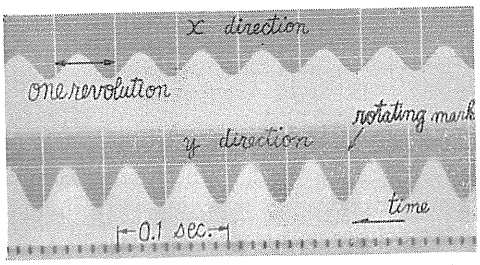

FIG. 3. Oscillographic paper of vibration of $[+\omega]$.

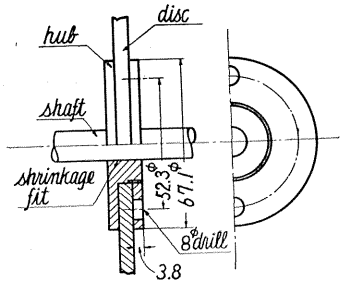

FIG. 4. Hub of the disc.

is the direction of the vertical center line of bearing pedestal) is selected as x-axis (see Fig. 2), and the direction OB as y-axis. A sample of the recording oscillographic paper obtained by this method is shown in Fig. 3. As shown in Fig. 4, the hub is fixed tightly onto the shaft by the shrink fit method and the disc is mounted on the hub. Holes of internal screw threads 1/4″ are made in the disc so as to attach the balancing weights. The discs and the shafts used in experiments are shown in the following tables.

TABLE 1. Dimensions of Discs

Disc No.	Dia. D in mm	Thickness in mm	Weight W in kg	Moment of inertia I in kg cm sec.^{2}	Radius of gyration k in mm
1	485.5	5.21	7.813	1.134	119.2
2	482.8	5.22	7.804	1.114	118.3
3	438.5	5.21	6.462	0.7530	106.9
4	366.0	9.26	6.927	0.5796	90.55
5	360.4	14.20	7.323	0.6075	90.17
6	150.1	60.15	6.479	0.1229	43.12

TABLE 2. Dimensions of Shaft*

Shaft No.	Shaft length l in mm	Dia. of shaft in mm	$a : b$ (see Fig. 2)	Remarks
1	507.9	11.85	4.5 : 5.5	
2	506.1	11.57	4 : 6	
3	508.3	11.89	3 : 7	
4	507.8	11.74	1 : 3	
5	506.3	11.72	1 : 4	
6	510.7	11.33	1 : 1	
7	505.9	11.15	1 : 1	
8	502.0	$a=11.74$, $b=10.89$	3 : 7	Cross section of the shaft is not circular.
9	505.6	11.71	3 : 7	
10	505.6	11.71	1 : 4	
11	506.8	12.00	3 : 7	Hub and shaft are made of one body. $a>b$
12	506.7	11.54	3 : 1	

*Example: Shaft No. 2 is illustrated in Fig. 5.

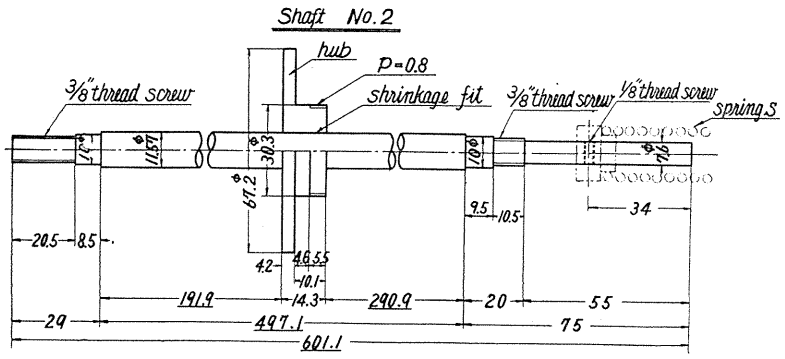

FIG. 5. Test-shaft (Shaft No. 2).

Self-aligning double-row ball bearings of 10 ϕ, except in special cases, are used in bearing pedestals.

3. The differential equations of motion

We treat with the rotating shaft system which consists of a light elastic shaft and a rotating disc with a mass m.

Consider the rectangular coordinate system o-xyz shown in Fig. 6 in which the z-axis is the bearing center line and let o be the position of the shaft center when no whirl exists; let $M(x, y)$ be the geometrical center of the shaft at the position where the rotating disc is mounted, and let $G(x_G, y_G)$ be the gravitational center of the disc. The configuration of the rigid body is determined by 6 coordinates, and the point M remains as always on the xy-plane when the shaft whirls, and the disc has 5 degrees of freedom.

Because it may be impossible for the axis perpendicular to the disc to exactly coincide with the center line of shaft, a small angle τ[50] as well as an inevitable eccentricity e may exist as a result of the deviation from an ideal mounting. The vibrations of a shaft are usually considered only by the eccentricity e, but in this case we should take into account a small angle τ as well as e because the deviation angle τ is the cause of the periodic disturbing forces exerted on the disc.

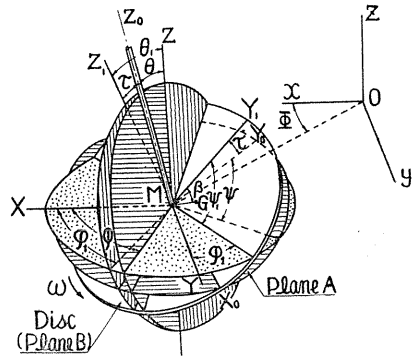

FIG. 6. Coordinate systems.

In Fig. 6 let M-XYZ be the rectangular coordinate system through the geometrical center M paralleling the system o-xyz. The disc surface will coincide with the plane A provided the small angle τ is zero. The following Eulerian angles θ, φ, ψ and $\theta_1, \varphi_1, \psi_1$ are used to denote the inclination of plane A and of the disc, respectively.

θ = inclination of the tangent Z_0M of deflection curve at M to the Z axis,
φ = angle of rotation of plane A about Z axis,
ψ = angle of rotation of plane A about Z_0M axis;
θ_1 = inclination of Z_1M which is perpendicular to the disc surface,
φ_1 = angle of rotation of the disc about Z axis,
ψ_1 = angle of rotation of the disc about Z_1M axis.

The configuration of the disc is decided by the coordinates x, y, θ_1, φ_1 and ψ_1. Let Y_1M be the intersecting line of the plane Z_0MZ_1 and the disc surface. Let Y_0M be the intersecting line of Z_0MZ_1 and plane A. Then obviously

$$\angle Z_0MZ_1 = \angle Y_1MY_0 = \tau, \tag{3. 1}$$

and the line X_0M, the intersecting line of the disc and plane A, is perpendicular to MZ_1, MZ_0, MY_1 and MY_0. The angle $\beta = \angle GMY_1$ is the angle between the eccentricity $GM = e$ and the small angle τ.

We proceed to obtain the differential equations of motion of the disc by using

Lagrage's equations. For this purpose we must obtain the kinetic energy and the potential energy of this vibratory system. In this procedure we may neglect the terms of powers higher than 3rd order of θ, θ_1, x, y, τ and e which are usually small compared with unity.

The kinetic energy of the disc is

$$T = T_1 + T_2, \tag{3. 2}$$

where

$$T_1 = \frac{1}{2} m(\dot{x}_G^2 + \dot{y}_G^2 + \dot{z}_G^2), \tag{3. 3}$$

$$T_2 = \frac{1}{2}\{I(\dot{\theta}_1^2 + \dot{\varphi}_1^2 \sin^2\theta_1) + I_p(\dot{\psi}_1 + \dot{\varphi}_1 \cos\theta_1)^2\}.^{(30)(43)} \tag{3. 4}$$

We now introduce new variables as follows:

$$\left.\begin{aligned} \varphi_1 + \psi_1 &= \Theta_1 \\ \theta_1 \cos\varphi_1 &= \theta_{x_1} \\ \theta_1 \sin\varphi_1 &= \theta_{y_1} \end{aligned}\right\} \qquad \left.\begin{aligned} \varphi + \psi &= \Theta \\ \theta \cos\varphi &= \theta_x \\ \theta \sin\varphi &= \theta_y \end{aligned}\right\} \tag{3. 5}$$

where θ_x, θ_y are the projectional angles of θ to xz- and yz-planes. With these variables, we have

$$\theta_1^2\dot{\varphi}_1 = \theta_1^2\dot{\varphi}_1(\cos^2\varphi_1 + \sin^2\varphi_1) = \dot{\theta}_{y_1}\theta_{x_1} - \dot{\theta}_{x_1}\theta_{y_1}, \quad \dot{\theta}_1^2 + \theta_1^2\dot{\varphi}_1^2 = \dot{\theta}_{x_1}^2 + \dot{\theta}_{y_1}^2. \tag{3. 6}$$

For the direction cosines of the three sets of axis M-$X_0Y_0Z_0$, M-$X_0Y_1Z_1$, and M-XYZ with respect to each other we obtain following tables:

	MX_0	MY_0	MZ_0
MX	$l_1 = \cos(\varphi+\psi) - \frac{\theta^2}{2}\cos\varphi\cos\psi$	$l_2 = -\sin(\varphi+\psi) + \frac{\theta^2}{2}\cos\varphi\sin\psi$	$l_3 = \theta\cos\varphi$
MY	$m_1 = \sin(\varphi+\psi) - \frac{\theta^2}{2}\sin\varphi\cos\psi$	$m_2 = \cos(\varphi+\psi) + \frac{\theta^2}{2}\sin\varphi\sin\psi$	$m_3 = \theta\sin\varphi$
MZ	$n_1 = -\theta\cos\psi$	$n_2 = \theta\sin\psi$	$n_3 = \cos\theta$

	MX_0	MY_1	MZ_1
MX	$l_1' = \cos(\varphi_1+\psi_1) - \frac{\theta_1^2}{2}\cos\varphi_1\cos\psi_1$	$l_2' = -\sin(\varphi_1+\psi_1) + \frac{\theta_1^2}{2}\cos\varphi_1\sin\psi_1$	$l_3' = \theta_1\cos\varphi_1$
MY	$m_1' = \sin(\varphi_1+\psi_1) - \frac{\theta_1^2}{2}\sin\varphi_1\cos\psi_1$	$m_2' = \cos(\varphi_1+\psi_1) + \frac{\theta_1^2}{2}\sin\varphi_1\sin\psi_1$	$m_3' = \theta_1\sin\varphi_1$
MZ	$n_1' = -\theta_1\cos\psi_1$	$n_2' = \theta\sin\psi_1$	$n_3' = \cos\theta_1$

	MX_0	MY_0	MZ_0
MX_0	1	0	0
MY_1	0	$\cos\tau$	$\sin\tau$
MZ_1	0	$-\sin\tau$	$\cos\tau$

Since $l_1 = l_1'$, $m_2' = \cos\tau\, m_2 + \sin\tau\, m_3$, we have

$$\cos(\varphi_1+\psi_1) - \frac{\theta_1^2}{2}\cos\varphi_1\cos\psi_1 = \cos(\varphi+\psi) - \frac{\theta^2}{2}\cos\varphi\cos\psi, \tag{3. 7}$$

$$\cos(\varphi_1+\psi_1) + \frac{\theta_1^2}{2}\sin\varphi_1\sin\psi_1 = \cos\tau\cos(\varphi+\psi) + \frac{\theta^2}{2}\sin\varphi\sin\psi + \sin\tau\sin\theta\sin\varphi. \tag{3. 8}$$

From Eq. (3. 7) and Eq. (3. 8), we have

$$\cos(\varphi_1+\psi_1)\left(2-\frac{\theta_1^2}{2}\right) = \cos(\varphi+\psi)\left(2-\frac{\tau^2}{2}\right) - \frac{\theta^2}{2}\cos(\varphi+\psi) + \tau\theta\sin\varphi. \tag{3. 9}$$

Since $m_1 = m_1'$, $l_2' = l_2\cos\tau + l_3\sin\tau$, we have similarly

$$\sin(\varphi_1+\psi_1)\left(2-\frac{\theta_1^2}{2}\right) = \sin(\varphi+\psi)\left(2-\frac{\tau^2}{2}-\frac{\theta^2}{2}\right) - \tau\theta\cos\varphi. \tag{3. 10}$$

Since $n_3' = -\tau n_2 + \cos\tau n_3$, we have

$$\cos\theta_1 = \cos\theta\cos\tau - \tau\sin\psi\sin\theta, \qquad \therefore\ \theta_1^2 = \tau^2+\theta^2+2\tau\theta\sin\psi. \tag{3. 11}$$

Insertion of $\theta\sin\psi = \theta\sin(\varphi+\psi-\varphi) = \theta_x\sin\Theta - \theta_y\cos\Theta$ into Eq. (3. 11) yields

$$\theta_1^2 = \tau^2+\theta^2+2\tau(\theta_x\sin\Theta - \theta_y\cos\Theta). \tag{3. 12}$$

Substituting this value of θ_1^2 in Eq. (3. 9) and Eq. (3. 10), we have

$$\cos(\varphi_1+\psi_1) = \cos\Theta_1 = \cos\Theta\left\{1+\frac{\tau}{2}(\theta_x\sin\Theta - \theta_y\cos\Theta)\right\} + \frac{\tau}{2}\theta_y, \tag{3. 13}$$

and

$$\sin(\varphi_1+\psi_1) = \sin\Theta_1 = \sin\Theta\left\{1+\frac{\tau}{2}(\theta_x\sin\Theta - \theta_y\cos\Theta)\right\} - \frac{\tau}{2}\theta_x, \tag{3. 14}$$

respectively.

Since $l_3' = -\tau l_2 + \cos\tau l_3$ and $m_3' = -\tau m_2 + \cos\tau\cdot m_3$, we have

$$\theta_1\cos\varphi_1 = \theta_{x_1} = \tau\sin\Theta + \cos\tau\theta_x, \quad \theta_1\sin\varphi_1 = \theta_{y_1} = -\tau\cos\Theta + \cos\tau\theta_y,$$

so that

$$\theta_{x_1}\dot\theta_{y_1} - \theta_{y_1}\dot\theta_{x_1} = \tau^2\dot\Theta + \tau\dot\Theta(\theta_x\sin\Theta - \theta_y\cos\Theta) + \tau(\dot\theta_x\cos\Theta + \dot\theta_y\sin\Theta) + (\theta_x\dot\theta_y - \theta_y\dot\theta_x), \tag{3. 15}$$

and

$$\dot\theta_{x_1}^2 + \dot\theta_{y_1}^2 = \tau^2\dot\Theta^2 + 2\tau\dot\Theta(\dot\theta_x\cos\Theta + \dot\theta_y\sin\Theta) + \dot\theta_x^2 + \dot\theta_y^2. \tag{3. 16}$$

Differentiating Eq. (3. 14) in respect to time t we get

$$\dot\Theta_1\cos\Theta_1 = \dot\Theta\cos\Theta\left\{1-\frac{\tau}{2}(\theta_x\sin\Theta - \theta_y\cos\Theta)\right\} + \frac{\tau}{2}\sin\Theta\{(\dot\theta_x\sin\Theta - \dot\theta_y\cos\Theta) + \dot\Theta(\theta_x\cos\Theta + \theta_y\sin\Theta)\} - \frac{\tau}{2}\dot\theta_x. \tag{3. 17}$$

Inserting $\cos\Theta_1$ of Eq. (3. 13) into the above expression, we have

$$\dot\Theta_1 = \dot\Theta + \frac{\tau\dot\Theta}{2}(\theta_x\sin\Theta - \theta_y\cos\Theta) - \frac{\tau}{2}(\dot\theta_x\cos\Theta + \dot\theta_y\sin\Theta). \tag{3. 18}$$

The relation

$$x_G = x + e\{\sin(\beta-\psi_1)\cos\varphi_1\cos\theta_1 - \sin\varphi_1\cos(\beta-\psi_1)\} = x + e\sin(\beta-\Theta_1),$$
$$y_G = y + e\{\sin(\beta-\psi_1)\sin\varphi_1\cos\theta_1 + \cos\varphi_1\cos(\beta-\psi_1)\} = y + e\cos(\beta-\Theta_1),$$

and

$$z_G = -\sin\theta_1\sin(\beta-\psi_1)e$$

lead to

$$\dot{x}_G^2 + \dot{y}_G^2 + \dot{z}_G^2 = \dot{x}^2 + \dot{y}^2 - 2e\dot{\Theta}\{\dot{x}\cos(\Theta-\beta) + \dot{y}\sin(\Theta-\beta)\} + e^2\dot{\Theta}^2. \quad (3.\ 19)$$

Substituting Eqs. (3. 3), (3. 4), (3. 6), (3. 15), (3. 16) and (3. 19) into Eq. (3. 2), we have

$$\begin{aligned} T = {} & \frac{\dot{\Theta}^2}{2}\{I_p(1-\tau_2) + I\tau^2\} + \tau\dot{\Theta}(I-I_p)(\dot{\theta}_x\cos\Theta + \dot{\theta}_y\sin\Theta) \\ & + \frac{1}{2}I_p\dot{\Theta}(\dot{\theta}_x\theta_y - \dot{\theta}_y\theta_x) + \frac{1}{2}I(\dot{\theta}_x^2 + \dot{\theta}_y^2) \\ & + \frac{1}{2}m[\dot{x}^2 + \dot{y}^2 - 2e\dot{\Theta}\{\dot{x}\cos(\Theta-\beta) + \dot{y}\sin(\Theta-\beta)\} + e^2\dot{\Theta}^2]. \end{aligned} \quad (3.\ 20)$$

The potential energy of this system should be represented by the following form

$$V = \frac{1}{2}\alpha(x^2+y^2) + \gamma(x\theta_x + y\theta_y) + \frac{1}{2}\delta(\theta_x^2+\theta_y^2), \quad (3.\ 21)$$

where α, γ and δ are the spring constants of the shaft. Substituting Eqs. (3. 20) and (3. 21) into Lagrage's equations, equations of motion regarding the rotating disc are

$$\begin{aligned} \{I_p - (I_p - I)\tau^2 + me^2\}\ddot{\Theta} = {} & \tau(I_p - I)(\ddot{\theta}_x\cos\Theta + \ddot{\theta}_y\sin\Theta) + \frac{1}{2}I_p(\ddot{\theta}_y\theta_x - \ddot{\theta}_x\theta_y) \\ & + me\{\ddot{x}\cos(\Theta-\beta) + \ddot{y}\sin(\Theta-\beta)\}, \end{aligned} \quad (3.\ 22)$$

$$m\ddot{x} - me\ddot{\Theta}\cos(\Theta-\beta) + \alpha x + \gamma\theta_x = -me\dot{\Theta}^2\sin(\Theta-\beta), \quad (3.\ 23)$$

$$m\ddot{y} - me\ddot{\Theta}\sin(\Theta-\beta) + \alpha y + \gamma\theta_y = me\dot{\Theta}^2\cos(\Theta-\beta), \quad (3.\ 24)$$

$$I\ddot{\theta}_x - \tau\ddot{\Theta}(I_p - I)\cos\Theta + \frac{1}{2}I_p\ddot{\Theta}\theta_y + I_p\dot{\Theta}\dot{\theta}_y + \gamma x + \delta\theta_x = -\tau\dot{\Theta}^2(I_p - I)\sin\Theta, \quad (3.\ 25)$$

$$I\ddot{\theta}_y - \tau\ddot{\Theta}(I_p - I)\sin\Theta - \frac{1}{2}I_p\ddot{\Theta}\theta_x - I_p\dot{\Theta}\dot{\theta}_x + \gamma y + \delta\theta_y = \tau\dot{\Theta}^2(I_p - I)\cos\Theta. \quad (3.\ 26)$$

Eqs. (3.22), (3.23), (3.24), (3.25) and (3.26) are the equations of motion Θ, x, y, θ_x and θ_y, respectively. Since $\ddot{x}$, $\ddot{y}$, $\ddot{\theta}_x$, $\ddot{\theta}_y$, $\dot{x}$, $\dot{y}$, $\dot{\theta}_x$, $\dot{\theta}_y$, x, y, θ_x, θ_y, τ and e are small compared with unity, we may neglect the higher powers in the equations of motion, so Eq. (3. 22) is approximately $I_p\ddot{\Theta} = 0$, and it leads to $\dot{\Theta} = \dot{\varphi} + \dot{\psi} = \text{constant}$. Obviously $\dot{\Theta}$ coincides with the angular velocity of the shaft ω. Using $\dot{\Theta} = \omega$ and $\Theta = \omega t + \frac{\pi}{2} + \beta$, we may express the equations of motion as follows:

$$\left.\begin{aligned} & \dot{\Theta} = \omega = \text{const}, \\ & m\ddot{x} + \alpha x + \gamma\theta_x = me\omega^2\cos\omega t, \\ & m\ddot{y} + \alpha y + \gamma\theta_y = me\omega^2\sin\omega t, \\ & I\ddot{\theta}_x + I_p\omega\dot{\theta}_y + \gamma x + \delta\theta_x = (I_p - I)\tau\omega^2\cos(\omega t + \beta), \\ & I\ddot{\theta}_y - I_p\omega\dot{\theta}_x + \gamma y + \delta\theta_y = (I_p - I)\tau\omega^2\sin(\omega t + \beta). \end{aligned}\right\} \quad (3.\ 27)$$

The particular solutions of Eqs. (3. 27) are

$$\left.\begin{aligned}
x &= \frac{1}{(\alpha-m\omega^2)\{\delta+(I_p-I)\omega^2\}-\gamma^2}[me\omega^2\{\delta+(I_p-I)\omega^2\}\cos\omega t \\
&\qquad -(I_p-I)\tau\omega^2\gamma\cos(\omega t+\beta)], \\
y &= \frac{1}{(\alpha-m\omega^2)\{\delta+(I_p-I)\omega^2\}-\gamma^2}[me\omega^2\{\delta+(I_p-I)\omega^2\}\sin\omega t \\
&\qquad -(I_p-I)\tau\omega^2\gamma\sin(\omega t+\beta)], \\
\theta_x &= \frac{1}{(\alpha-m\omega^2)\{\delta+(I_p-I)\omega^2\}-\gamma^2}[-me\omega^2\gamma\cos\omega t \\
&\qquad +(I_p-I)\tau\omega^2(\alpha-m\omega^2)\cos(\omega t+\beta)], \\
\theta_y &= \frac{1}{(\alpha-m\omega^2)\{\delta+(I_p-I)\omega^2\}-\gamma^2}[-me\omega^2\gamma\sin\omega t \\
&\qquad +(I_p-I)\tau\omega^2(\alpha-m\omega^2)\sin(\omega t+\beta)].
\end{aligned}\right\} \quad (3.\ 28)$$

Eqs. (3. 28) give the forced vibrations of the shaft.

The major critical speed ω_c is obtained by setting the denominator of Eqs. (3. 28) equal to zero.

$$\omega_c^2 = \frac{\{\alpha(I_p-I)-\delta m\}\pm\sqrt{\{\alpha(I_p-I)+\delta m\}^2-4m\gamma^2(I_p-I)}}{2m(I_p-I)} \quad (3.\ 29)$$

For the disc the thickness of which is small, we may put $I_p \fallingdotseq 2I$ and Eq. (3. 29) is

$$\omega_c^2 = \frac{\alpha I-\delta m\pm\sqrt{(\alpha I+\delta m)^2-4\gamma^2 mI}}{2mI}. \quad (3.\ 29\,a)$$

Introducing the dimensionless quantities ζ, μ and ν and denoting them as follows:

$$p_1^2=\alpha/m,\ p_2^2=\delta/I,\ p_3^4=\gamma^2/mI,\ \zeta=\omega/p_1,\ \mu=p_2/p_1,\ \nu=p_3^2/p_1^2, \quad (3.\ 30)$$

we have

$$\zeta_c^2=(\omega_c/p_1)^2=\frac{1-\mu^2\pm\sqrt{(1+\mu^2)^2-4\nu^2}}{2}. \quad (3.\ 29\,b)$$

Between the spring constants α, γ and δ, the relation $\alpha\delta-\gamma^2>0$ $(\mu^2-\nu^2>0)$ is always held, hence only the positive sign before the radical in Eqs. (3. 29), (3. 29a) and (3. 29b) may be adopted. Consequently it may be readily seen that the major critical speed of the shaft is unique. The frequency equation obtained from Eqs. (3. 27) is

$$\{(\alpha-mp^2)(\delta+2I\omega p-Ip^2)-\gamma^2\}\{(\alpha-mp^2)(\delta-2I\omega p-Ip^2)-\gamma^2\}=0, \quad (3.\ 31)$$

or

$$\{(1-\eta^2)(\mu^2+2\eta\zeta-\eta^2)-\nu^2\}\{(1-\eta^2)(\mu^2-2\eta\zeta-\eta^2)-\nu^2\}=0, \quad (3.\ 31\,a)$$

in which we put $I_p=2I$ and $\eta=p/p_1$, and p is the natural frequency of this system.

In Fig. 7 the $p-\omega$ diagrams are given and we may see that four natural frequencies p_1, p_2, p_3 and p_4 exist in a certain revolution ω.

In Fig. 7, Curve I and Curve II give the free vibrations with the mode of vibration of forward precession in which the direction of whirling is the same as that of rotation ω of the shaft; Curves III and IV represent the whirling of backward precession, in reversed direction to ω. In Fig. 7, point A at which the straight line $p=\omega$ and Curve II intersect, shows the major critical speed ω_c.

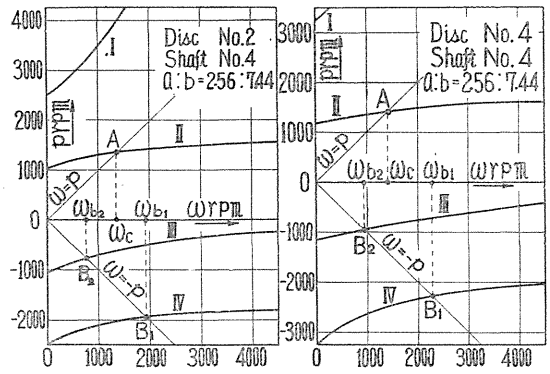

FIG. 7. Calculation diagram of $\omega - p$ curves.

4. Synopsis

According to the procedure mentioned in Section 2, we may obtain amplitude $-\omega$ curves (response curves), as illustrated in Figs. 8 and 9. In these figure, the motion of the disc is composed of various kinds of vibrations, and the resultant amplitudes including various modes of vibrations are shown by ordinates.

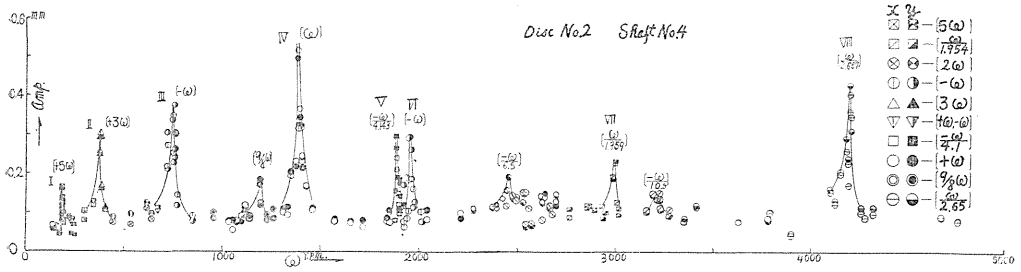

FIG. 8. Resonance diagram of Shaft No. 4 and Disc No. 2.

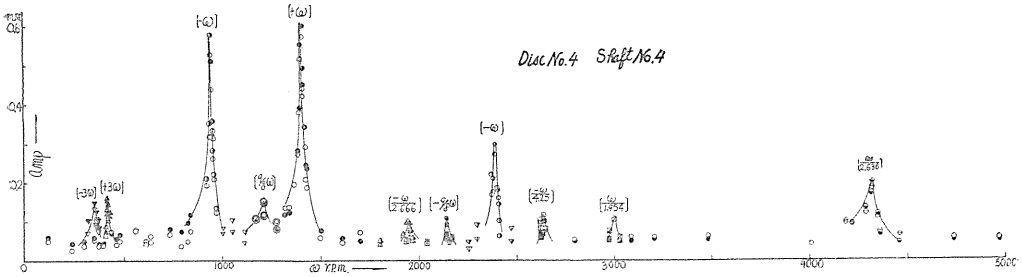

FIG. 9. Resonance diagram of Shaft No. 4 and Disc No. 4.

The following expressions are used to represent the mode of vibration. For instance, the notations $[+m\omega]$ and $[-n\omega]$ represent the following motions:

$$x = A\cos m\omega t,\quad y = A\sin m\omega t, \tag{4. 1}$$

and

$$x = A\cos n\omega t,\quad y = A\sin(-n\omega t) = -A\sin n\omega t, \tag{4. 2}$$

respectively.

The notation $[+m\omega]$ represents the motion which has a frequency of m times that of the angular velocity of shaft ω with whirling of the forward precession indicated by a positive sign. The notation $[-n\omega]$ represents the motion having n times frequency that of ω and the negative sign indicates the backward precession.

The experimental results obtained by using Disc No. 2 and Shaft No. 4 are illustrated in Fig. 8. In this figure there are 8 peaks of amplitudes of various modes of vibrations. Peak I of the motion $[+5\omega]$ occurs in 190 r.p.m., Peak II of $[+3\omega]$ in 383 r.p.m., Peak III of $[-\omega]$ in 750 r.p.m., Peak IV of $[+\omega]$ in 1,394 r.p.m., Peak V of $\left[-\frac{\omega}{4.143}\right]$ in 1,886 r.p.m., Peak VI of $[-\omega]$ in 1,995 r.p.m., Peak VII of $\left[+\frac{\omega}{1.959}\right]$ in 3,005 r.p.m. and Peak VIII of $\left[+\frac{\omega}{2.667}\right]$ in 4,205 r.p.m. The

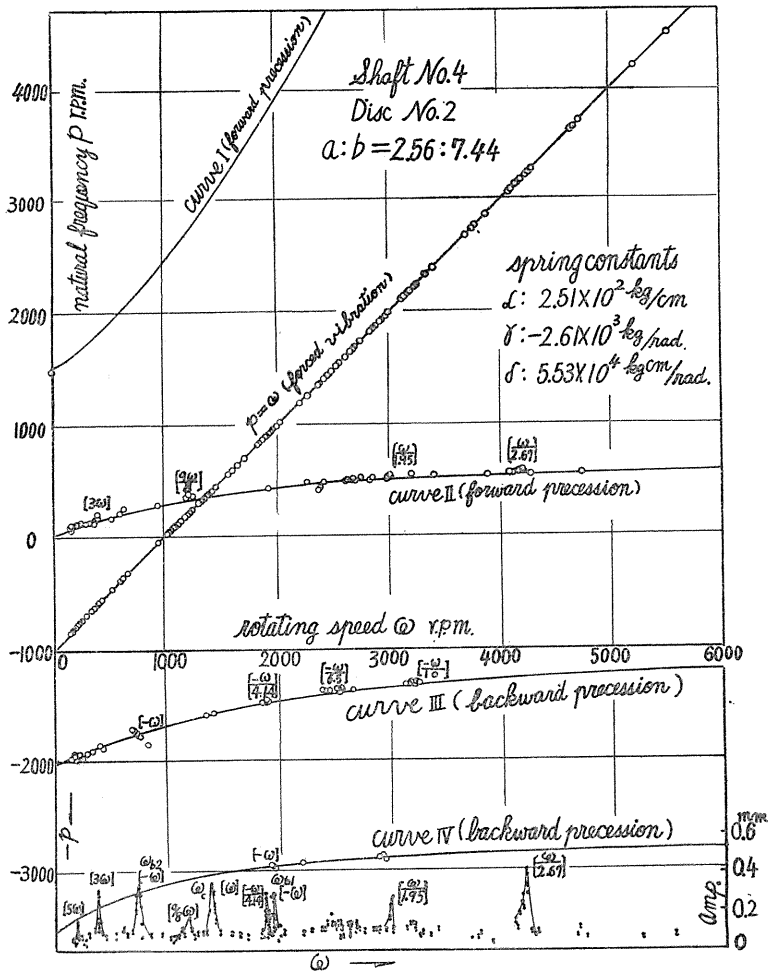

FIG. 10. Calculation diagram of $\omega - p$ curves and experimental results.

analogous response curves for Disc No. 4 and Shaft No. 4 are shown in Fig. 9. In Figs. 8 and 9 distinct marks are used to distinguish these modes of vibration.

Now we may see that there are many kinds of vibrations of the shaft and that rather complicated motions take place in a comparatively simple equipment as shown in Figs. 1 and 2.

The frequencies of vibrations shown in Fig. 8 are plotted against the angular velocity of shaft ω in Fig. 10. In this figure, Curves I, II, III and IV are the calculated $p-\omega$ curves from the frequency equation (3.31) and we may see that all vibrations in Fig. 8 consist of the vibrations having natural frequencies corresponding to any angular velocity of shaft and the forced vibrations of frequency induce by e and τ.

In the latter part of this paper we carry out detailed treatments of these vibrations and analyze the motions, clearing up the causes of various kinds of vibrations.

Chapter II. Synchronous Backward Precession[31]

5. Introduction

When the absolute value of frequency of a backward precession is equal to the angular velocity ω, such a backward precession is called "synchronous backward precession," represented by the notation $[-\omega]$.

Among numerous papers in which the whirling of rotating shaft has been discussed there has been treated the so-called shaft whipping[4)5)25)] having the mode of backward precession. In those cases, however, the frequencies of vibrations are equal to the natural frequencies of the system and those vibrations belong to self-sustained oscillations, and are substantially different from the synchronous backward precession with which we shall treat presently. Stodola[2)] pointed out experimentally the occurrence of synchronous backward precession in the turbine shaft. But the cause of this motion was not explained.

As shown in Figs. 8 and 9, there are two peaks of resonance curves of $[-\omega]$, one higher than the major critical speed ω_c, the other, lower. These two peaks correspond to the points B_1 and B_2 in Fig. 7, in which the straight line $\omega=-p$ intersects Curve III and Curve IV, and the frequency of the motion is exactly equal to $-\omega$ but not equal to the natural frequency of this system represented by Curves III and IV.

In Fig. 2, when the distances a and b of the disc D from both ends of the shaft are not equal, the deflections of the shaft and the inclinations of the disc are simultaneous. Consequently the motion in x-direction is not independant of that in y-direction because of the gyroscopic effect resulting from the unequal distances, $a \neq b$. In that case, the small differences in flexural rigidity of the system in all directions cause the backward precession. These differences in rigidity are due mainly to the deflections of bearing pedestals, detailed treatments on which are carried out later on.

6. Equations of motion

We now consider the vibratory system in which the stiffness in x-direction differs from that in y-direction. We denote the spring constants in x-direction to be $\alpha+\Delta\alpha$, $\gamma+\Delta\gamma$ and $\delta+\Delta\delta$, those in y-direction $\alpha-\Delta\alpha$, $\gamma-\Delta\gamma$ and $\delta-\Delta\delta$. Then

$2\Delta\alpha$, $2\Delta\gamma$ and $2\Delta\delta$ are the small differences of stiffness between those in x and y directions, and the differencial equations of motion (3.27) can be written in the following forms:

$$\left.\begin{aligned} &m\ddot{x}+(\alpha+\Delta\alpha)x+(\gamma+\Delta\gamma)\theta_x=me\omega^2\cos\omega t,\\ &m\ddot{y}+(\alpha-\Delta\alpha)y+(\gamma-\Delta\gamma)\theta_y=me\omega^2\sin\omega t,\\ &I\ddot{\theta}_x+2I\omega\dot{\theta}_y+(\delta+\Delta\delta)\theta_x+(\gamma+\Delta\gamma)x=I\tau\omega^2\cos(\omega t+\beta),\\ &I\ddot{\theta}_y-2I\omega\dot{\theta}_x+(\delta-\Delta\delta)\theta_y+(\gamma-\Delta\gamma)y=I\tau\omega^2\sin(\omega t+\beta), \end{aligned}\right\} \tag{6.1}$$

in which we put $I_p=2I$.

In general, $\Delta\alpha$, $\Delta\gamma$ and $\Delta\delta$ are small as compared with α, γ and δ, and we may assume the higher powers of these small quantities to be negligible. Thus the required particular solutions of Eqs. (6.1) become as follows:

$$\left.\begin{aligned} x=&\frac{me\omega^2(\delta+I\omega^2)}{(\alpha-m\omega^2)(\delta+I\omega^2)-\gamma^2}\cos\omega t+\frac{-I\tau\omega^2\gamma}{(\alpha-m\omega^2)(\delta+I\omega^2)-\gamma^2}\cos(\omega t+\beta)\\ &+\frac{me\omega^2\{-\Delta\alpha(\delta+I\omega^2)(\delta-3I\omega^2)+2\Delta\gamma\cdot\gamma(\delta-I\omega^2)-\Delta\delta\cdot\gamma^2\}}{\{(\alpha-m\omega^2)(\delta+I\omega^2)-\gamma^2\}\{(\alpha-m\omega^2)(\delta-3I\omega^2)-\gamma^2\}}\cos\omega t\\ &+\frac{I\tau\omega^2[\Delta\alpha\cdot\gamma(\delta-3I\omega^2)+\Delta\delta\cdot\gamma(\alpha-m\omega^2)-\Delta\gamma\{\gamma^2+(\delta-3I\omega^2)(\alpha-m\omega^2)\}]}{\{(\alpha-m\omega^2)(\delta+I\omega^2)-\gamma^2\}\{(\alpha-m\omega^2)(\delta-3I\omega^2)-\gamma^2\}}\\ &\qquad\times\cos(\omega t+\beta),\\ y=&\frac{me\omega^2(\delta+I\omega^2)}{(\alpha-m\omega^2)(\delta+I\omega^2)-\gamma^2}\sin\omega t+\frac{-I\tau\omega^2\gamma}{(\alpha-m\omega^2)(\delta+I\omega^2)-\gamma^2}\sin(\omega t+\beta)\\ &-\frac{me\omega^2\{-\Delta\alpha(\delta+I\omega^2)(\delta-3I\omega^2)+2\Delta\gamma\cdot\gamma(\delta-I\omega^2)-\Delta\delta\cdot\gamma^2\}}{\{(\alpha-m\omega^2)(\delta+I\omega^2)-\gamma^2\}\{(\alpha-m\omega^2)(\delta-3I\omega^2)-\gamma^2\}}\sin\omega t\\ &-\frac{I\tau\omega^2[\Delta\alpha\cdot\gamma(\delta-3I\omega^2)+\Delta\delta\cdot\gamma(\alpha-m\omega^2)-\Delta\gamma\{\gamma^2+(\delta-3I\omega^2)(\alpha-m\omega^2)\}]}{\{(\alpha-m\omega^2)(\delta+I\omega^2)-\gamma^2\}\{(\alpha-m\omega^2)(\delta-3I\omega^2)-\gamma^2\}}\\ &\qquad\times\sin(\omega t+\beta),\\ \theta_x=&\frac{-me\gamma\omega^2}{(\alpha-m\omega^2)(\delta+I\omega^2)-\gamma^2}\cos\omega t+\frac{I\tau\omega^2(\alpha-m\omega^2)}{(\alpha-m\omega^2)(\delta+I\omega^2)-\gamma^2}\cos(\omega t+\beta)\\ &+\frac{me\omega^2[\Delta\alpha\cdot\gamma(\delta+I\omega^2)+\Delta\delta\cdot\gamma(\alpha-m\omega^2)-\Delta\gamma\{\gamma^2+(\alpha-m\omega^2)(\delta+I\omega^2)\}]}{\{(\alpha-m\omega^2)(\delta+I\omega^2)-\gamma^2\}\{(\alpha-m\omega^2)(\delta-3I\omega^2)-\gamma^2\}}\\ &\qquad\times\cos\omega t\\ &+\frac{I\tau\omega^2\{2\Delta\gamma\cdot\gamma(\alpha-m\omega^2)-\Delta\delta(\alpha-m\omega^2)^2-\Delta\alpha\cdot\gamma^2\}}{\{(\alpha-m\omega^2)(\delta+I\omega^2)-\gamma^2\}\{(\alpha-m\omega^2)(\delta-3I\omega^2)-\gamma^2\}}\cos(\omega t+\beta),\\ \theta_y=&\frac{-me\gamma\omega^2}{(\alpha-m\omega^2)(\delta+I\omega^2)-\gamma^2}\sin\omega t+\frac{I\tau\omega^2(\alpha-m\omega^2)}{(\alpha-m\omega^2)(\delta+I\omega^2)-\gamma^2}\sin(\omega t+\beta)\\ &-\frac{me\omega^2[\Delta\alpha\cdot\gamma(\delta+I\omega^2)+\Delta\delta\cdot\gamma(\alpha-m\omega^2)-\Delta\gamma\{\gamma^2+(\alpha-m\omega^2)(\delta+I\omega^2)\}]}{\{(\alpha-m\omega^2)(\delta+I\omega^2)-\gamma^2\}\{(\alpha-m\omega^2)(\delta-3I\omega^2)-\gamma^2\}}\\ &\qquad\times\sin\omega t\\ &-\frac{I\tau\omega^2\{2\Delta\gamma\cdot\gamma(\alpha-m\omega^2)-\Delta\delta(\alpha-m\omega^2)^2-\Delta\alpha\cdot\gamma^2\}}{\{(\alpha-m\omega^2)(\delta+I\omega^2)-\gamma^2\}\{(\alpha-m\omega^2)(\delta-3I\omega^2)-\gamma^2\}}\sin(\omega t+\beta). \end{aligned}\right\} \tag{6.2}$$

The 1st and 2nd terms in the right-hand side of Eqs. (6.2) represent the normal vibrations of $[+\omega]$, but as can be easily seen from Eqs. (6.2), the 3rd and

4th terms give the motions of synchronous backward precession of $[-\omega]$. Usually, since the numerators of the 1st ard 2nd terms in the above equations are larger than those of the 3rd and 4th terms, the motions $[+\omega]$ predominate over the synchronous backward precession. The amplitudes of synchronous backward precession, however, tend to increase rapidly as ω approaches the frequency ω_{b_1} or ω_{b_2} in Fig. 7 and they become larger than the amplitudes of $[+\omega]$. The critical speeds of synchronous backward precession are obtained by making the denominators zero in the 3rd and 4th terms in Eqs. (6.2), *i.e.*,

$$\{(\alpha - m\omega^2)(\delta + I\omega^2) - \gamma^2\}\{(\alpha - m\omega^2)(\delta - 3I\omega^2) - \gamma^2\} = 0.$$

Equating the first bracketed equation to zero, the major critical speed ω_c can be obtained, *cf.* Eqs. (3.28), so that the motion of $[+\omega]$ predominates over the motion of $[-\omega]$ in the rotating speed of shaft. Then the critical speeds of $[-\omega]$ can be given only by making the second bracketed equation zero.

$$(\alpha - m\omega^2)\{(\delta - 3I\omega^2) - \gamma^2\} = 0 \tag{6.3}$$

It is to be noted that Eq. (6.3) is independent of $\Delta\alpha$, $\Delta\gamma$ and $\Delta\delta$. Similarly the frequency eauation obtained by Eq. (6.1) coincides with Eq. (3.31) and the natural frequencies of this system are independent of $\Delta\alpha$, $\Delta\gamma$ and $\Delta\delta$, provided that the higher powers of $\Delta\alpha$ etc. are negligible. From Eqs. (6.1) we obtain the frequency equation:

$$\begin{vmatrix} (\alpha+\Delta\alpha)-m\omega^2 & 0 & \gamma+\Delta\gamma & 0 \\ 0 & (\alpha-\Delta\alpha)-m\omega^2 & 0 & \gamma-\Delta\gamma \\ \gamma+\Delta\gamma & 0 & (\delta+\Delta\delta)-I\omega^2 & 2I\omega^2 \\ 0 & \gamma-\Delta\gamma & 2I\omega^2 & (\delta-\Delta\delta)-I\omega^2 \end{vmatrix}$$

$$= \{(\alpha - m\omega^2)(\delta + I\omega^2) - \gamma^2\}\{(\alpha - m\omega^2)(\delta - 3I\omega^2) - \gamma^2\}$$
$$+ [-(\Delta\alpha)^2(\delta + I\omega^2)(\delta - 3I\omega^2) - (\Delta\delta)^2(\alpha - m\omega^2)^2 - 2(\Delta\gamma)^2\{(\alpha - m\omega^2)(\delta - I\omega^2) + \gamma^2\}$$
$$+ 4\Delta\alpha\cdot\Delta\gamma\cdot\gamma(\delta - I\omega^2) + 4\Delta\gamma\cdot\Delta\delta\cdot\gamma(\alpha - m\omega^2) + \{(\Delta\gamma)^2 - \Delta\alpha\cdot\Delta\delta\}^2] = 0.$$

The above quation does not include the linear terms of $\Delta\alpha$ etc. and we may neglect the higher powers of $\Delta\alpha$ ect.; therefore this equation coincides with Eqs. (3.31) and is independent of $\Delta\alpha$ etc..

In all cases, the relation $\alpha\delta - \gamma^2 > 0$ is satisfied and it is easy to see that Eq. (6.3) has two positive roots for ω^2, *i.e.*,

$$\left.\begin{aligned} \omega_{b_1}^2 &= \frac{1}{6mI}\{(\delta m + 3\alpha I) + \sqrt{(\delta m - 3\alpha I)^2 + 12mI\gamma^2}\}, \\ \omega_{b_2}^2 &= \frac{1}{6mI}\{(\delta m + 3\alpha I) - \sqrt{(\delta m - 3\alpha I)^2 + 12mI\gamma^2}\}. \end{aligned}\right\} \tag{6.4}$$

Introducing the dimensionless quantities, we have

$$\zeta_{b_{1,2}}^2 = \frac{1}{6}\{3 + \mu^2 \pm \sqrt{(3 - \mu^2)^2 + 12\nu^2}\}. \tag{6.4a}$$

Obviously ω_{b_1} and ω_{b_2} obtained by the above equations coincide with those in

Fig. 7. From Eq. (6.4), we may conclude that the shaft with one disc always has two critical speeds of the mode of $[-\omega]$. We can also conclude that the relation $\omega_{b_1} \geqq \omega_c \geqq \omega_{b_2}$ can be held, provided $\alpha\delta - \gamma^2 > 0$, consequently one of the critical speeds of synchronous backward precession is higher than the major critical speed, the other is lower.

When Disc No. 2 and Shaft No. 4 are used, $\omega_c = 1{,}383$ r.p.m., $\omega_{b_1} = 1{,}948$ r.p.m. and $\omega_{b_2} = 750$ r.p.m. are obtained either by Eq. (6.4) or Fig. 7 and the experimental results lead to $\omega_c = 1{,}389$ r.p.m., $\omega_{b_1} = 1{,}940$ r.p.m. and $\omega_{b_2} = 759$ r.p.m. as shown in Fig. 8. Obviously good agreement is obtained.

7. The flexural rigidity of bearing pedestals and synchronous backward precession[4) 11) 16) 17) 18)]

The present section is devoted to a detailed discussion of the influence of the flexibility of bearing pedestals on the critical speeds of $[-\omega]$. If the bearing pedestals have some but not much elasticity, the equations of motion in this system reduce to Eqs. (6.1) and then the conclusion in the previous section holds good.

As can be easily seen from Fig. 2, the flexibility of pedestals in the direction OB is more than that in OA, and taking this into consideration, the rigidity of the shaft in OB is less than that in OA. For the pedestals used in experiments, the deflections in OA direction are so small as to be negligible. Furthermore, we should take the masses of pedestals into account and that the degrees of freedom in this system are higher than those of the freedom treated in Section 3. As shown in Fig. 11, we should consider the vibrations of flexible shaft supported by flexible bearing pedestals. We assume that the pedestals have the stiffness of k_a and k_b in OB direction (y-direction) and are not deflected in OA direction (x-direction). For the masses of pedestals, let us consider the concentrated masses of m_a and m_b attached to the top of pedestals. The spring constants of the shaft itself α_1, γ_1 and δ_1 are usually smaller than k_a and k_b. In Fig. 12, let F and M_t be force and moment exerted on the disc on yz-plane (*cf.* Fig. 6), y_a and y_b be small displacements of pedestals due to F and M_t, y_2 and θ_{y_2} be the deflection and inclination of disc due to y_a and y_b. The kinetic energy T_0 and potential energy V_0 in this system may be represented as follows:

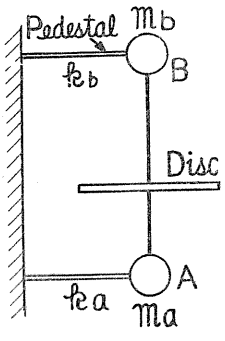

FIG. 11

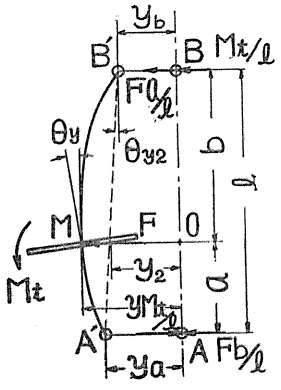

FIG. 12

$$T_0 = T + \frac{1}{2} m_a \dot{y}_a^2 + \frac{1}{2} m_b \dot{y}_b^2, \tag{7. 1}$$

$$\begin{aligned} V_0 &= \left(\frac{1}{2}\alpha_1 x^2 + \gamma_1 x\theta_x + \frac{1}{2}\delta_1\theta_x^2\right) + \left\{\frac{1}{2}\alpha_1(y-y_2)^2 + \gamma_1(y-y_2)(\theta_y - \theta_{y_2})\right. \\ &\quad \left. + \frac{1}{2}\delta_1(\theta_y - \theta_{y_2})^2\right\} + \frac{1}{2}k_a y_a^2 + \frac{1}{2}k_b y_b^2 \\ &= \frac{1}{2}\alpha_1(x^2+y^2) + \gamma_1(x\theta_x + y\theta_y) + \frac{1}{2}\delta_1(\theta_x^2+\theta_y^2) \\ &\quad + \frac{1}{2}\alpha_1\left(\frac{a}{l}y_b + \frac{b}{l}y_a\right)^2 - \alpha_1 y\left(\frac{a}{l}y_b + \frac{b}{l}y_a\right) - \gamma_1 y\left(\frac{y_b - y_a}{l}\right) \\ &\quad - \gamma_1\theta_y\left(\frac{a}{l}y_b + \frac{b}{l}y_a\right) + \gamma_1\left(\frac{a}{l}y_b - \frac{b}{l}y_a\right)\left(\frac{y_b - y_a}{l}\right) \\ &\quad + \frac{1}{2}\delta_1\left(\frac{y_b - y_a}{l}\right)^2 - \delta_1\theta_y\left(\frac{y_b - y_a}{l}\right) + \frac{1}{2}(k_a y_a^2 + k_b y_b^2). \end{aligned} \tag{7. 2}$$

in which T is represented in Eq. (3. 20) and y_2 and θ_{y_2} will be

$$\left.\begin{aligned} y_2 &= \frac{a}{l}y_b + \frac{b}{l}y_a, \\ \theta_{y2} &= \frac{y_b - y_a}{l}. \end{aligned}\right\} \tag{7. 3}$$

Substituing Eq. (7. 1) and Eq. (7. 2) into Lagrange's equations, the equations of motion become

$$\left.\begin{aligned} &\ddot{\varphi} + \ddot{\psi} = \dot{\omega} = 0, \\ &m\ddot{x} + \alpha_1 x + \gamma_1\theta_x = me\omega^2\cos\omega t, \\ &m\ddot{y} + \alpha_1\left\{y - \left(\frac{a}{l}y_b + \frac{b}{l}y_a\right)\right\} + \gamma_1\left\{\theta_y - \left(\frac{y_b - y_a}{l}\right)\right\} = me\omega^2\sin\omega t, \\ &I\ddot{\theta}_x + 2I\omega\dot{\theta}_y + \delta_1\theta_x + \gamma_1 x = I\tau\omega^2\cos(\omega t + \beta), \\ &I\ddot{\theta}_y - 2I\omega\dot{\theta}_x + \delta_1\left\{\theta_y - \left(\frac{y_b - y_a}{l}\right)\right\} + \gamma_1\left\{y - \left(\frac{a}{l}y_b + \frac{b}{l}y_a\right)\right\} \\ &\qquad\qquad = I\tau\omega^2\sin(\omega t + \beta), \\ &\frac{m_a}{k_a}\ddot{y}_a + y_a + \frac{1}{k_a}\left(-\alpha_1\frac{b}{l} + \alpha_1\frac{b^2}{l^2} + \frac{2b}{l^2}\gamma_1 + \frac{\delta_1}{l^2}\right)y_a \\ &\quad + \frac{1}{k_a}\left(\alpha_1\frac{ab}{l^2} - \frac{\gamma_1}{l} - \frac{\delta_1}{l^2}\right)y_b + \frac{1}{k_a}\left(\frac{\gamma_1}{l} - \alpha_1\frac{a}{l}\right)y + \frac{1}{k_a}\left(-\gamma_1\frac{b}{l} + \frac{\delta_1}{l}\right)\theta_y = 0, \\ &\frac{m_b}{k_b}\ddot{y}_b + y_b + \frac{1}{k_b}\left(-\alpha_1\frac{a}{l} + \alpha_1\frac{a^2}{l^2} + \frac{2a}{l^2}\gamma_1 + \frac{\delta_1}{l^2}\right)y_b \\ &\quad + \frac{1}{k_b}\left(\alpha_1\frac{ab}{l^2} - \frac{\gamma_1}{l} - \frac{\delta_1}{l^2}\right)y_a - \frac{1}{k_b}\left(\frac{\gamma_1}{l} + \alpha_1\frac{b}{l}\right)y - \frac{1}{k_b}\left(\gamma_1\frac{a}{l} + \frac{\delta_1}{l}\right)\theta_y = 0. \end{aligned}\right\} \tag{7. 4}$$

As we have already remarked, since the stiffness of pedestals k_a and k_b are greater than the spring constants of shaft, then $1/k_a$, $1/k_b$, y_a and y_b are small compared with other quantities and we may neglect the terms of these products.

Consequently, from the 6th and 7th equations of Eqs. (7.4), we have

$$\left.\begin{aligned} y_a &= \frac{1}{k_a}\left\{\left(\alpha_1\frac{b}{l}-\frac{\gamma_1}{l}\right)y+\left(\gamma_1\frac{b}{l}-\frac{\delta_1}{l}\right)\theta_y\right\}, \\ y_b &= \frac{1}{k_b}\left\{\left(\alpha_1\frac{a}{l}-\frac{\gamma_1}{l}\right)y+\left(\gamma_1\frac{a}{l}+\frac{\delta_1}{l}\right)\theta_y\right\}. \end{aligned}\right\} \tag{7.5}$$

Eqs. (7.5) means that the terms of inertia forces of pedestals $\frac{m_a}{k_a}\times\ddot{y}_a$ and $\frac{m_b}{k_b}\times\ddot{y}_b$ become negligible and y_a, y_b are approximately evaluated by the relations of statics of Eqs. (7.5), provided that the approximation is possible, *i.e.*, the products of $1/k_a$, $1/k_b$, y_a and y_b are negligible.

We now insert y_a and y_b given by Eqs. (7.5) into Eqs. (7.4) and obtain the differential equations of motion of disc

$$\left.\begin{aligned} &m\ddot{x}+(\alpha+\Delta\alpha)x+(\gamma+\Delta\gamma)\theta_x=me\omega^2\cos\omega t, \\ &m\ddot{y}+(\alpha-\Delta\alpha)y+(\gamma-\Delta\gamma)\theta_y=me\omega^2\sin\omega t, \\ &I\ddot{\theta}_x+2I\omega\dot{\theta}_y+(\delta+\Delta\delta)\theta_x+(\gamma+\Delta\gamma)x=I\tau\omega^2\cos(\omega t+\beta), \\ &I\ddot{\theta}_y-2I\omega\dot{\theta}_x+(\delta-\Delta\delta)\theta_y+(\gamma-\Delta\gamma)y=I\tau\omega^2\sin(\omega t+\beta), \end{aligned}\right\} \tag{7.6}$$

in which we have introduced the quantities

$$\alpha_1=\alpha+\Delta\alpha,\qquad \gamma_1=\gamma+\Delta\gamma,\qquad \delta_1=\delta+\Delta\delta, \tag{7.7}$$

and

$$\left.\begin{aligned} 2\Delta\alpha &= \frac{1}{l^2}\left\{\alpha^2\left(\frac{a^2}{k_b}+\frac{b^2}{k_a}\right)+2\alpha\gamma\left(\frac{a}{k_b}-\frac{b}{k_a}\right)+\gamma^2\left(\frac{1}{k_a}+\frac{1}{k_b}\right)\right\}, \\ 2\Delta\gamma &= \frac{1}{l^2}\left\{\alpha\gamma\left(\frac{a^2}{k_b}+\frac{b^2}{k_a}\right)+(\alpha\delta+\gamma^2)\left(\frac{a}{k_b}-\frac{b}{k_a}\right)+\gamma\delta\left(\frac{1}{k_a}+\frac{1}{k_b}\right)\right\}, \\ 2\Delta\delta &= \frac{1}{l^2}\left\{\gamma^2\left(\frac{a^2}{k_b}+\frac{b^2}{k_a}\right)+2\gamma\delta\left(\frac{a}{k_b}-\frac{b}{k_a}\right)+\delta^2\left(\frac{1}{k_a}+\frac{1}{k_b}\right)\right\}. \end{aligned}\right\} \tag{7.8}$$

In the above equations, the differences of spring contants in x and y directions are represented by the terms of stiffness of pedestals k_a, k_b. Obviously Eqs. (7.6) coincide with Eqs. (6.1) and we have observed that the motions of the disc when the pedestals have flexibility are reduced to the vibrations explained in the previous section.

8. Experimental analysis of synchronous backward precession

It is easy to see from Eqs. (6.2), that the amplitudes of synchronous backward precession become larger as the differences in flexibilities of shaft $\Delta\alpha$, $\Delta\gamma$ and $\Delta\delta$ increase, *i.e.*, with the values of flexibility of pedestals $1/k_a$ and $1/k_b$ in Eq. (7.8) there is an increase in the magnitudes of the peaks at ω_{b_1} and ω_{b_2} where the resonance of $[-\omega]$ takes place.

In order to observe the effect of $1/k_a$ and $1/k_b$ on synchronous backward precession, two kinds of pedestals are used in experiments as shown in Fig. 13, one comparatively rigid, the other more flexible. Measuring the deflections at the top of pedestals, we find that the former has the stiffness of about 9.8×10^5 kg/cm, the latter 1.15×10^3 kg/cm in OB direction, and neither pedestal deflects in OA

direction. In Fig. 14 the amplitudes for two types of pedestals are plotted against the rotating speed ω. As shown, the amplitudes for the flexible pedestals in the critical speeds of synchronous backward precession ω_{b_1} and ω_{b_2} are larger than those for the rigid pedestals.

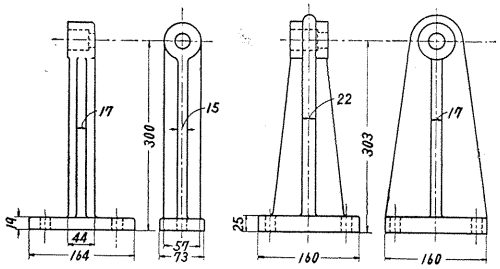

FIG. 13. Bearing pedestals.

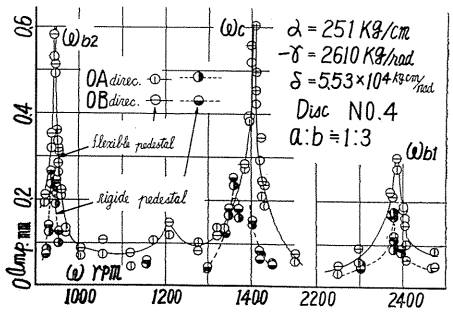

FIG. 14. Resonance diagrams.

These spring constants of Shaft No. 4 used in experiments shown in Fig. 14 are illustrated as follows:

OA direction	*OB* direction	mean values
$\alpha + \Delta\alpha = 2.70 \times 10^2$ kg/cm	$\alpha - \Delta\alpha = 2.31 \times 10^2$	$\alpha = 2.51 \times 10^2$
$-(\gamma + \Delta\gamma) = 2.72 \times 10^3$ kg/rad	$-(\gamma - \Delta\gamma) = 2.49 \times 10^3$	$-\gamma = 2.61 \times 10^3$
$\delta + \Delta\delta = 5.63 \times 10^4$ kg cm/rad	$\delta - \Delta\delta = 5.43 \times 10^4$	$\delta = 5.53 \times 10^4$

Reproduction of the oscillographic paper of synchronous backward precession $[-\omega]$ is given in Fig. 15. It is to be noted that in the mode of vibrations of synchronous forward precession $[+\omega]$, the phase angle between the rotating mark and the wave of vibration in x direction is the same angle as in y direction, as shown in Fig. 3, but in synchronous backward precession $[-\omega]$ there is the phase difference of 180 degrees between x and y directions, as we may observe in Fig. 15. In Fig. 16, we show that the waves of vibrations with amplitudes in x direc-

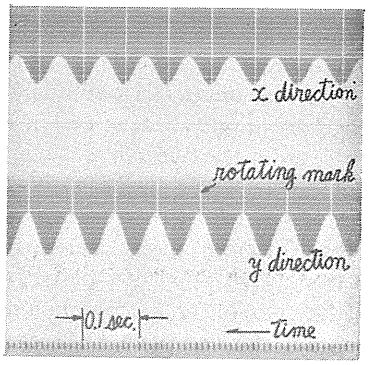

FIG. 15. Oscillographic paper of vibration of $[-\omega]$.

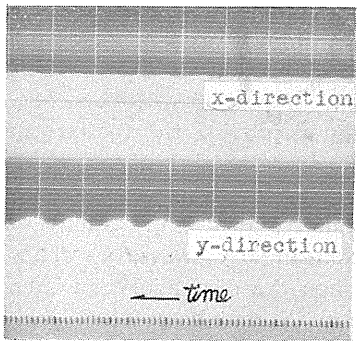

FIG. 16. Oscillographic paper of vibration of ∇.

tion are zero. Such waves appear in transient regions $[+\omega]$ to $[-\omega]$ and *vice versa*, and are represented by ▽ and ▼ in Figs. 8 and 9.

Now we show that even when the disc is mounted very tightly on the shaft, the critical speeds of synchronous backward precession can appear. Stodola[2] suggested that the synchronous backward precession would occur in the disc mounted loosely on shaft. However, for Disc No. 5 mounted very tightly on Shaft No. 11, the peaks of synchronous backward precession appear. As shown in Fig. 17, Shaft No. 11 and its hub of 66.2 ϕ on which Disc No. 5 is mounted tightly by the method of shrinkage fit, are made of one body. These experimental results are shown in Fig. 18 where the peak of $[-\omega]$ and the behavior of vibrations similar to that in Fig. 14 are still found. Thus the "loosely mounted disc" is not the cause of synchronous backward precession. Finally, we may conclude that the pedestals having different flexibilities cause the critical speeds of synchronous backward precession and that the amplitudes of $[-\omega]$ increase with this non-uniformity of rigidity of $\Delta\alpha$ etc..

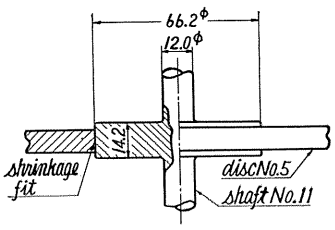

FIG. 17 (*left*). Hub of Shaft No. 11 and Disc No. 5.

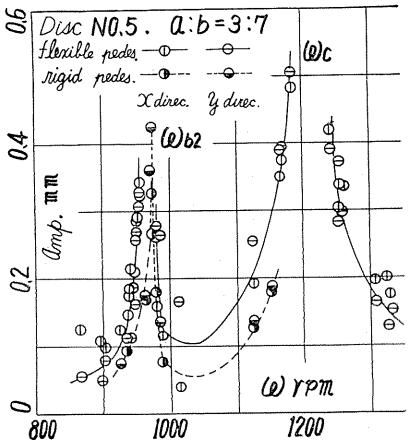

FIG. 18 (*right*). Resonance diagram of Disc No. 5 in the neighborhood of the critical speed ω_{b_2}.

9. Balancing to eliminate critical speeds of synchronous backward precession

In general, the balancing conditions in ω_{b_1} or ω_{b_2} are different from those in major critical speed ω_c and there is no remedy for complete balance but the simultaneous elimination of e and τ for the system in which $\Delta\alpha$ etc. exist. As shown in Fig. 19, (sections a and b), the balance at ω_c in section (a) is obviously better than that in section (b), however, the difference of amplitudes at ω_{b_2} in both is rather small proving the fact we have just mentioned. By two correction masses which lie in respective planes at right angles to the axis of rotation, it is theoretically possible, of course, that any rigid body can always be brought into a complete balancing state in which simultaneously both eccentricity e and deviational inclination angle τ are zero. The distance between two separate planes is also small when the disc thickness is small, so that the sensibility for balance may not be good and it may be practically impossible to obtain the complete balance. Then we are compelled to be satisfied with obtaining the balancing state in which e and τ cancel each other.

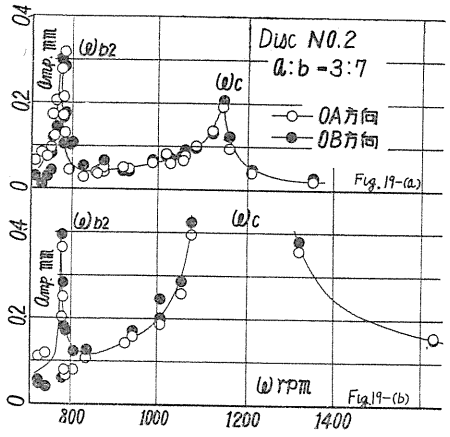

FIG. 19. Effects of balancing conditions in the major critical speed ω_c.

Moreover, another trouble develops in balancing synchronous backward precession. In the major critical speed ω_c, the conditions of balance of x and y are equal to those of θ_x and θ_y, and the balance of x, y, θ_x and θ_y can be made at the same time. On the other hand, in the critical speeds of synchronous backward precession ω_{b_1} and ω_{b_2}, as we see later, the conditions of balance of x and y are not equal to those of θ_x and θ_y and we cannot find the conditions by which the balance of x, y and θ_x, θ_y are satisfied at the same time, unless $\Delta\alpha$ etc. are zero.

In order to bring x and y into balance in the major critical speed, it is required that we make the sum of the 1st and 2nd terms in the right-hand side of the 1st or 2nd equation in Eqs. (6.2) equal to zero, that is,

$$\cos\beta = 1, \qquad me\omega^2(\delta + I\omega^2) = I\tau\omega^2\gamma. \tag{9. 1}$$

Similarly for θ_x and θ_y,

$$\cos\beta = 1, \qquad \tau\omega^2(\alpha - m\omega^2) = me\omega^2\gamma. \tag{9. 2}$$

As we have already remarked, the relation $(\alpha - m\omega^2)(\delta + I\omega^2) - \gamma^2 = 0$ is satisfied in the major critical speed ω_c and obviously the conditions of Eq. (9.1) are equivalent to those of Eq. (9.2). Consequently the balance of x, y and θ_x, θ_y is immediately carried out.

The conditions of balance at ω_{b_1} and ω_{b_2} are introduced by making the sum of the 3rd and 4th terms in the right-hand side of Eqs. (6.2) equal to zero, *i.e.*,

for x and y, $\quad \cos\beta = 1, \quad me\omega^2\gamma(A + 4\,\Delta\gamma \cdot I\omega^2) = I\tau\gamma B\omega^2,$ (9. 3)

for θ_x and θ_y, $\quad \cos\beta = 1, \quad I\tau\omega^2(\alpha - m\omega^2)B = me\omega^2(\alpha - m\omega^2)A,$ (9. 4)

in which we denote

$$\left.\begin{aligned} A &= 2\,\Delta\gamma\cdot\gamma^2(\alpha - m\omega^2)^{-1} - \Delta\delta\cdot\gamma - \Delta\alpha\cdot\gamma(\delta + I\omega^2)(\alpha - m\omega^2)^{-1}, \\ B &= \Delta\alpha\cdot\gamma^2(\alpha - m\omega^2)^{-1} + \Delta\delta(\alpha - m\omega^2) - 2\,\Delta\gamma\cdot\gamma. \end{aligned}\right\} \tag{9. 5}$$

In order that Eqs. (9.3) and (9.4) may be satisfied at the same time, the relation

$$meA = me(A + 4\,\Delta\gamma\cdot I\omega^2) \tag{9. 6}$$

is required. But Eq. (9.6) does not hold good unless $\Delta\alpha$ etc. and e are zero. Consequently we may conclude that it is very difficult to obtain the balance in ω_{b_1} and ω_{b_2} unless $\Delta\alpha$ etc. are zero, and that the best means to remove the critical speeds of synchronous backward precession is to adopt the rigid pedestals.

10. The locations of ω_{b_1} and ω_{a_2}

The values of ω_{b_1} and ω_{b_2} vary with the values of mass m, the moment of inertia of disc I, and the position of disc on shaft $a:b$ (Fig. 2). For the freely supported shaft, the spring constants may be represented as follows:[32]

$$\alpha = 3lB\frac{a^2-ab+b^2}{a^3b^3}, \quad \gamma = 3lB\frac{a-b}{a^2b^2}, \quad \delta = 3lB\frac{1}{ab}, \tag{10. 1}$$

in which $B=EI_0$, E is Young's modulus of shaft and I_0 is moment of inertia of the area of cross section of shaft. From Eqs. (3. 29), (6. 4) and (10. 1), we have

$$\frac{\omega_b^2}{\omega_c^2} = \frac{3(1-3a_1b_1)\Gamma+a_1^2b_1^2 \pm \sqrt{\{3(1-3a_1b_1)\Gamma-a_1^2b_1^2\}^2+12\Gamma a_1^2b_1^2(a_1-b_1)^2}}{3[3(1-3a_1b_1)\Gamma-a_1^2b_1^2+\sqrt{\{3(1-3a_1b_1)\Gamma+a_1^2b_1^2\}^2-4\Gamma a_1^2b_1^2(a_1-b_1)^2}]}, \tag{10. 2}$$

where $a_1=\frac{a}{l}$, $b_1=\frac{b}{l}$, $I=mk^2$, $\Gamma=\frac{k^2}{l^2}$, and Γ is the dimensionless quantity proportional to the square of radius of gyration of disc k, and ω_b is the notation representing either ω_{b1} or ω_{b_2}. For the fixed shaft, we have

$$\alpha = 12lB\frac{a^2-ab+b^2}{a^3b^3}, \quad \gamma = 6lB\frac{a-b}{a^2b^2}, \quad \delta = 4lB\frac{1}{ab}, \tag{10. 3}$$

and

$$\frac{\omega_b^2}{\omega_c^2} = \frac{9(1-3a_1b_1)\Gamma+a_1^2b_1^2 \pm \sqrt{\{9(1-3a_1b_1)\Gamma-a_1^2b_1^2\}^2+27\Gamma a_1^2b_1^2(a_1-b_1)^2}}{3[3(1-3a_1b_1)\Gamma-a_1^2b_1^2+\sqrt{\{3(1-3a_1b_1)\Gamma+a_1^2b_1^2\}^2-9\Gamma a_1^2b_1^2(a_1-b_1)^2}]}. \tag{10. 4}$$

The $\omega_b/\omega_c - a/l$ curves are shown in Fig. 20 for various values of Γ. The full lines are the curves for the freely supported shaft and the value of $\Gamma=0.0542$ corresponds to Disc No. 2. The dotted lines represent the curves for the fixed supported shaft mounting Disc No. 2 ($\Gamma=0.0542$). The circular marks plotted on Curve IV are obtained by experiments and it may be proved that a freely supported condition can be spproximately obtained by use of self-aligning double-row ball bearings. Clearly the curves in Fig. 20 are symmetrical with respect the straight line $a/l=0.5$. The behaviors of curves vary accordingly as Γ is larger or smaller than 1/12. For $\Gamma>1/12$, the lower critical speed of synchronous backward precession

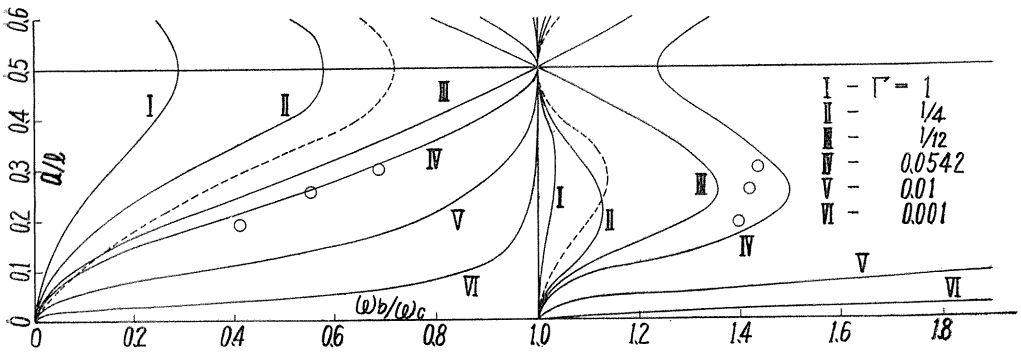

FIG. 20. Calculation diagram of $\omega_b/\omega_c - a/l$ curves.

ω_{b_2}/ω_c reaches a maximum value lower than unity at $a/l=0.5$, and decreases as the disc moves away from the middle point of shaft $a/l=0.5$. The higher critical speed ω_{b_1}/ω_c coincides with unity at $a/l=0$ and $a/l=0.5$, and for the intermediate value of a/l, it is higher than unity. For $\Gamma<1/12$ on the other hand, ω_{b_2}/ω_c has a maximum value of unity at $a/l=0.5$, and ω_{b_1}/ω_c has a maximum value at an intermediate position between $a/l=0$ and $a/l=0.5$, and ω_{b_1}/ω_c is equal to unity at $a/l=0$, and larger than unity at $a/l=0.5$.

Consequently ω_{b_2}/ω_c for $\Gamma<1/12$, and ω_{b_1}/ω_c for $\Gamma>1/12$ approach the value of unity as a/l approaches 0.5, so that in these cases the critical speeds of $[-\omega]$ approach the predominant major critical speed and a new phenomena take place with which we shall treat later.

From Fig. 20, we can easily see where the critical speeds of $[-\omega]$ occur.

For the fixed supported shaft, $\Gamma=1/36$ is the critical value of Γ changing the nature of $\omega_b/\omega_c-a/l$ curves.

11. The magnitudes of amplitudes of synchronous backward precession and the position of disc a : b

In this section we present the way in which the amplitudes of peaks of $[-\omega]$ in ω_{b_1} and ω_{b_2} change in their relation to the value of $a:b$. For this purpose it is useful to introduce the following new quantities:

$$\left.\begin{aligned}
x_e &= \frac{me\omega^2\{-\Delta\alpha(\delta+I\omega^2)(\delta-3I\omega^2)+2\Delta\gamma\cdot\gamma(\delta-I\omega^2)-\Delta\delta\cdot\gamma^2\}}{\{(\alpha-m\omega^2)(\delta+I\omega^2)-\gamma^2\}\{(\alpha-m\omega^2)(\delta-3I\omega^2)-\gamma^2\}},\\
x_\tau &= \frac{I\tau\omega^2[\Delta\alpha\cdot\gamma(\delta-3I\omega^2)+\Delta\delta\cdot\gamma(\alpha-m\omega^2)-\Delta\gamma\{\gamma^2+(\delta-3I\omega^2)(\alpha-m\omega^2)\}]}{\{(\alpha-m\omega^2)(\delta+I\omega^2)-\gamma^2\}\{(\alpha-m\omega^2)(\delta-3I\omega^2)-\gamma^2\}},\\
\theta_e &= \frac{me\omega^2[\Delta\alpha\cdot\gamma(\delta+I\omega^2)+\Delta\delta\cdot\gamma(\alpha-m\omega^2)-\Delta\gamma\{\gamma^2+(\delta+I\omega^2)(\alpha-m\omega^2)\}]}{\{(\alpha-m\omega^2)(\delta+I\omega^2)-\gamma^2\}\{(\alpha-m\omega^2)(\delta-3I\omega^2)-\gamma^2\}},\\
\theta_\tau &= \frac{I\tau\omega^2\{2\Delta\gamma\cdot\gamma(\alpha-m\omega^2)-\Delta\delta(\alpha-m\omega^2)^2-\Delta\alpha\cdot\gamma^2\}}{\{(\alpha-m\omega^2)(\delta+I\omega^2)-\gamma^2\}\{(\alpha-m\omega^2)(\delta-3I\omega^2)-\gamma^2\}}.
\end{aligned}\right\}\quad(11.1)$$

In Eqs. (6.2), we can interpret x_e, as the amplitude of deflection of shaft of the motion $[-\omega]$ due to the eccentricity e ; θ_e as the amplitude of inclination angle of disc of $[-\omega]$ due to e ; $x\tau$ as the amplitude of deflection of shaft of $[-\omega]$ due to the deviational angle τ, and θ_τ as the amplitude of inclination angle of $[-\omega]$ due to τ.

Now we calculate for the freely supported shaft the values of x_e, x_τ, θ_e and θ_τ at the rotating speed $\omega=\omega_b+\Delta\omega$ which deviates slightly from the critical speeds of ω_b. In our calculations $\omega_b+\Delta\omega$ replaces ω in Eqs. (11.1), insert Eq. (7.8) and Eq. (10.1) into Eqs. (11.1) making $k_a=k_b$ in Eqs. (7.8). By considering that ω_b satisfies Eq. (6.3), we develop the numerators and denominators in the right-hand side of Eqs. (11.1) in powers of $\Delta\omega$, and reject all but the linear terms in $\Delta\omega$; then we reach the following results.

$$
\left.\begin{aligned}
x_{e(\omega=\omega_b+\Delta\omega)} &= AB_1(a_1b_1)^{-9/2}\Big[(a_1^6+b_1^6)\Big(3a_1^2b_1^2+\frac{A}{2}\Big)\Big(a_1^2b_1^2-\frac{A}{2}\Big)+2a_1^3b_1^3\\
&\quad\times(a_1-b_1)(b_1^5-a_1^5)\Big(3a_1^2b_1^2-\frac{A}{2}\Big)+3a_1^4b_1^4(a_1^4+b_1^4)(a_1-b_1)^2\Big],\\
\theta_e\cdot k_{(\omega=\omega_b+\Delta\omega)} &= -AB_1\Gamma^{1/2}(a_1b_1)^{-7/2}\Big[(a_1^6+b_1^6)(a_1-b_1)\Big(3a_1^2b_1^2+\frac{A}{2}\Big)\\
&\quad+a_1^2b_1^2(a_1^4+b_1^4)(a_1-b_1)\Big\{3(1-3a_1b_1)-\frac{A}{2\Gamma}\Big\}+6a_1^2b_1^2(b_1^5-a_1^5)(a_1^2-b_1^2)\Big],\\
\frac{1}{k}x_{\tau(\omega=\omega_b+\Delta\omega)} &= -3BB_1\Gamma^{-1/2}(a_1b_1)^{-7/2}\Big[3(a_1^6+b_1^6)(a_1-b_1)\Big(a_1^2b_1^2-\frac{A}{2}\Big)\\
&\quad+a_1^2b_1^2(a_1^4+b_1^4)(a_1-b_1)\Big\{3(1-3a_1b_1)-\frac{A}{2\Gamma}\Big\}+6a_1^2b_1^2(b_1^5-a_1^5)(a_1-b_1)^2\Big],\\
\theta_{\tau(\omega=\omega_b+\Delta\omega)} &= BB_1(a_1b_1)^{-5/2}\Big[6(a_1-b_1)(b_1^5-a_1^5)\Big\{3(1-3a_1b_1)-\frac{A}{2\Gamma}\Big\}\\
&\quad+(a_1^4+b_1^4)\Big\{3(1-3a_1b_1)-\frac{A}{2\Gamma}\Big\}^2+9(a_1-b_1)^2(a_1^6+b_1^6)\Big],
\end{aligned}\right\}\quad(11.2)
$$

in which

$$
\left.\begin{aligned}
B_1 &= \Big[3a_1^2b_1^2(a_1-b_1)^2+\Gamma\Big\{3(1-3a_1b_1)-\frac{A}{2\Gamma}\Big\}^2\Big]^{-1}\cdot A^{-1/2},\\
A &= a_1^2b_1^2+3\Gamma(1-3a_1b_1)\pm\sqrt{\{a_1^2b_1^2-3\Gamma(1-3a_1b_1)\}^2+12\Gamma a_1^2b_1^2(a_1-b_1)^2},\\
A &= \frac{9\sqrt{2}\,B^{3/2}e}{16k_aI^{1/2}\Gamma^{1/2}\Delta\omega},\qquad B=\frac{3\sqrt{2}\,I^{1/2}B^{3/2}\tau}{16mk_aI^{11/2}\Delta\omega}.
\end{aligned}\right\}\quad(11.3)
$$

The positive sign before the radical in the right-hand side expression of A corresponds to ω_{b_1}, the negative sign to ω_{b_2}, and A and B are constants which are independent of the position of disc $a:b$. Since in the system with no damping force, the amplitudes of x_e etc. take infinite value at ω_b, we may reasonably introduce the following expressions as the quantities to show the magnifications of amplitudes in ω_b,

$$
X_e=\frac{x_{e(\omega=\omega_b)}}{x_{e\left(\substack{a_1=0.3\\ \omega=\omega_{b2}}\right)}}=\lim_{\Delta\omega\to0}\frac{x_{e(\omega=\omega_b+\Delta\omega)}}{x_{e\left(\substack{a_1=0.3\\ \omega=\omega_{b2}+\Delta\omega}\right)}}=\frac{x_{e(\omega=\omega_b+\Delta\omega)}}{x_{e\left(\substack{a_1=0.3\\ \omega=\omega_{b2}+\Delta\omega}\right)}},\qquad \Theta_e=\frac{\theta_e k_{(\omega=\omega_b)}}{x_{e\left(\substack{a_1=0.3\\ \omega=\omega_{b2}}\right)}}.\quad(11.4)
$$

The amplitudes x_e at ω_{b_2} for $a:b=3:7$ are taken as basis of comparison in the dimensionless quanties X_e etc. in the above equations. Obviously X_e etc. in Eq. (11.4) have decided definite values, and we may see how the amplitudes in ω_b change in accordance with the position of disc $a:b$. In Fig. 21, X_e etc. are plotted against $a_1=a/l$ for Disc No. 2 ($\Gamma=0.0542$). Suffixes 1 and 2 correspond to ω_{b_1} and ω_{b_2}, respectively. As shown in Fig. 21, x_{e_2}, x_{τ_2}, θ_{e_2} and θ_{τ_2} at the lower critical speed ω_{b_2} increase as a_1 approaches 0.5 and the predominant resonance can occur in ω_{b_2}. With $\Gamma<1/12$, however, as we have already shown in Fig. 20, ω_{b_2} also approaches ω_c as a_1 approaches 0.5, so that the superposition of the vibrations of $[-\omega]$ and $[+\omega]$ introduces new phenomenon with which we shall treat later. Fig. 21 shows that the amplitudes in ω_{b_1} are larger than those of ω_{b_2} as a_1 decreases. Actually the experimental results prove these facts, as shown in Fig. 22. For $a_1=0.19$ shown in Fig. 22, the amplitudes in ω_{b_1} are larger than those in ω_{b_2}, but for

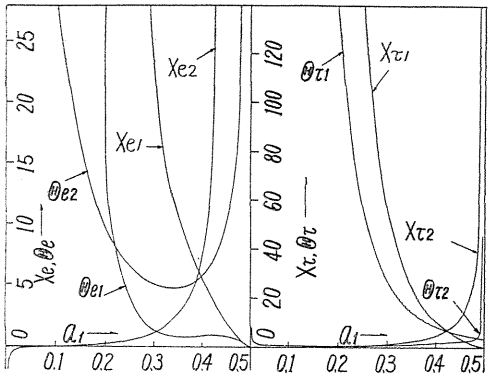

FIG. 21. Calculation curves of X_e, Θ_e, X_τ and Θ_τ.

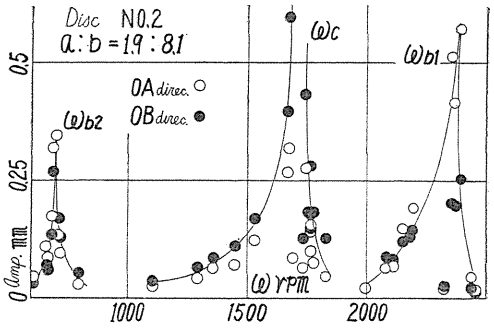

FIG. 22. Resonance diagram of Disc No. 2 ($a : b = 1.9 : 8.1$).

Disc No.	$a : b$	Max. amp. in ω_{b_1} (mm)	Max. amp. in ω_{b_2} (mm)	Max. amp. in ω_{b_1} / Max. amp. in ω_{b_2}
No. 1	3 : 7	0.20	0.715	0.280
No. 1	3 : 7	0.22	0.65	0.338
No. 2	3 : 7	0.08	0.45	0.178
No. 4	1 : 3	0.175	0.22	0.875
No. 2	1 : 3	0.185	0.19	0.975
No. 4	1 : 3	0.160	0.265	0.604
No. 2	1 : 4	0.57	0.345	1.65
No. 2	1 : 4	0.335	0.22	1.48

$a_1 = 0.256$ as shown in Figs. 8 and 9, the amplitudes in ω_{b_2} are larger than those in ω_{b_1}. The above table further confirms this, where the ratio of maximum amplitudes in ω_{b_1} and ω_{b_2} obtained by experiments are shown against various values of $a : b$.

Consequently, when the disc is mounted near the end of shaft, the higher critical speed ω_{b_1} increases in importance.

It is to be noted that since $\theta\tau_1$ is not zero for $\Gamma < 1/12$ and $a_1 = 0.5$, there is the resonance of inclination angle θ_x and θ_y of synchronous backward precession at a higher rotating speed than the major critical speed ω_c even in the simple system where one disc is mounted on the shaft at the middle point.

As shown in Fig. 20, when Γ (diameter of disc and moment of inertia I) is small, ω_{b_2} is almost equal to ω_c in wide range of a_1, then the resonance of peak in ω_{b_2} does not occur. In Fig. 23, we show the experimental results of Disc No. 6 having a comparatively small moment of inertia I. Obviously the peaks of $[-\omega]$ do not appear. As we have mentioned, ω_{b_1} for $\Gamma > 1/12$ and ω_{b_2} for $\Gamma < 1/12$ with $a_1 \fallingdotseq 0.5$ are nearly equal to ω_c and it may be feasible to treat this case by the following procedure. As we see in Eqs. (10.1) or (10.3), the spring constant γ is usually very small for $a \fallingdotseq b$, and γ may be assumed to be of the same small order as $\Delta\alpha$ ect. Rejecting the higher powers of small values in the 1st and 2nd equation in Eq. (6.2), we have

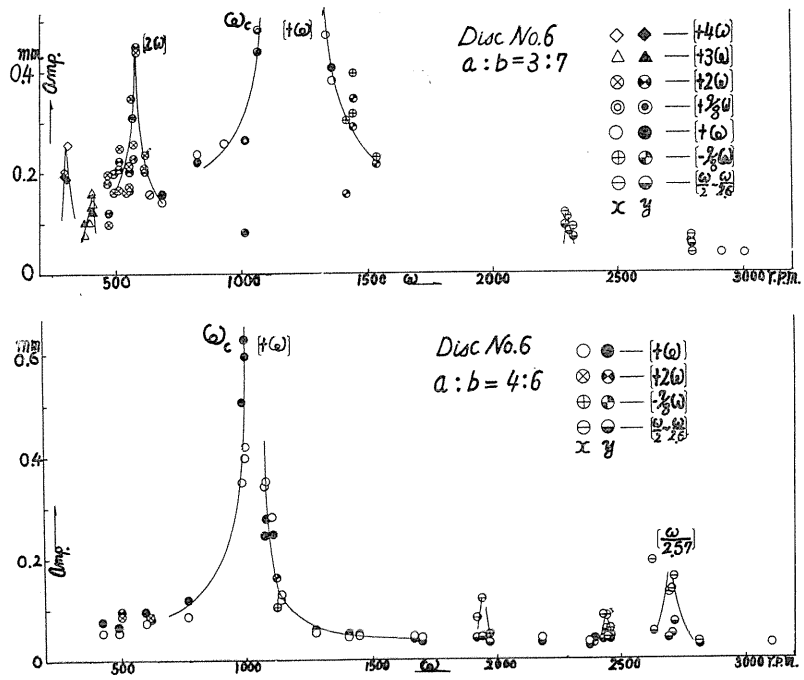

FIG. 23. Resonance diagram of Disc No. 6.

$$\left.\begin{aligned} x &\fallingdotseq \frac{me\omega^2}{\alpha - m\omega^2}\cos\omega t + \frac{-me\omega^2\Delta\alpha}{(\alpha - m\omega^2)^2}\cos\omega t \fallingdotseq \frac{me\omega^2}{(\alpha+\Delta\alpha) - m\omega^2}\cos\omega t, \\ y &\fallingdotseq \frac{me\omega^2}{(\alpha-\Delta\alpha) - m\omega^2}\sin\omega t, \end{aligned}\right\} \quad (11.\ 5)$$

and the critical speed in OA and OB directions are

$$\omega_{c_1} = \sqrt{\frac{\alpha+\Delta\alpha}{m}}, \qquad \omega_{c_2} = \sqrt{\frac{\alpha-\Delta\alpha}{m}}, \quad (11.\ 6)$$

respectively. The resonance curves are shown in Fig. 24. On the other hand, when γ is not very small, all terms in the right-hand side of Eqs. (6.2) include $\{(\alpha - m\omega^2)(\delta + I\omega^2) - \gamma^2\}$ which, changing its sign at ω_c, change all the signs in ω_c at the same time. Consequently the resonance curves in ω_c are represented as shown in Fig. 25 which is entirely different from Fig. 24.

As an example, the experimental results for $a : b = 4.5 : 5.5$ are shown in Fig. 26 and as previously mentioned, the peaks of synchronous backward precession do not appear.

In spite of the fact that we have obtained the response curves as shown in Fig. 24, we should point out that all coordinates coupled together usually have the identical natural frequencies as the coupled mechanical system, and the major critical speed and other resonance frequencies with respect to each coordinate have the same values. Hence even if γ is very small, ω_c, ω_{b_1} and ω_{b_2} in x-direction are not differnt when in y-direction, unless $\gamma = 0$ is held exactly. Therefore the differ-

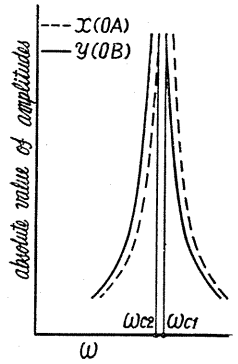

FIG. 24. Resonance curves in the neighborhood of the maior critical speed ω_c.

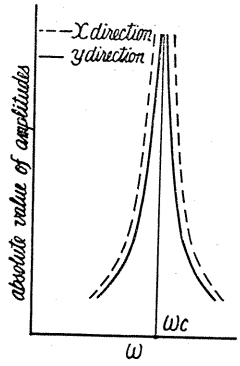

FIG. 25. Resonance curves in the neighborhood of the major critical speed ω_c.

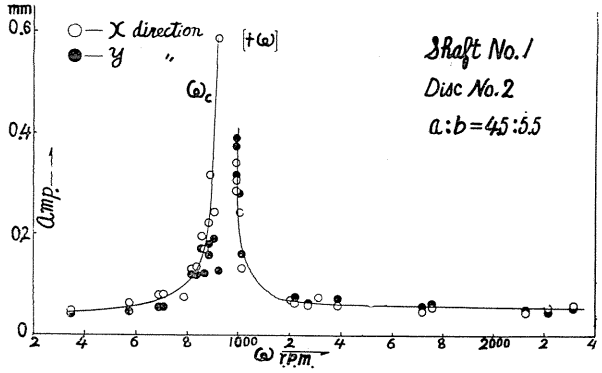

FIG. 26. Resonance curves in the neighborhood of the major critical speed of Shaft No. 1 ($a : b = 4.5 : 5.5$).

ence between ω_{c_1} and ω_{c_2} in Fig. 24 is only an apparent one due solely to superposing two kinds of vibrations $[+\omega]$ and $[-\omega]$, and in Fig. 24 or Eqs. (11.5) to treating them as one vibration. An analysis of these motions leads to identical critical speeds of ω_c and ω_b for x and y directions.

Summarizing, the resonance of synchronous backward precession can occur when the bearing pedestals deflect in OB direction and the shaft has unequal flexibility, provided $a \neq b$. In this chapter we discussed the nature of the vibrations of $[-\omega]$ due to the flexibility of bearing pedestals.

Chapter III. On the Critical Speeds of Shaft due to Ball Bearings

Part I. Vibrations of Forward Precession due to Ball Bearings[33) 49)]

12. *Preliminaries*

Obviously in the results of numerous experiments with various kinds of discs and shafts, we may find that vibrations of $\left[+\frac{\omega}{2.65}\right]$ and $\left[-\frac{\omega}{4.1}\right]$ take place at high

rotating speeds. For example, such vibrations are found in Figs. 8 and 9 indicated by ⊖, ◒ and □, ■. Owing to the difference in diameter of each ball in a bearing, these vibrations occur as covered in the present chapter. In Part I, the vibrations $\left[+\frac{\omega}{2.65}\right]$ are studied, and in Part II the vibrations of backward precession $\left[-\frac{\omega}{4.1}\right]$ are discussed.

13. Behavior of vibrations in resonant rotating speed

The critical speed of the vibrations $\left[+\frac{\omega}{2.65}\right]$ takes place in all cases in which various kinds of discs and shafts are used, and the value of $+\frac{1}{2.65}$ is universally constant. This fact suggests that the occurrence of this kind of vibration is not becaused of the discs and shafts themselves. The critical speed ω_a of mode of $\left[+\frac{\omega}{2.65}\right]$ always exists at a rotating speed higher than the major critical speed ω_c.

An example of the vibratory waves in this critical speed ω_a is shown in Fig. 27. The direction of whirl is found by combining the vibrations in the x- and the y-directions in Fig. 27. Observing the shapes of waves in Fig. 27, the motion of disc center M must be represented as follows:

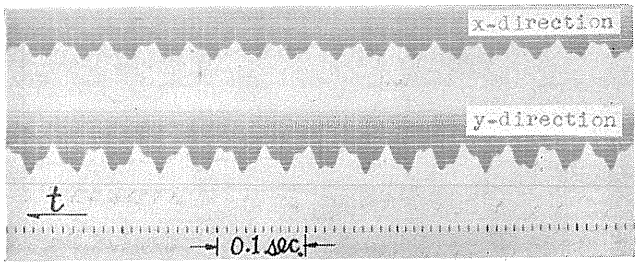

FIG. 27. Oscillographic paper of vibration of $[+\omega_1]$.

$$\left.\begin{aligned} x &= A\cos\omega t + B\cos\alpha_1\omega t, \\ y &= A\sin\omega t + B\sin\alpha_1\omega t, \qquad (A>0,\ B>0) \end{aligned}\right\} \quad (13.1)$$

i.e., the motion is composed of two vibrations the periods of which are $2\pi/\omega$ and $2\pi/\alpha_1\omega$. When self-aligning double-row ball bearings 10 ϕ are used, the value of α_1 is about $+\frac{1}{2.65}$ as just mentioned, and because α_1 takes a positive value, the locus of disc center M in the xy-plane is obviously epitrochoid, plainly showed in Eqs. (13.1). An example of such a locus obtained from the recording oscillographic paper is shown in Fig. 28 where the interval from circular mark to the next mark means one revolution of shaft, and the curve shown there is the locus on which the disc center M moves during the time interval of 8 revolutions of shaft. The direction of rotation of shaft is anti-clockwise in the figure. In the region about this critical speed ω_a, the amplitudes A in Eqs. (13.1) are unchanged and the amplitudes B alone increase and form the critical speed ω_a. This fact is shown in Fig. 29. Separating the amplitudes A and B by analyzing the vibratory waves

on oscillographic paper, these amplitudes are plotted against the rotating speed ω in Fig. 29. For comparison, the peak of the major critical speed is shown additionally. Considering that the amplitudes A are almost unchanged in the neighborhood of the critical speed ω_a, amplitudes B in ω_a or closely thereto must be remarkably larger than A, so that the locus of disc center M may form the figure shown in Fig. 30 or a similar one. On the other hand, the rotating speed ω deviates slightly from ω_a and since the difference between A and B is not very large, the path of whirl forms the figure shown in Fig. 31 or one like it. Figs. 30 and 31 are the geometrical figures obtained from Eqs. (13.1), putting $\alpha_1 = +\frac{1}{2.65}$, the circular marks showing the interval of rotation of shaft, as in Fig. 28.

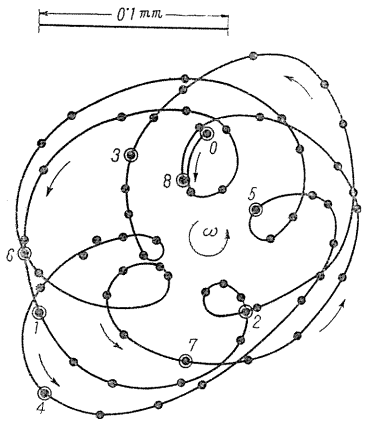

FIG. 28. Path of whirl in vibration of $[+\omega_1]$.

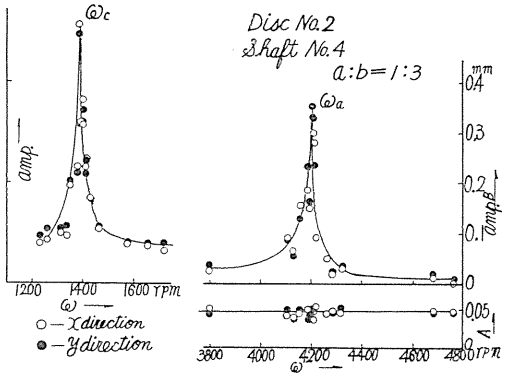

FIG. 29. Resonance curve in the neighborhood of the critical speed ω_a.

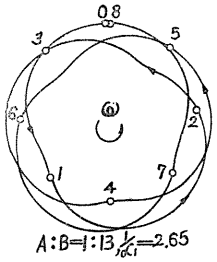

FIG. 30. Geometrical figure of epitrochoid. ($A : B = 1 : 13$, $1/\alpha_1 = 2.65$.)

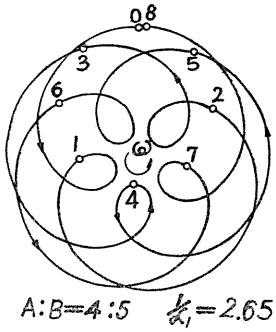

FIG. 31. Geometrical figure of epitrochoid. ($A : B = 4 : 5$, $1/\alpha_1 = 2.65$.)

14. Motion of steel balls in a ball bearing

Observing the motion of steel balls in a bearing during the rotation of shaft, we may clear up, at least partially, the cause of occurrence of the critical speed with which we will treat presently.

As a general rule, the motion of the balls is carried out under circumstances in which the rolling contact is kept between balls and inner and outer rings. Studying the motion of rollers in a roller bearing, it is concluded that as far as precessional motion of rollers is concerned (motion of roller center around the center of inner ring), that rule is held rigorously, independant of the conditions of load, rotating speed and lubrication.[34] In the self-aligning double-row ball bearings used in our experiments, the motion of balls was somewhat complicated in comparison to that of rollers in roller bearings with their more simple bearing construction. However by the following experiment, it can be proved that steel balls rotate around the center of the inner ring in their rolling contact, in self-aligning double-row ball bearing as well as in roller bearings.

As shown in Fig. 32, a piece of thin steel plate is soldered on the outside of the retainer of one ball bearing, held in such a way so that the steel plate does not touch the balls and outer ring, during rotation of shaft. Rotating at the same speed as the precessional motion of the balls, the piece of steel plate interrupts the light at each revolution of the retainer and a record is made of precessional rotation of balls ω_1 on oscillographic paper. The values thus obtained of ratio of precessional revolutions to revolutions of the shaft ω are plotted against ω between 100 r.p.m. and 4,100 r.p.m. in Fig. 33. The mean value of ω/ω_1 in Fig. 33 is $+2.647$. The diameter D of inner ring is $14.72\,\phi$ when measured by micrometer microscope at the bottom of groove (see Fig. 32), and by the reading of ortho-tester, diameter of steel ball is $d=4.673\,\phi$. Assuming that the motion of steel balls is made in the state of rolling contact, obviously the following relation is obtained,

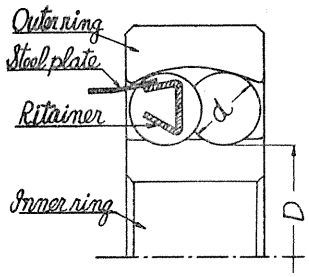

FIG. 32. Self-aligning double-row ball bearing.

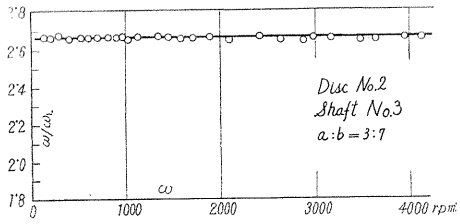

FIG. 33. Diagram of the precessional angular velocity of ball ω_1 obtained by experiments ($\omega/\omega_1-\omega$ curve).

$$\frac{\omega}{\omega_1}=2+2\frac{d}{D}. \tag{14. 1}$$

Inserting the values of D and d shown above in Eq. (14.1), $\omega/\omega_1=+2.647$ is obtained, and this value agrees accurately with the result of experiments. Therefore even in self-aligning double-row ball bearings used in our experiments, it may be concluded that the precessional revolution ω_1 of balls is constant, independent of rotating speed ω, amplitudes and load. Even with the same kind of ball bearings, when individually compared, there will be found between them small variations of D and d in dimensions, and small differences in the value of ω/ω_1. Furthermore the magnitudes of ω/ω_1 may be affected according to whether the shaft is arranged horizontally or vertically, and whether the radial clearance is small or large. But

by numerous experiments under various circumstances, the deviation of ω/ω_1 is found to be very small.

Now we should note that the value of α_1 in Eqs. (13.1) obtained by analyzing the shapes of vibratory waves on the oscillographic papers agrees with ω_1/ω, *i.e.*,

$$\alpha_1 = \omega_1/\omega, \qquad \alpha_1\omega = \omega_1. \tag{14. 2}$$

Consequently the vibrations of shaft in the critical speed ω_a have the same frequencies as the precessional revolution of balls ω_1.

15. Difference in diameter between each ball in a bearing

As our next step, we should inquire into the reasons why the vibrations of mode of $[\omega_1 = \alpha_1\omega]$ predominate and why the critical speed ω_a occurs in the specific rotating speed ω.

If we assume that the periodic disturbing force having the circular frequency ω_1 is applied to this vibratory system, there is the possible occurrence of the critical speed ω_a having the mode of vibration $[\omega_1]$. By experiment it is ascertain that when there is a difference in the diameter of each ball inserted in one bearing, there is such a disturbing force exerted on the disc and the occurrence of the critical speed ω_a becomes possible. Errors in dimensions of inner and outer rings do not cause the disturbance having the same frequency as that of the precessional angular velocity of balls ω_1. However accurate the inner and outer rings may be, if there is any difference in the diameters of the balls, the center line of the journal of the shaft does not coincide accurately with the bearing center line. When one comparatively large ball is inserted into the bearing, the inner ring is displaced by this larger ball and the ring is forced off center toward the opposite side of the bearing along the diameter in which the larger ball lies. If a ball smaller than the others is inserted in the bearing, the inner ring is forced toward the smaller ball and the opposite side of the bearing is pushed off center along the diameter toward the smaller ball. Therefore owing to this small eccentricity e_0 of inner ring, the center of disc M is also deviated from the bearing center line as shown in Fig. 34. The magnitude of the deviation of disc center M is represented by e_1 and is decided according to e_0 and $a : b$, as shown in Fig. 34.

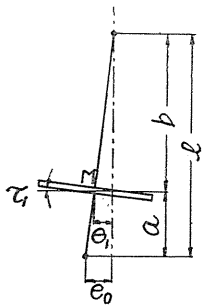

FIG. 34. e_1 and τ_1.

The direction of the deviation e_1 due to the difference in the diameter of the balls rotates with the same velocity as the precessional rotating speed of balls ω_1. Briefly described, the shaft is supported on its ends by the eccentric wheels which rotate at angular velocity ω_1. Under such conditions the periodic disturbing force having circular frequency ω_1 is applied to the disc and the forced vibration of $[\omega_1]$ is induced, thus the critical speed ω_a of $\left[+\frac{\omega}{2.65}\right]$ appears.

16. Differential equations of motion

As shown in Fig. 34, we denote e_1 and τ_1 to be the eccentricity and the inclination angle due to the differences in ball diameters. Then the kinetic energy T of this system is still represented as shown in Eq. (3.20) but the potential energy V is modified as follows:

$$V=\frac{1}{2}\alpha\{(x-e_1\cos\omega_1 t)^2+(y-e_1\sin\omega_1 t)^2\}+\gamma\{(x-e_1\cos\omega_1 t)(\theta_x-\tau_1\cos\omega_1 t)+(y-e_1\sin\omega_1 t)(\theta_y-\tau_1\sin\omega_1 t)\}+\frac{1}{2}\delta\{(\theta_x-\tau_1\cos\omega_1 t)^2+(\theta_y-\tau_1\sin\omega_1 t)^2\} \tag{16. 1}$$

Substituting Eq. (3. 20) and Eq. (16. 1) into Lagrange's equations and considering $\Theta=\omega t+\frac{\pi}{2}+\beta$ the equations of motion are obtained as follows:

$$\left.\begin{aligned} &m\ddot{x}+\alpha x+\gamma\theta_x=me\omega^2\cos\omega t+(\alpha e_1+\gamma\tau_1)\cos\omega_1 t,\\ &m\ddot{y}+\alpha y+\gamma\theta_y=me\omega^2\sin\omega t+(\alpha e_1+\gamma\tau_1)\sin\omega_1 t,\\ &I\ddot{\theta}_x+I_p\omega\dot{\theta}_y+\delta\theta_x+\gamma x=(I_p-I)\tau\omega^2\cos(\omega t+\beta)+(\gamma e_1+\delta\tau_1)\cos\omega_1 t,\\ &I\ddot{\theta}_y-I_p\omega\dot{\theta}_x+\delta\theta_y+\gamma y=(I_p-I)\tau\omega^2\sin(\omega t+\beta)+(\gamma e_1+\delta\tau_1)\sin\omega_1 t. \end{aligned}\right\} \tag{16 .2}$$

When the disc is mounted at the middle point of the shaft ($a=b$), Eq. (16. 2) is simplified and we have

$$\left.\begin{aligned} &m\ddot{x}+\alpha x=me\omega^2\cos\omega t+\alpha e_1\cos\omega_1 t,\\ &m\ddot{y}+\alpha y=me\omega^2\sin\omega t+\alpha e_1\sin\omega_1 t. \end{aligned}\right\} \tag{16. 3}$$

Because the periodic disturbing forces with period $2\pi/\omega_1$ are contained in the right-hand side of Eqs. (16.2) and (16.3), the peak of the amplitudes are formed at the rotating speed ω_a in which ω_1 coincides with the natural frequencies of this system.

Since the critical speed ω_a of $\left[+\frac{\omega}{2.65}\right]$ always occurs at speeds higher than the major critical speed ω_c, the rotation of the disc must pass through ω_c in order to make possible any experiment in ω_a. Consequently, if there is a large eccentricity, the shaft invariably breaks, so that the disc must always be brought into some degree of balance. In our experiments, the eccentricity usually remained in an unbalanced state of about 0.01 mm. As we see by Figs. 8, 9 and 29, the major critical speed still predominates under such a state of unbalance. Though the magnitude of deviation of disc center e_1 is varied according to circumstances, it is about 1~10 μ. Consequently while the amplitude of the critical speed of ω_a is smaller than that in the major critical speed, the peak may still be remarkable considering the magnitude of e_1. The forced vibrations given as the particular solutions of Eq. (16.2) become:

$$\left.\begin{aligned} x=&\frac{me\omega^2(\delta-I\omega^2+I_p\omega^2)\cos\omega t-\gamma(I_p-I)\tau\omega^2\cos(\omega t+\beta)}{(\alpha-m\omega^2)(\delta-I\omega^2+I_p\omega^2)-\gamma^2}\\ &+\frac{(\alpha e_1+\gamma\tau_1)(\delta-I\omega_1^2+I_p\omega\omega_1)-(\gamma e_1+\delta\tau_1)\gamma}{(\alpha-m\omega_1^2)(\delta-I\omega_1^2+I_p\omega\omega_1)-\gamma^2}\cos\omega_1 t,\\ \theta_x=&\frac{-me\omega^2\gamma\cos\omega t+(I_p-I)\tau\omega^2(\alpha-m\omega^2)\cos(\omega t+\beta)}{(\alpha-m\omega^2)(\delta-I\omega^2+I_p\omega^2)-\gamma^2}\\ &+\frac{(\gamma e_1+\delta\tau_1)(\alpha-m\omega_1^2)-(\alpha e_1+\gamma\tau_1)\gamma}{(\alpha-m\omega_1^2)(\delta-I\omega_1^2+I_p\omega\omega_1)-\gamma^2}\cos\omega_1 t. \end{aligned}\right\} \tag{16. 4}$$

Putting sin in place of cos in the above equations, the solutions for y and θ_y are obtained. The 1st terms in the right-hand side of Eqs. (16.4) represent the

amplitudes A in Eqs. (13.1), and the 2nd terms in the right-hand side of Eqs. (16.4) represent the amplitudes B in Eqs. (13.1). The critical speed ω_a is formed by increase of amplitudes B, suggesting that the denominatior becomes small in the neighborhood of ω_a in the 2nd term in the right-hand side in Eqs. (16.4).

17. The difference of diameter between each ball and the magnitudes of amplitudes

As we see in Eqs. (16.2), (16.3) and (16.4), the amplitudes of vibrations of $\left[+\frac{\omega}{2.65}\right]$ increase as the magnitudes of e_1 and τ_1 increase. The values of e_1 and τ_1, when there is the same difference in diameters, may vary accordingly as the following conditions exist: the shaft equipped horizontally or vertically, there is a combination of ball bearings at both ends of the shaft, to the order of arrangement of balls in a bearing, the magnitude of radial clearance, and the position of disc $a : b$. In Fig. 35, the arrangement of balls used in our experiments is shown. This self-aligning double-row ball bearing contains 18 balls, having 9 balls each in one row. For instance, supposing that two of the balls are somewhat larger than the others and that these two large balls are inserted in the symmetrical position shown 1 and 5′, Fig. 35, both e_1 and τ_1 being very small. On the other hand, supporsing that the two large balls are put side-by-side as 1 and 1′, then e_1 and τ_1 become larger. Furthermore, when the disc is not mounted at the middle point of shaft but is one-sided toward either upper or lower bearing pedestal, *i.e.*, $a \neq b$, the bearing nearer the disc exerts more influence upon e_1 and τ_1, and the other bearing less.

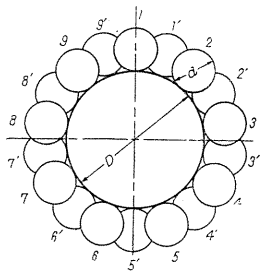

FIG. 35 (*left*). Arrangement of balls in self-aligning double-row ball bearing.

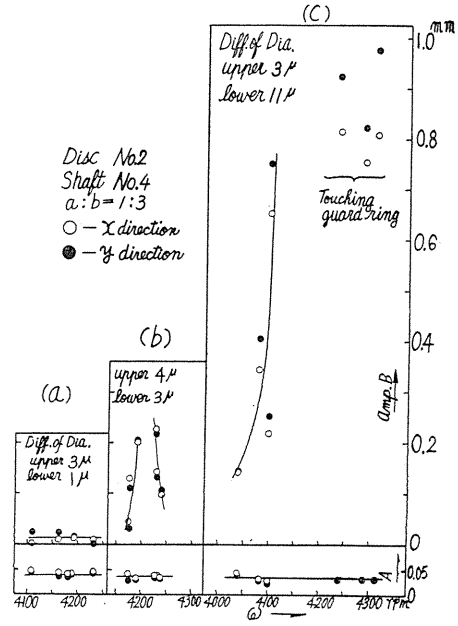

FIG. 36 (*right*). Effects of difference in diameter of balls.

It may be observed in the experiments shown in Fig. 36, how the amplitudes of vibrations of $\left[+\frac{\omega}{2.65}\right]$ vary with the difference in diameters of the balls. In

this figure, because the position of disc $a : b$ is 1 : 3, the influence of the ball bearing on the lower pedestal is three times greater than that on the upper pedestal. In Figs. 36 a, 36 b and 36 c, all conditions are unchanged except the differences in diameters of balls. In Figs. 36 a and 36 b, commercial ball bearings purchased on the market were used. In Fig. 36 c, the difference in diameters of balls in the lower bearing is artificially enlarged. In Fig. 36 c, two balls of 4.768ϕ with diameters larger by 11 μ than those of the others were inserted side-by-side into a ball bearing in which there were balls of $d = 4.757\phi$, as shown in 1 and 1′, Fig. 35. Therefore, the amplitudes of the peak ω_a greatly increase and build up so large that the shaft touches the guard ring which is there to check the increase of deflections of shaft. In Fig. 36 the amplitudes A of vibrations of $[+\omega]$ are almost unchanged, as we have already mentioned. We can see in Fig. 36 that the amplitudes of vibrations of $\left[+\frac{\omega}{2.65}\right]$ increase with the magnitude of differences in diameters of balls. Results of numerous experiments show that in all cases where ball bearings on the market are used, the critical speed ω_a always appears in which irrespective of the magnitudes of amplitudes; the cases in which it does not appear are the few exceptions. In the following table we give the standards of JIS for steel balls in ball bearings with diameters within the limits of 1/16″–11/16″.

The difference between the max. and min. diameters of one ball			The difference of dia. between each ball inserted in one bearing		
Class 1	Class 2	Class 3	Class 1	Class 2	Class 3
0.5 μ	1.0 μ	1.5 μ	0.8 μ	1.5 μ	2.5 μ

By actual measurement, not all ball bearings on the market are within the above tolerances. Furthermore it seems that wear through use to some extent increases the differences in diameters.

18. *The location of the critical speed* ω_a *of* $\left[+\frac{\omega}{2.65}\right]$

Equating the denominator of the 2nd term in the right-hand side of Eq. (16.4) to zero and considering $\omega_1 = \alpha_1\omega$, we have

$$(\alpha - m\omega_1^2)(\delta - I\omega_1^2 + I_p\omega\omega_1) - \gamma^2 = (\alpha - \alpha_1^2 m\omega^2) \times (\delta - \alpha_1^2 I\omega^2 + \alpha_1 I_p\omega^2) - \gamma^2 = 0. \qquad (18.1)$$

Solving the above equation with respect to ω^2, the critical speed of $\left[+\frac{\omega}{2.65}\right]$ is obtained as follows:

$$\omega_a^2 = \frac{\{\alpha(I_p - \alpha_1 I) - \alpha_1\delta m\} \pm \sqrt{\{\alpha(I_p - \alpha_1 I) + \alpha_1\delta m\}^2 - 4\alpha_1 m(I_p - \alpha_1 I)\gamma^2}}{2\alpha_1^2 m(I_p - \alpha_1 I)}. \qquad (18.2)$$

Putting $\alpha_1 = 1$ in the above equation, the result coincides with Eq. (3.29) which gives the major critical speed ω_c. Considering only $\alpha\delta - \gamma^2 > 0$ and $\alpha_1 < 1$, the positive sign before the radical in Eq. (18.2) should be adopted and the critical speed of ω_a is unique. In Fig. 7 or Fig. 37, as we proved in Section 3, the straight line $p = \omega$ cuts Curve II at only one point, A; then the line $p = \alpha_1\omega$ ($\alpha_1 < 1$) ob-

viously cannot intersect Curve I having only one intersecting point B, on Curve II. From this standpoint, it is also readily understood that the critical speed of ω_a is unique. In Fig. 37 the abscissa of point B on Curve II gives the critical speed ω_a coinciding with the value obtained from Eq. (18.2). Because the natural frequency p is constant when the disc is located at the middle point of shaft, the ratio ω_a/ω is equal to $1/\alpha_1$ and for a disc not so located (*i.e.*, $a \neq b$), ω_a is situated at a comparatively higher rotating speed of shaft and the relation $\omega_a/\omega_c > 1/\alpha_1$ always holds good. This inclination becomes more marked as the disc approaches the end of shaft and this fact can be proved by Eq. (18.2), representing the spring constants α, γ and δ as functions of a and b. By results of experiments on several kinds of shafts shown in the following table, this tendency is obvious.

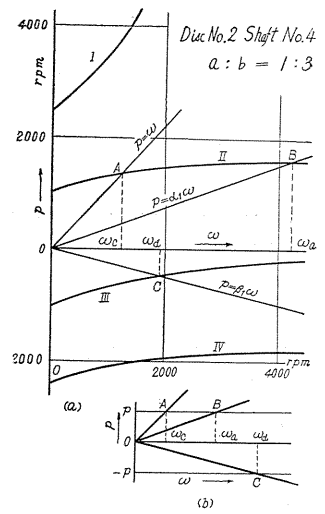

FIG. 37. Calculation diagram of $\omega - p$ curves and the location of ω_a and ω_d.

The location of disc $a : b$	1 : 1	1 : 2.33	1 : 3
ω_a/ω_c	2.665	2.860	3.036

In these experiments, Disc No. 2 was used. When a ball bearing with a fixed inner ring is used, the equation corresponding to Eq. (14.1) becomes

$$\frac{\omega}{\omega_1} = 1 + \frac{D}{D+2d}. \tag{18.3}$$

For self-aligning double-row ball bearings used in our experiments $\omega/\omega_1 = 1/\alpha_1 \fallingdotseq 1.612$ is obtained from the above equation. Thus for the fixed inner ring the critical speed ω_a reduces to a lower rotating speed of shaft as compared with that of a fixed outer ring. As is readily seen from Eqs. (14.1) and (18.3), when the fixed outer ring is used ω/ω_1 is always larger than 2 and when the fixed inner ring is used, ω/ω_1 is smaller than 2. For the thrust ball bearing, ω/ω_1 takes the value of 2, which is the critical value for these two cases.

The radial single-row ball bearing with deep groove is most widely used. This type of ball bearing with 10 ϕ bore (bearing number $\neq$ 6,200) was used in our experiments. The diameter of ball d is 5.501 ϕ, the diameter of the inner ring at the bottom of the deep groove is 14.23 ϕ, and then ω/ω_1 or $1/\alpha_1$ has a value of 2.773 from Eq. (14.1). Diameters D and d are shown in Fig. 38. An example of oscillographic paper obtained in the experiment using this type of ball bearing, is shown in Fig. 39. Observing the shapes of vibratory waves on oscillographic paper, we obtain $1/\alpha_1 = 25/9 = 2.778$. This value agrees with that obtained by Eq. (14.1) as mentioned above.

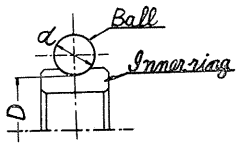

FIG. 38. Single-row radial ball bearing.

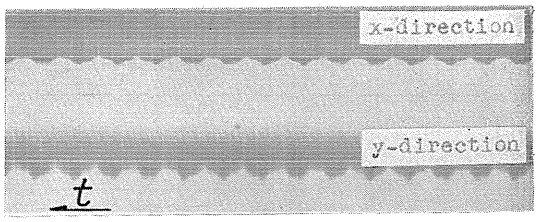

FIG. 39. Oscillographic paper of vibration $[+\omega_1]$ for single-row radial ball bearing.

Summarizing, the difference in diameters between each ball in a bearing causes the critical speed of ω_a which has the following natures:

1. The peculiar mode of vibration decided by the dimensions of ball bearing
2. Occurring at the solitary revolution ω_a
3. Appearing at a speed higher than the major critical speed ω_c
4. As the difference of diameter increases, the amplitudes become larger.

This kind of vibration necessarily comes into question for the shaft rotating at high speeds where quiet operation is demanded. For example, in the spindle of internal grinders and the spinning spindle.

In addition, it is to be noted that when several kinds of ball or roller bearings are equipped on a shaft, individual critical speeds of many kinds appear and the circumstances become more troublesome. Counter-measures for this vibration may be self-evident by what has been described.

Since the sensibility of occurrence of the peak of the critical speed ω_a is remarkably large even in the simple apparatus as shown in Figs. 1 and 2, a testing machine may perhaps be devised for measuring the accuracy of ball bearings by observing the magnitude of amplitudes of vibrations of $[\alpha_1\omega]$ at the critical speed.

Part II. Vibrations of Backward Precession due to Ball Bearings[35)-49)]

19. Introduction

We have stated in Part I that the vibrations $[\alpha_1\omega]$ can occur in the shaft supported by ball bearings. In Part II we treat with those vibrations which have the mode of vibrations $\left[-\frac{\omega}{4.1}\right]$ as we treated the vibrations $[\alpha_1\omega]$ due to the difference in diameters of each ball. Though the amplitudes of vibrations $\left[-\frac{\omega}{4.1}\right]$ are usually smaller than those of $[\alpha_1\omega]$, they build up considerably under certain circumstances. It is somewhat difficult to state clearly the causes of the occurrence of these vibrations. In Part II we intend to clear up the reasons for these vibrations and to investigate their behavior.

20. The relation between stiffness of shaft and difference in diameters of balls

In ball bearings the radial clearance is usually provided by increased temperatures during operation. If there is a difference in diameter of the balls, this radial clearance becomes smaller or it may entirely disappear, or the interference between balls and inner and outer rings may occur in the position in which the larger ball is inserted. Consequently when the stiffness of shaft is considered together with

the ball bearings, the stiffness increases slightly at that position and the shaft is never equally stiff in all directions. Obviously this non-uniformity of stiffness of shaft rotates with an angular velocity of ω_1 which is the precessional rotating speed of balls around the center of inner ring. Therefore the difference in diameters of balls causes the shaft to have the directional non-uniformity of stiffness with angular velocity ω_1. According to thoretical and experimental results, it may be concluded that such a rotating directional character of rigidity of shaft makes the disc vibrate with the peculiar mode of vibration which will be treated with presently. Bearings on the market with balls having various diameters within the prescribed tolerance are inserted at random without considering the order of arrangement. But the magnitude of the difference in stiffness of shaft in all directions can not be explained only by the difference in diameters of balls without considering the order of arrangement of balls. The existence of radial clearance in ball bearings induces the nonlinear spring force which causes the new phenomena not appearing in the linear system.

As just mentioned, the condition is complicated under which the directional difference of stiffness in shaft exists. For example, if there is, to some extent, radial clearance in all directions, the spring force can be represented by the broken line $ABCD$ in Fig. 40 or another similar line, and if a ball somewhat larger is inserted and interference occurs at that point, the character of restoring force can be shown by the straight line AOB in Fig. 40. Under certain circumstances the stiffness may indicate a behavior of an intermediary character between those of the above two cases, as shown by the dotted line in Fig. 40. Although some complex nature may exhibit itself in the spring force, we must consider that since the radial clearance is in general very small, the restoring force has approximately the linear character, and the stiffness where the larger ball is inserted is to some extent more rigid than that in other directions, because the shaft is supported more tightly by the larger ball.

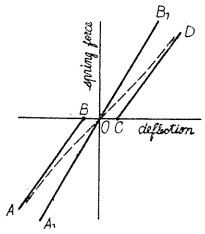

FIG. 40. Characteristics of spring forces.

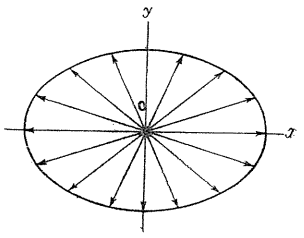

FIG. 41. Vectors representing spring forces.

Now we consider Fig. 41 which is obtained by connecting the tops of vectors representing all directions of the stiffness of shaft. This figure is symmetrical in shape with respect to the origin O as shown in Fig. 41, except under special circumstances. We cannot assume simply that the direction of maximum stiffness is at right angles to the direction of minimum stiffness as shown in Fig. 41, and it may be considered that in general the figure will be more complicated than as shown in Fig. 41 depending upon the order of arrangement of balls. In most cases the figure will resemble Fig. 41 in shape for reasons given later.

21. The equations of motion

For the stiffness of the shaft which is influenced by the differences in diameters of the balls mentioned in the preceding section, the following treatment may be the simplest and most plausible. We assume the character of stiffness of shaft to be of liner type and the angle between the angular positions of the maximum and minimum stiffness to be a right angle. In Fig. 42, let the center of ball bearing be point o and o-x_1y_1 be a rotating rectangular coordinate system revolving with the precessional angular velocity of balls ω_1. Now we assume that the minimum and the maximum stiffness represented by $\alpha-\Delta\alpha$ and $\alpha+\Delta\alpha$, respectively, lie in the directions ox_1 and oy_1. Then the notation $\Delta\alpha$ is one-half the difference between the maximum and minimum stiffness. The angle $\angle x_1ox$ is equal to $\omega_1 t$, if we assume that x_1 axis agrees with the x axis of the fixed rectangular coordinate system when time t is equal to zero. We will treat with the simple system in which the shaft has a uniform cross section and the disc is mounted on the shaft at the middle point and where the supporting conditions of shaft are equal at the upper and the lower bearings. Let the spring forces in x_1, y_1, x and y directions be P_{x_1}, P_{y_1}, P_x and P_y, respectively, and the components of the deflections of disc center M in these directions be x_1, y_1, x and y. Then we have

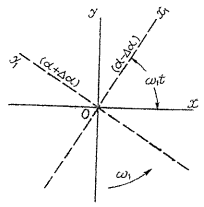

FIG. 42. Rotating rectangular coordinate system with ω_1.

$$P_{x_1}=-(\alpha-\Delta\alpha)x_1, \qquad P_{y_1}=-(\alpha+\Delta\alpha)y_1, \tag{21. 1}$$

and

$$\left.\begin{aligned} P_x &= P_{x_1}\cos\omega_1 t - P_{y_1}\sin\omega_1 t,\\ P_y &= P_{x_1}\sin\omega_1 t + P_{y_1}\cos\omega_1 t, \end{aligned}\right\} \qquad \left.\begin{aligned} x_1 &= x\cos\omega_1 t + y\sin\omega_1 t,\\ y_1 &= -x\sin\omega_1 t + y\cos\omega_1 t. \end{aligned}\right\} \tag{21. 2}$$

From Eqs. (21. 1) and (21. 2), the spring forces in the x and y dirctions are

$$\begin{aligned} -P_x &= \alpha x - \Delta\alpha(y\sin 2\omega_1 t + x\cos 2\omega_1 t),\\ -P_y &= \alpha y - \Delta\alpha(x\sin 2\omega_1 t - y\cos 2\omega_1 t). \end{aligned} \tag{21. 3}$$

The differencial equations of motions are

$$\left.\begin{aligned} m\ddot{x} + \alpha x - \Delta\alpha(y\sin 2\omega_1 t + x\cos 2\omega_1 t) &= me\omega^2\cos\omega t,\\ m\ddot{y} + \alpha y - \Delta\alpha(x\sin 2\omega_1 t - y\cos 2\omega_1 t) &= me\omega^2\sin\omega t. \end{aligned}\right\} \tag{21. 4}$$

Obviously the differential equations of motion include the terms in which the coefficients are regular periodic functions of time t with period $2\pi/\omega_1$. Putting the solutions of Eqs. (21. 4) in the following forms

$$\left.\begin{aligned} x &= A\cos\omega t + B\cos(2\omega_1-\omega)t,\\ y &= A\sin\omega t + B\sin(2\omega_1-\omega)t, \end{aligned}\right\} \tag{21. 5}$$

and substituting the above equations into Eq. (21. 4), we readily have,

$$A=\frac{e\omega^2\{p^2-(2\omega_1-\omega)^2\}}{(p^2-\omega^2)\{p^2-(2\omega_1-\omega)^2\}-(\Delta\alpha)^2}, \quad B=\frac{\Delta\alpha e\omega^2}{m[(p^2-\omega^2)\{p^2-(2\omega_1-\omega)^2\}-(\Delta\alpha)^2]}, \tag{21. 6}$$

in which $p^2=\alpha/m$. Assuming that the higher powers of $\Delta\alpha$ are negligible, Eqs. (21. 6) may be written in the following forms

$$A=\frac{e\omega^2}{p^2-\omega^2},\qquad B=\frac{\Delta\alpha e\omega^2}{m(p^2-\omega^2)\{p^2-(2\omega_1-\omega)^2\}}. \tag{21. 7}$$

Eqs. (21. 7) yield the solutions of Eqs. (21. 4) of

$$\left.\begin{aligned} x&=\frac{e\omega^2}{p^2-\omega^2}\cos\omega t+\frac{\Delta\alpha e\omega^2}{m(p^2-\omega^2)\{p^2-(2\omega_1-\omega)^2\}}\cos(2\omega_1-\omega)t,\\ y&=\frac{e\omega^2}{p^2-\omega^2}\sin\omega t+\frac{\Delta\alpha e\omega^2}{m(p^2-\omega^2)\{p^2-(2\omega_1-\omega)^2\}}\sin(2\omega_1-\omega)t.\end{aligned}\right\} \tag{21. 8}$$

The most widely used iteration method gives the same results as Eqs. (21. 8) starting with the negligence of $\Delta\alpha$ as the first step. Eqs. (21. 8) are the particular solutions of Eqs. (21. 4). The 1st terms in the right-hand side of Eqs. (21. 8) are the normal forced vibrations having the period $2\pi/\omega$ induced by e. The 2nd terms represent the peculiar vibrations having the period $\left|\frac{2\pi}{2\omega_1-\omega}\right|$ induced by the difference in stiffness of the shaft which rotates with ω_1. These vibrations cause the critical speed to occur at a certain rotating speed ω given by $p^2=(2\omega_1-\omega)^2$ (p the natural frequency of this system).

The differential equations of motion in general systems, $(a\neq b)$, are also readily obtained as follows:

$$\left.\begin{aligned} &m\ddot{x}+\alpha x+\gamma\theta_x-\Delta\alpha(y\sin 2\omega_1t+x\cos 2\omega_1t)-\Delta\gamma(\theta_y\sin 2\omega_1t+\theta_x\cos 2\omega_1t)\\ &\qquad=me\omega^2\cos\omega t,\\ &m\ddot{y}+\alpha y+\gamma\theta_y-\Delta\alpha(x\sin 2\omega_1t-y\cos 2\omega_1t)-\Delta\gamma(\theta_x\sin 2\omega_1t-\theta_y\cos 2\omega_1t)\\ &\qquad=me\omega^2\sin\omega t,\\ &I\ddot{\theta}_x+I_p\omega\dot{\theta}_y+\delta\theta_x+\gamma x-\Delta\delta(\theta_y\sin 2\omega_1t+\theta_x\cos 2\omega_1t)-\Delta\gamma(y\sin 2\omega_1t\\ &\qquad+x\cos 2\omega_1t)=(I_p-I)\tau\omega^2\cos(\omega t+\beta),\\ &I\ddot{\theta}_y-I_p\omega\dot{\theta}_x+\delta\theta_y+\gamma y-\Delta\delta(\theta_x\sin 2\omega_1t-\theta_y\cos 2\omega_1t)-\Delta\gamma(x\sin 2\omega_1t\\ &\qquad-y\cos 2\omega_1t)=(I_p-I)\tau\omega^2\sin(\omega t+\beta),\end{aligned}\right\} \tag{21. 9}$$

in which $2\Delta\alpha$, $2\Delta\gamma$ and $2\Delta\delta$ are the differences of stiffnesses α, γ and δ, respectively, all having the same nature as $\Delta\alpha$ in Eqs. (21. 1), (21. 3) and (21. 4). We easily obtain the solutions of Eqs. (21. 9) using the itration method. As the first step, we make $\Delta\alpha$, $\Delta\gamma$ and $\Delta\delta$ in Eqs. (21. 9) zero, and Eqs. (21. 9) becomes Eqs. (3. 27), with the particular solutions as the first approximation are given by Eqs. (3. 28). Substituting Eqs. (3. 28) into Eqs. (21. 9), we obtain the linear differential equations (21. 10) having constant coefficients in which are included two kinds of disturbing forces with frequencies ω and $2\omega_1-\omega$.

$$\left.\begin{aligned}
m\ddot{x}+\alpha x+\gamma\theta_x &= me\omega^2\cos\omega t+(\Delta\alpha A_1+\Delta\gamma B_1)\cos(2\omega_1-\omega)t\\
&\quad+(\Delta\alpha A_2+\Delta\gamma B_2)\cos\{(2\omega_1-\omega)t-\beta\},\\
m\ddot{y}+\alpha y+\gamma\theta_y &= me\omega^2\sin\omega t+(\Delta\alpha A_1+\Delta\gamma B_1)\sin(2\omega_1-\omega)t\\
&\quad+(\Delta\alpha A_2+\Delta\gamma B_2)\sin\{(2\omega_1-\omega)t-\beta\},\\
I\ddot{\theta}_x+I_p\omega\dot{\theta}_y+\delta\theta_x+\gamma x &= (I_p-I)\tau\omega^2\cos(\omega t+\beta)+(\Delta\delta B_1+\Delta\gamma A_1)\\
&\quad\times\cos(2\omega_1-\omega)t+(\Delta\delta B_2+\Delta\gamma A_2)\cos\{(2\omega_1-\omega)t-\beta\},\\
I\ddot{\theta}_y-I_p\omega\dot{\theta}_x+\delta\theta_y+\gamma y &= (I_p-I)\tau\omega^2\sin(\omega t+\beta)+(\Delta\delta B_1+\Delta\gamma A_1)\\
&\quad\times\sin(2\omega_1-\omega)t+(\Delta\delta B_2+\Delta\gamma A_2)\sin\{(2\omega_1-\omega)t-\beta\}.
\end{aligned}\right\}\quad(21.\ 10)$$

In the foregoing equations, following notations are used.

$$\left.\begin{aligned}
A_1&=\frac{me\omega^2\{\delta+(I_p-I)\omega^2\}}{(\alpha-m\omega^2)\{\delta+(I_p-I)\omega^2\}},\\
A_2&=\frac{-(I_p-I)\tau\omega^2\gamma}{(\alpha-m\omega^2)\{\delta+(I_p-I)\omega^2\}},\\
B_1&=\frac{-me\omega^2\gamma}{(\alpha-m\omega^2)\{\delta+(I_p-I)\omega^2\}},\\
B_2&=\frac{(I_p-I)\tau\omega^2(\alpha-m\omega^2)}{(\alpha-m\omega^2)\{\delta+(I_p-I)\omega^2\}}.
\end{aligned}\right\}\quad(21.\ 11)$$

These differential equations may be solved easily by normal procedure and assuming the higher powers of $\Delta\alpha$ etc. to be negligible, the solutions are written as follows:

$$\left.\begin{aligned}
x&=A_1\cos\omega t+A_2\cos(\omega t+\beta)\\
&\quad+\frac{[\delta+(2\omega_1-\omega)\{I_p\omega-I(2\omega_1-\omega)\}]}{\{\alpha-m(2\omega_1-\omega)^2\}[\delta+(2\omega_1-\omega)\{I_p\omega-I(2\omega_1-\omega)\}]-\gamma^2}\\
&\qquad\times\frac{[(\Delta\alpha A_1+\Delta\gamma B_1)\cos(2\omega_1-\omega)t+(\Delta\alpha A_2+\Delta\gamma B_2)\cos\{(2\omega_1-\omega)t-\beta\}]}{\{\alpha-m(2\omega_1-\omega)^2\}[\delta+(2\omega_1-\omega)\{I_p\omega-I(2\omega_1-\omega)\}]-\gamma^2}\\
&\quad-\frac{\gamma[(\Delta\alpha B_1+\Delta\gamma A_1)\cos(2\omega_1-\omega)t+(\Delta\delta B_2+\Delta\gamma A_2)\cos\{(2\omega_1-\omega)t-\beta\}]}{\{\alpha-m(2\omega_1-\omega)^2\}[\delta+(2\omega_1-\omega)\{I_p\omega-I(2\omega_1-\omega)\}]-\gamma^2},\\
\theta_x&=B_1\cos\omega t+B_2\cos(\omega t+\beta)\\
&\quad+\frac{\{\alpha-m(2\omega_1-\omega)^2\}[(\Delta\delta B_1+\Delta\gamma A_1)\cos(2\omega_1-\omega)t+(\Delta\delta B_2+\Delta\gamma A_2)\cos\{(2\omega_1-\omega)t-\beta\}]}{\{\alpha-m(2\omega_1-\omega)^2\}[\delta+(2\omega_1-\omega)\{I_p\omega-I(2\omega_1-\omega)\}]-\gamma^2}\\
&\quad-\frac{\gamma[(\Delta\alpha A_1+\Delta\gamma B_1)\cos(2\omega_1-\omega)t+(\Delta\alpha A_2+\Delta\gamma B_2)\cos\{(2\omega_1-\omega)t-\beta\}]}{\{\alpha-m(2\omega_1-\omega)^2\}[\delta+(2\omega_1-\omega)\{I_p\omega-I(2\omega_1-\omega)\}]-\gamma^2}.
\end{aligned}\right\}\quad(21.\ 12)$$

Putting sin in place of cos in the above equations, the solutions for y and θ_y are obtained. The 1st and 2nd terms in right-hand side of Eqs. (21.12) represent the normal forced vibrations given by Eqs. (3.28); the 3rd and 4th terms give the vibrations of $[2\omega_1-\omega]$.

If Fig. 41 becomes more complicated, the terms of sin $n\omega_1 t$ and cos $n\omega_1 t$ (n is any integer) may also be included in Eqs. (21.10), and the vibrations of mode

of $[n\omega_1 \pm \omega]$ may appear. But it would seem that the figure obtained by connecting the tops of vectors of stiffnesses may resemble an ellipse as shown in Fig. 41 regardless of the order of arrangement of balls. For instance, if there are three larger balls of equal diameter and they are arranged equally in a bearing at an angular interval of 120 degrees, at first glance it may seem that Fig. 41 would resemble a triangle. As a matter of fact the figure becomes more like a circle which can be clearly understood when we consider that the shaft having three key-ways at equal intervals of 120 degrees does not have the difference of stiffness in all directions.[5] Therefore Fig. 41 is a circle. Not considering the magnitudes of difference in stiffness, when two larger balls are inserted, the figure may also resemble an ellipse whether the balls are insterted side-by-side, as in Fig. 35 1 and 1′, or at right angles as 1 and 3, or in a symmetrical position as 1 and 5′. Consequently in many cases the figure may resemble an ellipse. These facts would indicate that the stiffness of the shaft having any cross section in all directions can be represented by the inertia ellipse. Accordingly Eqs. (21.4) and (21.9) which are induced by laying the directions of the maximum and minimum stiffness at right angles to each other may be the simplest and the most plausible forms for all cases. Actually the vibrations of mode of $[n\omega_1 \pm \omega]$ hardly ever appeared in our numerous experiments under various circumstances. Then we may conclude that the terms of $\sin n\omega_1 t$ and $\cos n\omega_1 t$ can be regarded as negligibly small whatever they may be.

22. Behavior of vibrations and the shapes of vibratory waves

Now putting

$$2\omega_1 - \omega = \beta_1 \omega, \tag{22.1}$$

we obtain the following relation from $\omega_1 = \alpha_1 \omega$,

$$\beta_1 = 2\alpha_1 - 1. \tag{22.2}$$

Since the value of α_1 is peculiar to all kinds of ball bearings, the value of β_1 depends upon the bearing. For the fixed outer ring, α_1 is smaller than 1/2, then β_1 takes a negative value, as we see by Eq. (22.2) and the vibrations of $[\beta_1 \omega]$ have the mode of vibration of backward precession for any kind of radial ball bearing. For the self-aligning double-row ball bearing with 10 ϕ bore used in the experiments, α_1 is equal to about $+\frac{1}{2.65}$ as shown in Part I, and then the value of β_1 becomes about $-\frac{1}{4.1}$. Consequently the vibrations take the following forms:

$$\left.\begin{aligned} x &= A\cos\omega t + B\cos\frac{\omega}{4.1}t, \\ y &= A\sin\omega t - B\sin\frac{\omega}{4.1}t. \end{aligned}\right\} \tag{22.3}$$

As we see by Eqs. (21.8) and (21.12), in the region of such critical speeds of $[2\omega_1 - \omega]$, the amplitudes A in Eq. (22.3) are almost unchanged and only the amplitudes B increase, forming the peak of critical speed and this fact is the same as in the vibrations treated in Part I. Eqs. (22.3) plainly show that the motion is

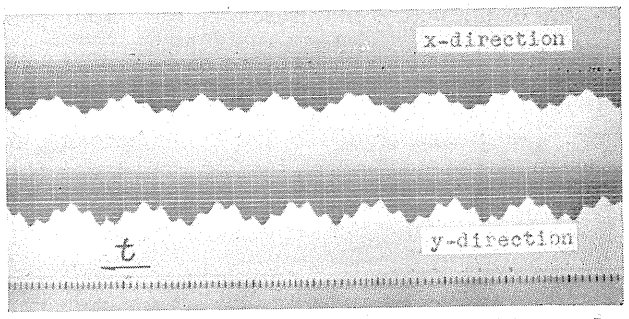

FIG. 43. Oscillographic paper of vibrations of $[2\omega_1-\omega]$.

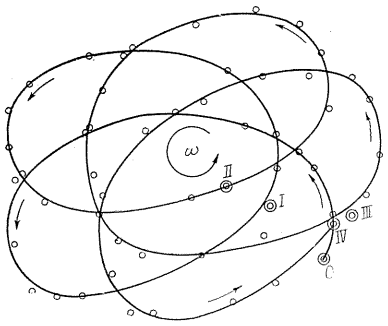

FIG. 44. Path of whirl in vibrations of $[2\omega_1-\omega]$.

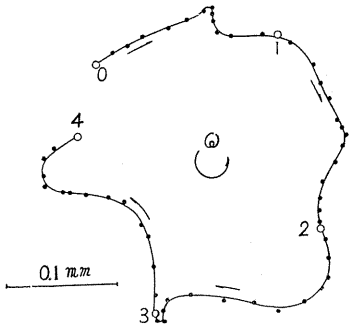

FIG. 45. Path of whirl in vibrations of $[2\omega_1-\omega]$. $(A<B)$.

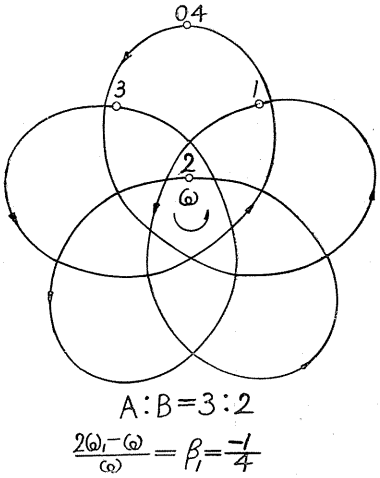

FIG. 46. Geometrical figure of hypotrochoid, $(A:B=3:2,\ \beta_1=-1/4)$.

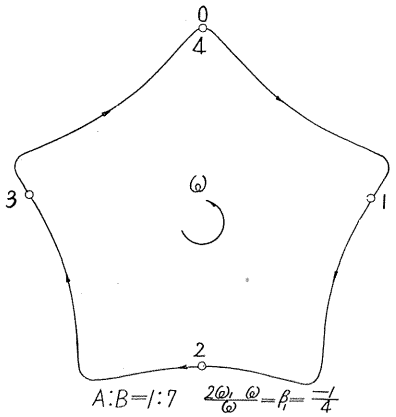

FIG. 47. Geometrical figure of hypotrochoid, $(A:B=1:7,\ \beta_1=-1/4)$.

composed of two vibrations with respective periods of $2\pi/\omega$ and $2\pi\frac{4.1}{\omega}$. An example of oscillographic paper is shown in Fig. 43. Whether the motion is backward percession or not is proved by combining the vibrations in x- and y- directions in Fig. 43. For the fixed outer ring β_1 is negative, so that the locus of disc center M in the xy-plane obviously must be hypotrochoid as seen in Eq. (22.3). An example of this locus as obtained by the oscillographic paper is shown in Fig. 44, where the difference between the magnitudes of the amplitudes A and B in Eqs. (22.3) is not very large. In Fig. 44, the interval between the circular mark and the next means one revolution of shaft, so that this figure shows the path of disc center M during 4 revolutions of shaft, the direction of rotation of shaft being anti-clockwise. When the difference between the magnitudes of the amplitudes A and B is large, the path of the disc center M is as in Fig. 45. Figs. 46 and 47 are the geometrical figures obtained from Eqs. (22.3).

23. Results of experiments

In this section we will first examine whether the value of β_1 obtained by experiments coincides with the values of Eqs. (22.1) and (22.2). As we have already stated, even in the same kinds of ball bearings there is a small variation of α_1 according to the dimensions D and d, the size of radial clearance, and the magnitude of difference in diameter between each ball. From the table given below, it may be concluded that in proportion to the variation of α_1 above mentioned, β_1 obtained by experiments also varies according to the value given by Eq. (22.1). The results of experiments with Disc No. 2 using various shafts and bearings, are given in the following table.

Position of disc $a:b$	$1/\alpha_1$	$1/\beta_1$ calculated	$1/\beta_1$ by experiments
1 : 3	2.643	−4.110	−4.143
3 : 7	2.625	−4.200	−4.250
3 : 7	2.625	−4.200	−4.220
1 : 1	2.647	−4.092	−4.111
1 : 1	2.625	−4.200	−4.167

The values $1/\beta_1$ in the 3rd column are obtained by Eq. (22.1) and those in the 4th column by investigating vibratory waves on oscillographic papers. The values in both these columns agree and it can be ascertained experimentally that these vibrations are those of mode of $[2\omega_1-\omega]$.

As we see in Eqs. (21.8) and (21.12), the amplitudes of these vibrations of $[2\omega_1-\omega]$ increase with the increase in eccentricity e and the deviational inclination angle τ. Figs. 48 *b* and 48 *c* make this fact experimentally plain. The disc in Fig. 48 *c* has a larger eccentricity than that in Fig. 48 *b*, all other circumstances being the same in both cases. The amplitudes B of the vibrations $[2\omega_1-\omega]$ in the former figure build up larger than those in the latter. Eqs. (21.8) and (21.12) also indicate that the amplitudes B are proportional to the differences in stiffnesses $\Delta\alpha$ etc.

The substantial cause for $\Delta\alpha$ etc. is the difference itself in diameter of balls, although the magnitudes of $\Delta\alpha$ etc. may also be affected by the radial clearance, the difference in diameter of balls, and the order of arrangement of balls; there-

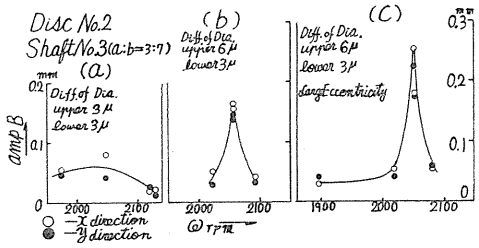

FIG. 48 (*left*). Effects of the difference in diameter of balls and the arrangement of balls.

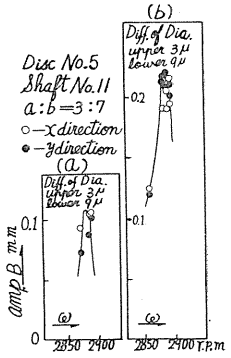

FIG. 49 (*right*). Effects of the arrangement of balls.

fore, generally speaking, it may be expected that $\Delta\alpha$ etc. increase with the greater differences in diameters of balls. In Fig. 48 *b*, the difference in diameters of balls is larger than that in Fig. 48 *a*, all the other conditions being the same in both cases. Obviously with larger differences in diameters, the amplitudes B are larger.

The influence of the order of arrangement of balls are examined in Fig. 49. In this figure the differences in diameters of balls in the lower ball bearing is artificially enlarged. In Fig. 49 *a*, two larger balls of 4.766 ϕ and 4.765 ϕ are inserted side-by-side into the bearing of $d = 4.757\ \phi$. In Fig. 49 *b*, two larger balls of 4.766 ϕ are put symmetrically in each side in the bearing of $d = 4.757\ \phi$, *i.e.*, in the positions as 1, 1′, 5′ and 6 in Fig. 35. As already mentioned, it is expected that Fig. 49 *b* has amplitudes larger than those of Fig. 49 *a*, and the experimental results clearly showing this fact are in Fig. 49.

Now we denote the critical speed of mode of $[2\omega_1 - \omega]$ by the notation ω_d. The peak at the critical speed ω_d is usually smaller than that at the major critical speed ω_c and at the critical speed ω_a of $[\alpha_1\omega]$. But under certain circumstances, it is possible to make the amplitudes of the critical speed ω_d build up to a considerable extent until they are larger than those of the critical speed ω_a. As above mentioned, in order to enlarge the peak of ω_d, the following conditions should be satisfied.

1) The eccentricity e and the deviational angle τ to be large.
2) The difference in diameter of balls to be large.
3) The balls to be arranged in a bearing so as to yield the greatest difference in stiffness of $\Delta\alpha$ etc.

Since the critical speed ω_d usually appears at a rotating speed higher than the major critical speed ω_c, it is dangerous when the disc having large eccentricity passes through ω_c, so that considering the points set forth in 2) and 3), very larges amplitudes are obtained experimentally, as shown in Fig. 50. The differences in diameters in the upper and lower pedestals are 9 μ and 11 μ, respectively, and they are very large. In Fig. 50 *a* although the balls are inserted at random, the amplitudes are remarkably larger than those in other experiments. It is to be noted that in Fig. 50 the scale of the ordinate is shortened compared with other diagrams. In the ball bearing used in Fig. 50 *b*, the balls are arranged symmetrically as shown in Fig. 51, *i.e.*, the larger balls are inserted in positions directly opposite each other, the smaller ones also directly opposite and at right angles with the larger. In this case, the peak of the critical speed ω_d builds up considerably so as to make the shaft strike the guard ring violently.

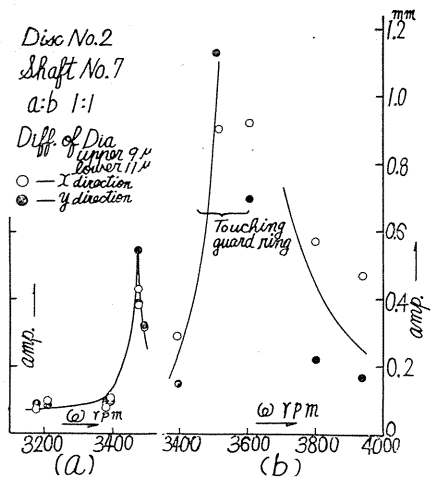

FIG. 50 (*left*). Resonance curves of vibrations $[2\omega_1-\omega]$ having large amplitudes.

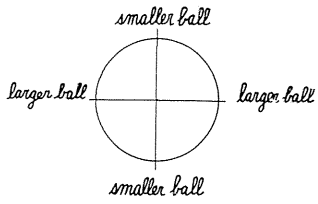

FIG. 51 (*right*). Arrangement of balls.

24. The location of the critical speed ω_d of $[\beta_1\omega]$

In Fig. 37 the abscissa of the point C on which the straight line $p=\beta_1\omega$ cuts the Curve III gives the critical speed ω_a. Equating the denominator of the 3rd and 4th terms in the right-hand side of Eqs. (21.12) to zero and considering $\omega_1=\alpha_1\omega$, $\beta_1=2\alpha_1-1$, we have

$$\left.\begin{aligned}&\{\alpha-m(2\omega_1-\omega)^2\}[\delta+(2\omega_1-\omega)\{I_p\omega-I(2\omega_1-\omega)\}]-\gamma^2\\&=\{\alpha-m(2\alpha_1-1)^2\omega^2\}[\delta+(2\alpha_1-1)\{I_p-(2\alpha_1-1)I\}\omega^2]-\gamma^2\\&=(\alpha-\beta_1^2\omega^2m)\{\delta+\beta_1\omega^2(I_p-\beta_1I)\}-\gamma^2=0.\end{aligned}\right\}\qquad(24.\ 1)$$

Solving the above equation with respect to ω^2, the critical speeds ω_d of $[\beta_1\omega]$ are to be obtained as follows:

$$\omega_d^2=\frac{\{\alpha(I_p-\beta_1I)-\alpha_1\delta m\}\pm\sqrt{\{\alpha(I_p-\beta_1I)+\beta_1\delta m\}^2-4\beta_1m(I_p-\beta_1I)\gamma^2}}{2\beta_1^2m(I_p-\beta_1I)}\qquad(24.\ 2)$$

The value of ω_d in the above equation coincides with that in Fig. 37. As we see in Fig. 37 *a*, the straight line $p=\beta_1\omega$ can not only cut the Curve III but also the Curve IV, then two critical speeds of $[\beta_1\omega]$ appear. Since the higher critical speed of ω_d appears in our apparatus at the considerably high speed ω_1 we cannot actually observe this critical speed. In the simple case $a=b$, the critical speed ω_d is only one and is equal to $|\beta_1\omega|$ as shown in Fig. 37 *b*. The nearer the disc is mounted to the end of shaft, the nearer the critical speed ω_d approaches the major critical speed ω_c and consequently ω_d is not always larger than ω_c. This is in direct contrast to the fact that ω_a is always larger than ω_c. In fact, in $a:b=1:4$, the peak of the critical speed ω_d of $[\beta_1\omega]$ appears near the major critical speed ω_c as shown in Fig. 52.

For the deeply grooved sigle-row ball bearing, reproduction of the oscillographic paper showing vibrations of $[\beta_1\omega]$ is given in Fig. 53, and $\beta_1=\frac{-7}{25}$ is obtained by the shape of vibratory waves in this figure. Here the value of α_1 is given by the relation $\beta_1=2\alpha_1-1$, and this value is $\alpha_1=9/25$. Since the value $\alpha_1=9/25$

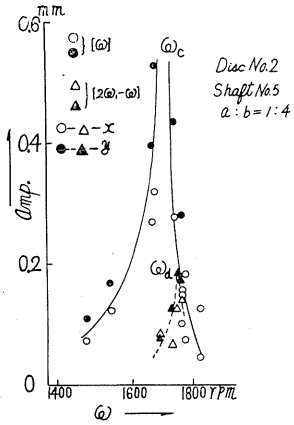

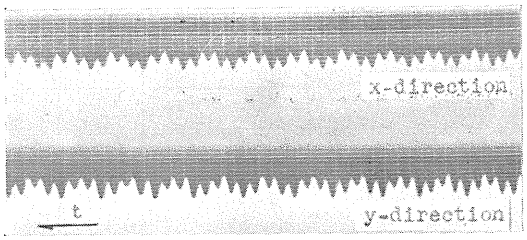

FIG. 52 (*left*). Resonance curves in the neighborhood of the major critical speed. (Disc No. 2 and Shaft No. 5, $a : b = 1 : 4$).

FIG. 53 (*right*). Oscillographic paper of vibrations $[2\omega_1 - \omega]$ for single-row radial ball bearing.

coincides with that in Fig. 39, the bearing used in Fig. 53 may have the same dimensions of D and d as in Fig. 39.

Incidentally, when the fixed inner ring is used, α_1 is always larger than 1/2, so the vibrations of $[\beta_1\omega]$ are the forward precessional motions. Since the thrust ball bearing has the value of $\alpha_1 = 1/2$ consequently $\beta_1 = 0$, and the vibrations of $[\beta_1\omega]$ may not appear.

Summarizing, the vibrations of $[\beta_1\omega]$ of backward precession occur because of the differences in stiffness of shaft which rotate with ω_1, and the differences in stiffness are produced by the differences in diameter of balls. The amplitudes of these vibrations are influenced by the differences in diameters and the order of arrangement of balls. Furthermore, the radial clearance may also affect these vibrations.

These vibrations necessarily come into question for the shaft at high speed. Using ball bearings on the market, the vibrations of $[\beta_1\omega]$ nearly always appear.

Part III. Various Kinds of Vibrations Having Small Amplitudes Due to Ball Bearings

25. Preliminaries

Observing the results of numerous experiments with various kinds of discs and shafts, we may find that many kinds of vibrations having comparatively small amplitudes take place in the shaft. For instance, such vibrations are found in Figs. 8 and 9, represented by notations $[+5\omega]$, $[+3\omega]$, $[-3\omega]$, $\left[-\frac{\omega}{6.5}\right]$, $\left[\frac{\omega}{1.959}\right]$, $\left[-\frac{\omega}{10.5}\right]$, $\left[-\frac{\omega}{2.666}\right]$, $\left[+\frac{9}{8}\omega\right]$, etc..

As shown in Figs. 8 and 9, amplitudes of these vibrations are so small that they may be of little importance in practical problems. Some of these vibrations can be explained by machining errors in ball bearings.

26. Errors in dimensions of outer and inner rings

In general, it may be expected that there are errors in machining outer and inner rings which may not be made in an exact circle. In other words, their shapes may be nearly ellipse or in other more complicated figures. Magnitudes of these irregularities in dimensions may be of the same order as the differences in diame-

ters between each ball in a ball bearing, as has been discussed in Parts I and II. Therefore we should consider not only the differences in diameter but the effects of such irregularities.

Simplifying the problem of such irregularities, we will consider the following:

1) The shape of outer ring is ellipse.

2) The shape of inner ring is ellipse.

Though there are more complicated shapes which could be considered, the tendency toward the ellipse is the most frequent and most likely to cause vibrations.

Usually there is considerable magnitude of eccentricity of inner ring due to error in machining, but this eccentricity causes only the vibration of mode of $[+\omega]$ and no new modes of vibration appear.

27. Various kinds of modes of vibrations due to irregularities in inner and outer rings

A. Elliptical outer ring and the difference in diameters of balls

If both the inclination of ellipse in outer ring and the difference in diameter of balls (see Parts I and II) are present, the conditions develope as shown in Fig. 54. In Fig. 54, when the larger ball B is inserted into the bearing, the inner ring is pushed outward on the opposite side along the directional line ob and the inner ring is deviated from the center line of bearing in the amount of e_0, as shown in Fig. 54, line of direction *ab*. If the outer ring forms in a perfect circle, the magnitude of this eccentricity e_0 is constant at every position of the ball B. But when the shape of the outer ring is an ellipse and the internal diameter of outer ring in x-direction is larger than the diameter in y-direction, as shown in Fig. 54, the value of e_0 varies every half-revolution. When the larger ball B is in x-direction where the radial clearance is largest, the inner ring tends to be pressed outward by B, and the eccentricity e_0 becomes large. On the other hand, if B locates in y-direction where the radial clearance is smallest, the deviation of inner ring from the bearing center line is somewhat small, then e_0 takes the minimum value in y-direction. Since the larger ball B rotates with the precessional angular velocity ω_1 and e_0 takes the maximum value in x- and $-x$- directions and minimum value in y- and $-y$-directions, there is a periodic change of the magnitude of e_0, and two periodic changes of e_0 during one revolution of ball B. Consequently the deviation of disc center e_1 from the bearing center line which changes in proportion as e_0 also varies periodically (see Fig. 34), and is represented approximately as follows:

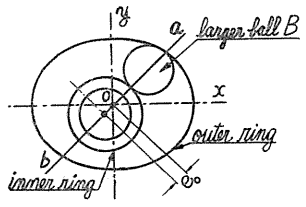

FIG. 54

$$e_1 = e_{10} + 2\,e_2 \cos 2\,\omega_1 t, \tag{27. 1}$$

in which e_{10} and e_{20} are contants.

The diviational angle τ_1 shown in Fig. 34 is also to be

$$\tau_1 = \tau_{10} + 2\,\tau_2 \cos 2\,\omega_1 t. \tag{27. 1a}$$

Inserting Eq. (27. 1) into Eqs. (16. 3), we have

$$m\ddot{x} + \alpha x = me\omega^2 \cos \omega t + \alpha e_{10} \cos \omega_1 t + \alpha e_2 \cos 3\omega_1 t + \alpha e_2 \cos \omega_1 t,$$
$$m\ddot{y} + \alpha y = me\omega^2 \sin \omega t + \alpha e_{10} \sin \omega_1 t + \alpha e_2 \sin 3\omega_1 t - \alpha e_2 \sin \omega_1 t. \qquad (27.\ 2)$$

Since the 3rd and 4th terms in the right-hand sides of the abovs equations represent the external disturbing forces having the circular frequencies $[+3\omega_1]$ and $[-\omega_1]$, the forced vibrations of modes of $[+3\omega_1]$ and $[-\omega_1]$ can take place in the shaft. A similar conclusion is obtained from Eqs. (16.2), for $a \neq b$.

Observing Peak VIII in Fig. 8, we find that $\alpha_1 (= \omega_1/\omega)$ is equal to 3/8 $\left(= \frac{1}{2.667}\right)$ so that $3\alpha_1 = 9/8$. Consequently we can see that the vibrations themselves represented by $[+9/8\omega]$ in Fig. 8 are of $[+3\omega_1]$. The peak in Fig. 9 is also of $[+3\omega_1]$.

The magnitudes of amplitudes obtained by numerous experiments are shown in the following table. In this table, resultant amplitudes are shown.

Vibrations of $[+3\omega_1]$

Max. amp. in mm	Disc No.	Shaft No.	Location of disc $a : b$	Location of peak of $[+3\omega_1]$ in r.p.m.	Remarks
0.18	2	4	2.56 : 7.44 $\fallingdotseq$ 1 : 3	1,190	See Fig. 8.
0.15	4	4	2.56 : 7.44 $\fallingdotseq$ 1 : 3	1,208	See Fig. 9.
0.14	3	4	2.61 : 7.39 $\fallingdotseq$ 1 : 3	1,261	
0.27	6	3	3 : 7	1,019	
0.13	4	12	7 : 3	1,195	

In the experiments shown in the above table, self-aligning double-row ball bearings with 10 ϕ bore are used. Since $3\alpha_1$ is equal to about $+9/8$ for this type of ball bearing, the peak of $[3\omega_1]$ inevitably appeares near the peak of the major critical speed ω_c in any position of disc $a : b$. Therefore even at the peak of $[9/8\omega]$, the amplitudes of vibrations $[+\omega]$ are somewhat large. The difference of frequency between $[9/8\omega]$ and $[+\omega]$ are comparatively small, so that the beat phenomena[36] appear in shaft at the peak of $[+9/8\omega]$. In Fig. 55 a tracing of an oscillographic paper of vibrations $[+9/8\omega]$ is shown.

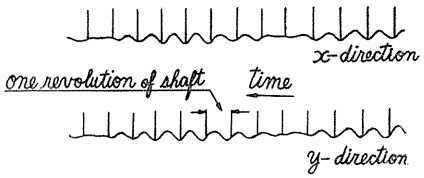

FIG. 55. Copy of vibratory waves of $[+3\omega_1]$.

For single-row radial ball bearing, α_1 is equal to about 9/25 as mentioned in Part I, then $3\alpha_1 = 27/25 < 9/8$, and the peak of $[+3\omega_1]$ appears closer to the major critical speed ω_c.

Though vibrations of mode of $[-\omega_1]$ do not appear in Fig. 8, they occur in the experiment as the peak of $\left[-\frac{\omega}{2.666}\right]$ shown in Fig. 9. In this figure the peak of $[-\omega_1]$ appears in 1,932 r.p.m. and the maximum amplitude is 0.10 mm.

If the eccentricity of inner ring e_0 due to the differences in diameters of balls is considerably large, the flexibility of bearing pedestal may also cause the vibrations of $[-\omega_1]$, but e_0 is usually so much smaller than the eccentricity e of disc, that it is not sufficient to cause the peak $[-\omega_1]$.

Since e_1 and τ_1 vary periodically, as shown in Eqs. (27.1) and (27.1*a*), the differences in stiffness of shaft $\Delta\alpha$ (see Section 21) also varies and is represented as follows:

$$\Delta\alpha = \Delta\alpha_1 + 2\,\Delta\alpha_2 \cos 2\,\omega_1 t. \tag{27.3}$$

Consequently Eqs. (21.4) become

$$m\ddot{x} + \alpha x - (\Delta\alpha_1 + 2\,\Delta\alpha_2 \cos 2\,\omega_1 t)(y \sin 2\,\omega_1 t + x \cos 2\,\omega_1 t) = me\omega^2 \cos \omega t,$$
$$m\ddot{y} + \alpha y - (\Delta\alpha_1 + 2\,\Delta\alpha_2 \cos 2\,\omega_1 t)(x \sin 2\,\omega_1 t - y \cos 2\,\omega_1 t) = me\omega^2 \sin \omega t.$$

By a similar procedure as in Section 21, we obtain

$$\left.\begin{aligned} x &= A\cos\omega t + B\cos(2\,\omega_1 - \omega)t + C\cos(-\omega t) + D\cos(4\,\omega_1 - \omega)t, \\ y &= A\sin\omega t + B\sin(2\,\omega_1 - \omega)t + C\sin(-\omega t) + D\sin(4\,\omega_1 - \omega)t, \end{aligned}\right\} \tag{27.4}$$

in which

$$\left.\begin{aligned} A &= \frac{e\omega^2}{p^2 - \omega^2}, & C &= \frac{A\Delta\alpha_2}{m(p^2 - \omega^2)} \\ B &= \frac{A\Delta\alpha_1}{m\{p^2 - (2\,\omega_1 - \omega)^2\}}, & D &= \frac{A\Delta\alpha_2}{m\{p^2 - (4\,\omega_1 - \omega)^2\}}, & p^2 &= \alpha/m. \end{aligned}\right\} \tag{27.5}$$

The 3rd terms in the right-hand side of Eqs. (27.4) represent the vibrations $[-\omega]$: the 4th terms show the vibrations $[4\,\omega_1 - \omega]$.

The peak of vibrations of $[4\,\omega_1 - \omega]$ are shown as the Peak VII of $\left[\frac{\omega}{1.959}\right]$ in Fig. 8. The peak $\left[\frac{\omega}{1.954}\right]$ in Fig. 9 is also of $[4\,\omega_1 - \omega]$.

If the peaks of $\left[\frac{\omega}{1.954}\right]$ and $\left[\frac{\omega}{1.959}\right]$ are of $[4\,\omega_1 - \omega]$, we obtain the relation

$$\tau_1 = \frac{1}{1.954} = 4\,\alpha_1 - 1, \qquad \tau_1 = \frac{1}{1.959} = 4\,\alpha_1 - 1, \tag{27.6}$$

From the above equations we get $1/\alpha_1 = 2.645$ and $1/\alpha_1 = 2.648$, respectively, and these values of α_1 agree with the values discussed in Part I, so that we proved that the vibrations of $[4\,\omega_1 - \omega]$ are of $\left[\frac{\omega}{1.954}\right]$ or $\left[\frac{\omega}{1.959}\right]$.

In Fig. 56 we give a tracing of oscillographic paper of the vibrations $\left[\frac{\omega}{1.959}\right]$. In Fig. 56, the smaller vibratory wave is that of $[+\omega]$ and the superposition is represented by $\left[\frac{\omega}{1.959}\right]$ and $[+\omega]$. Since $[4\,\omega_1 - \omega]$ is almost equal to $[2\,\omega]$, the slow shift of phase angle between two different vibrations $[4\,\omega_1 - \omega]$ and $[\omega]$ can be easily seen.

B. Elliptical outer ring and elliptical inner ring

Now we will point to the fact that not only the outer ring but the inner

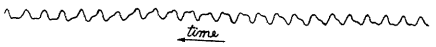

FIG. 56. Copy of vibratory waves of $[4\,\omega_1 - \omega]$.

ring also has the tendency toward an ellipse. A new mode of vibration [$+3\omega$] takes place in the shaft even when there is no difference in diameters of the ball and if e_0 disappears.

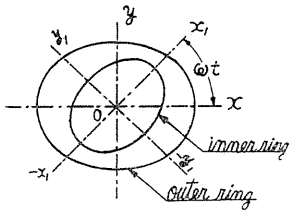

FIG. 57

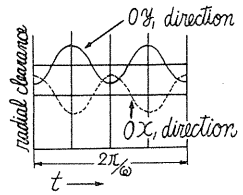

FIG. 58. Variation of radial clearance.

Considering the rotating rectangular coordinate system o-x_1y_1 with angular velocity ω, let us assume the direction of maximum outer diameter of inner ring to be x_1-axis, and the directions of minimum diameter y_1-direction as shown in Fig. 57. The directions of the maximum and the minimum internal diameters of outer ring are o-x and o-y, respectively. Obviously the radial clearance varies periodically, and when ox_1 axis agrees with ox axis, the radial clearance in ox_1-direction takes the maximum value and that in oy_1-direction, the minimum value. Considering that the inner ring rotates with ω, the radial clearances in ox_1- and oy_1-directions vary approximately as shown in Fig. 58. Let the spring forces in x_1, y_1, x and y directions be P_{x_1}, P_{y_1}, P_x and P_y, respectively, and the components of the deflections of disc center M in these directions be x_1, y_1, x and y, respectively. Then we have

$$\left.\begin{aligned} P_x &= P_{x_1}\cos\omega t - P_{y_1}\sin\omega t, \\ P_y &= P_{x_1}\sin\omega t + P_{y_1}\cos\omega t, \end{aligned}\right\} \qquad \left.\begin{aligned} x_1 &= x\cos\omega t + y\sin\omega t, \\ y_1 &= -x\sin\omega t + y\cos\omega t. \end{aligned}\right\} \tag{27. 7}$$

As discused in Part II, the stiffness of shaft varies with the radial clearance and observing Fig. 58, the spring forces P_{x_1} and P_{y_1} become

$$\left.\begin{aligned} -P_{x_1} &= (\alpha + \Delta\alpha - 2\,\Delta\alpha_1\cos 2\omega t)x_1, \\ -P_{y_1} &= (\alpha - \Delta\alpha + 2\,\Delta\alpha_1\cos 2\omega t)y_1. \end{aligned}\right\} \tag{27. 8}$$

From Eqs. (27. 7) and (27. 8), we have

$$\left.\begin{aligned} -P_x &= \alpha x + (\Delta\alpha - 2\,\Delta\alpha_1\cos 2\omega t)(y\sin 2\omega t + x\cos 2\omega t), \\ -P_y &= \alpha y + (\Delta\alpha - 2\,\Delta\alpha_1\cos 2\omega t)(x\sin 2\omega t - y\cos 2\omega t). \end{aligned}\right\} \tag{27. 9}$$

Then the differential equations of motion are

$$\left.\begin{aligned} m\ddot{x} + \alpha x + (\Delta\alpha - 2\,\Delta\alpha_1\cos 2\omega t)(y\sin 2\omega t + x\cos 2\omega t) &= me\omega^2\cos(\omega t + \beta), \\ m\ddot{y} + \alpha y + (\Delta\alpha - 2\,\Delta\alpha_1\cos 2\omega t)(x\sin 2\omega t - y\cos 2\omega t) &= me\omega^2\sin(\omega t + \beta), \end{aligned}\right\} \tag{27. 10}$$

in which β is a phase angle.

By a procedure similar to that used in Eqs. (21. 4) of Part II, we have

$$\left.\begin{aligned} x &= A\cos(\omega t+\beta) - \frac{\Delta\alpha' A}{p^2-\omega^2}\cos(\omega t-\beta) + \frac{\Delta\alpha_1' A}{p^2-\omega^2}\cos(-\omega t-\beta) \\ &\qquad + \frac{\Delta\alpha_1' A}{p^2-9\omega^2}\cos(3\omega t-\beta), \\ y &= A\sin(\omega t+\beta) - \frac{\Delta\alpha' A}{p^2-\omega^2}\sin(\omega t-\beta) + \frac{\Delta\alpha_1' A}{p^2-\omega^2}\sin(-\omega t-\beta) \\ &\qquad + \frac{\Delta\alpha_1' A}{p^2-9\omega^2}\sin(3\omega t-\beta), \end{aligned}\right\} \quad (27.11)$$

in which $A=\dfrac{e\omega^2}{p^2-\omega^2}$, $\Delta\alpha'=\Delta\alpha/m$ and $\Delta\alpha_1'=\Delta\alpha_1/m$.

The 1st and 2nd terms in the right-hand sides of the above equations give the vibrations $[+\omega]$, the 3rd terms show the vibration $[-\omega]$, and the 4th terms represent the vibrations $[+3\omega]$.

For $a \neq b$, a similar conclusion is obtained in Eqs. (3.27) and (21.9).

Vibrations of $[+3\omega]$ appearing in our experiments are shown in the following table.

Vibrations of $[+3\omega]$

Max. amp. in mm	Disc No.	Shaft No.	Position of disc $a:b$	Location of peak of $[+3\omega]$ in r.p.m.
0.30	2	4	1 : 3	380
0.16	4	4	1 : 3	416
0.23	2	6	1 : 1	288
0.37	2	7	1 : 1	282
0.14	3	4	1 : 3	420
0.17	6	3	3 : 7	402

An oscillographic paper of vibration $[+3\omega]$ is shown in Fig. 59.

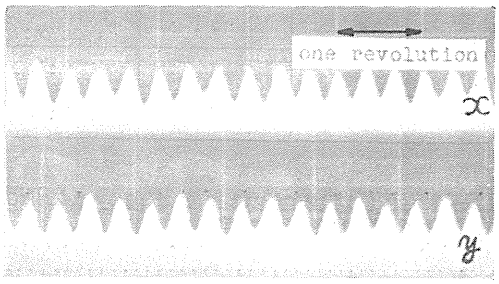

FIG. 59. Oscillographic paper of vibrations of $[+3\omega]$.

If the bending moment applied at the end of shaft varies periodically due to the irregularities in coupling, and this frequency of variation is $\nu\omega$, the vibrations of mode of

$$(\nu \pm 1)\omega \quad (27.12)$$

take place in shaft.[2)20)] Then for $\nu=2$, the vibrations of $[+3\omega]$ may also appear.

C. Eliptical outer ring and the differences in diameters of balls.

Since the larger ball B revolves at the precessional angular velocity ω_1 and the inner ring rotates at ω, the relative velocity of inner ring to the ball B is $\omega-\omega_1$. During the relative time it takes ball B to make one revolution around the inner ring, two cycles of variation of e_0 in Fig. 60 are performed, then e_1 may be represented as follows:

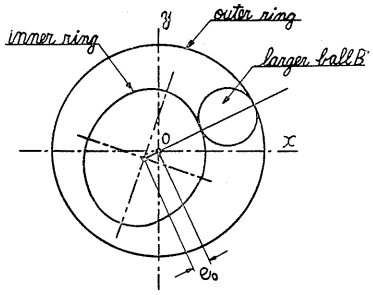

FIG. 60

$$e_1 = e_{10} + 2e_2\cos 2(\omega-\omega_1)t, \tag{27. 13}$$

in which e_1 is the deviation of disc center M due to the larger ball B. Inserting Eq. (27. 13) into Eq. (16. 3), we have

$$\left.\begin{aligned} m\ddot{x}+\alpha x &= me\omega^2\cos\omega t+\alpha e_{10}\cos\omega_1 t+\alpha e_2\cos(3\omega_1-2\omega)t+\alpha e_2\cos(2\omega-\omega_1)t,\\ m\ddot{y}+\alpha y &= me\omega^2\sin\omega t+\alpha e_{10}\sin\omega_1 t+\alpha e_2\sin(3\omega_1-2\omega)t+\alpha e_2\sin(2\omega-\omega_1)t. \end{aligned}\right\} \tag{27. 14}$$

As we have already mentioned, $\alpha_1=\omega_1/\omega$ is equal to about 3/8 for self-aligning double-row ball bearing with 10 ϕ bore, then

$$3\omega_1-2\omega \fallingdotseq -7/8\,\omega, \qquad 2\omega-\omega_1 \fallingdotseq 13/8\,\omega. \tag{27. 15}$$

Eqs. (27. 14) prove that the forced vibrations of $[-7/8\omega]$ and $[13/8\omega]$ can take place in the shaft.

Those vibrations appearing in our experiments are shown in the following table.

Vibrations $[-7/8\omega]$ and $[13/8\omega]$

Mode of vibration	Max. amp. in mm	Disc No.	Shaft No.	Position of disc $a:b$	Location of peak in r.m.p.
$[-7/8\omega]$	0.12	2	4	1 : 3	2131.3
$[13/8\omega]$	0.08	4	4	1 : 3	755

Since the peak of $[-7/8\omega]$ appears near the major critical spped ω_c, the beat phenomena take place.

28. Summary

In the previous section, we have discussed many kinds of vibrations having comparatively small amplitudes. We have cited rather simple cases only. Irregularities in dimensions of ball bearings may be more complicated, and other modes of vibrations may appear under such circumstances.

Moreover, the vibrations $[+2\omega]$ appear when the spring coupling S shown in Figs. 1 and 2 is not straight and the bending moment exerted at the shaft end varies periodically.[37] As an example, the peak of vibrations $[+2\omega]$ is shown in Fig. 23.

The oscillographic paper of vibrations $[+2\omega]$ is given in Fig. 61. In addition to the vibrations described in Part III, there are others having small amplitudes the causes of which are unknown. For instance, the backward precesions of $\left[-\frac{\omega}{6.5}\right]$, $\left[-\frac{\omega}{7}\right]$ and $\left[-\frac{\omega}{10}\right]$ appear occasionally. In Fig. 8 the peaks of $\left[-\frac{\omega}{6.5}\right]$ and $\left[-\frac{\omega}{10.5}\right]$ are shown. In Fig. 62 is shown the vibration $\left[-\frac{\omega}{10.5}\right]$ which is one of these of unknown origin. In Fig. 63, the path of whirl during 8 revolutions of shaft at the peak of $\left[-\frac{\omega}{7}\right]$ is shown. In the experiment shown in Fig. 63, Disc No. 2 and Shaft No. 5 ($a : b \fallingdotseq 1 : 4$) are used. Fig. 64 shows the locus of the disc center M in vibrations composed of $[+3\omega]$ and $[+\omega]$ which appear near the peak of $[+3\omega]$. In this case, Disc No. 6 and Shaft No. 3 ($a : b = 3 : 7$) are used. Fig. 65 represents the path of the shaft obtained by combining $[+2\omega]$ and $[+\omega]$ taking place near the peak of $[+2\omega]$. In this experiment Disc No. 6 and Shaft No. 3 ($a : b = 3 : 7$) are used. The loci in Figs. 64 and 65 are the path of shaft during one revolution.

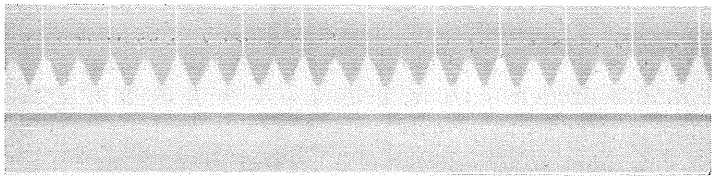

FIG. 61. Oscillographic paper of vibrations of $[+2\omega]$.

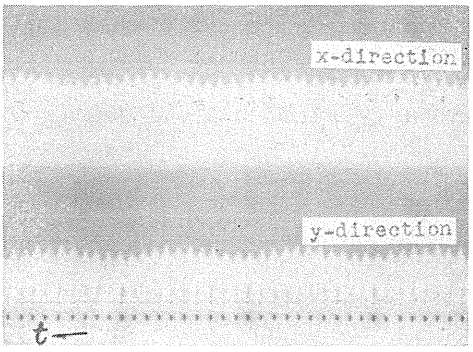

FIG. 62. Oscillographic paper of vibrations of $[-\omega/10.5]$.

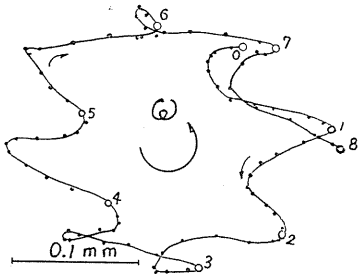

FIG. 63. Path of whirl of vibrations of $[-\omega/7]$.

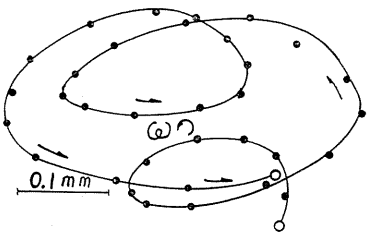

FIG. 64. Path of whirl of vibrations of $[+3\omega]+[+\omega]$.

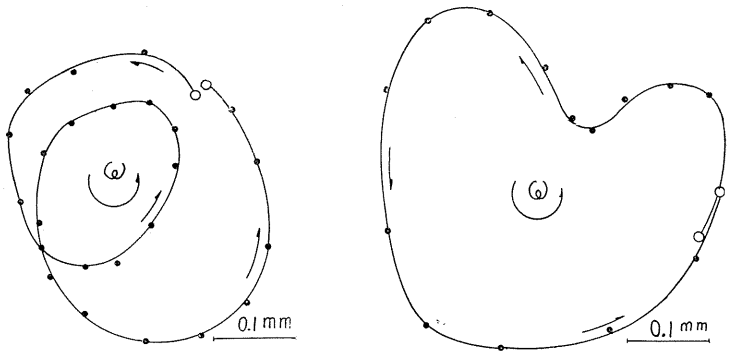

FIG. 65. Path of whirl of vibrations of $[+2\omega]+[+\omega]$.

Chapter IV. Forced Vibration of a Shaft supported by Bearings with Radial Clearances[44]

29. Preliminaries

There are many studies[38)39)45)46)47)48)] on vibratory characteristics of systems having a small clearance. These studies, however, have been treated when the reciprocal vibrations are on a straight line, *i.e.*, the system where the motion is of a sigle degree of freedom. When a shaft is supported by berings with small backlash and the shaft whirls, the system has a motion of several drgrees of freedom and differs from the system with a single degree of freedom. We studied both theoretically and experimentally the whirling of a vertical shaft supported by bearings with small radial clearances and we cleaced up the nature of respose curves and the criteria of stability of motion.

30. Differential eqations of motion and the stability criteria for the whirling motion of the shaft

We treat with the rotating shaft system which consists of a light elastic shaft and a rotating disc mounted at the middle point of the shaft ($a=b$). Let e_1 and e_2 be the magnitudes of the small radial clearances in the upper and the lower bearings, respectively, and let $S(x, y)$ be the geometrical center of the shaft and let $G(x_G, y_G)$ be the gravitational center of the disc. Fig. 66 represents the configuration of the system when the shaft whirls. In Fig. 66 *a*, AB is the center line of bearing and both of the shaft ends move A and B to A' and B' when the shaft deflects. As we see in Fig. 66, we have

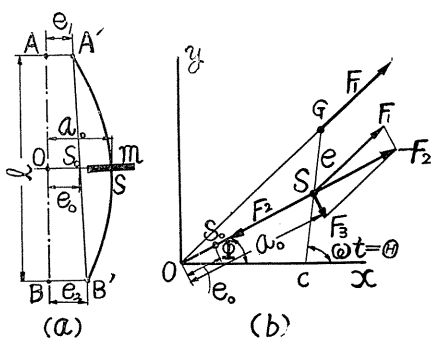

FIG. 66

$$OS_0 = e_0 = 1/2(e_1 + e_2), \tag{30. 1}$$

in which e_0 is the backlash. When there is no friction in bearings, the points S,

S_0 and O must lie on a straight line, as shown in Fig. 66 *b*.
The kinetic energy of the disc is

$$T=\frac{1}{2}m(\dot{x}_G^2+\dot{y}_G^2)+\frac{1}{2}I_p\dot{\theta}^2, \tag{30. 2}$$

in which $\theta=\angle Gcx$ (see Fig. 66. b) and $x_G=x+e\cos\theta$, $y_G=y+e\sin\theta$. The potential energy of this system should be represented by the following form

$$V=\frac{\alpha}{2}(x-e_0\cos\phi)^2+\frac{\alpha}{2}(y-e_0\sin\phi)^2, \tag{30. 3}$$

in which α is the spring constant of the shaft and $\phi=\angle Sox$. Substituting Eqs. (30. 2) and (30. 3) into Lagrange's equations, we have

$$\left.\begin{aligned} &I_p\ddot{\theta}+me^2\ddot{\theta}-me(\dot{x}\sin\theta-\dot{y}\cos\theta)=0,\\ &m\ddot{x}+\alpha(x-e_0\cos\phi)=me\dot{\theta}^2\cos\theta+me\ddot{\theta}\sin\theta,\\ &m\ddot{y}+\alpha(y-e_0\sin\phi)=me\dot{\theta}^2\sin\theta-me\ddot{\theta}\cos\theta. \end{aligned}\right\} \tag{30. 4}$$

Since $\dot{x}$, $\dot{y}$, x, y and e are small compared with unity and we can neglect the higher powers, we have

$$\left.\begin{aligned} &\dot{\theta}=\omega=\text{const.},\\ &m\ddot{x}+\alpha(x-e_0\cos\phi)=me\omega^2\cos\omega t,\\ &m\ddot{y}+\alpha(y-e_0\sin\phi)=me\omega^2\sin\omega t, \end{aligned}\right\} \tag{30. 5}$$

in which ω is the rotating speed of the shaft.

Even in the rotating shaft system with a backlash, we can treat with the disc rotating with a constant angular velocity. When the damping forces $-c\dot{x}$ and $-c\dot{y}$ exist, the differential equations of motion are

$$\left.\begin{aligned} &m\ddot{x}+c\dot{x}+\alpha(x-e_0\cos\phi)=me\omega^2\cos\omega t,\\ &m\ddot{y}+c\dot{y}+\alpha(y-e_0\sin\phi)=me\omega^2\sin\omega t. \end{aligned}\right\}^{51)} \tag{30. 6}$$

Since S, S_0 and O lie on a straight line, we have

$$\cos\phi=\frac{x}{\sqrt{x^2+y^2}},\qquad \sin\phi=\frac{y}{\sqrt{x^2+y^2}}, \tag{30. 7}$$

and Eqs. (30. 6) are represented by the following forms:

$$\left.\begin{aligned} &\ddot{x}+2n\dot{x}+p^2x-\frac{e_0p^2x}{\sqrt{x^2+y^2}}=e\omega^2\cos\omega t,\\ &\ddot{y}+2n\dot{y}+p^2y-\frac{e_0p^2y}{\sqrt{x^2+y^2}}=e\omega^2\sin\omega t, \end{aligned}\right\} \tag{30. 8}$$

where $p^2=\alpha/m$, $2n=c/m$ and p is the natural frequency of the system when the backlash is not present.

Now we obtain the response curves, using the method by which van der Pol[52]

developed the self-sustained vibration theory. Forced vibrations are represented as follows:

$$x = a\cos(\omega t + \beta'), \qquad y = a\sin(\omega t + \beta'), \tag{30. 9}$$

where β' is a phase angle. When the motion is slightly deviated from the steady state by a disturbing force, free vibrations with small amplitudes take place and the amplitudes a in Eqs. (30.9) are not constant, therefore da/dt and d^2a/dt^2 are not equal to zero. The quantities da/dt and d^2a/dt^2 are small of 1st and 2nd order, respectively. Inserting Eqs. (30.9) into Eqs. (30.8), and rejecting all terms of order higher than the 1st, we obtain

$$\left.\begin{aligned} &2n\dot{a}_1 - 2\omega\dot{a}_2 + (p^2-\omega^2)a_1 - 2n\omega a_2 - p^2e_0\cos\beta' = e\omega^2, \\ &2\omega\dot{a}_1 + 2n\dot{a}_2 + 2n\omega a_1 + (p^2-\omega^2)a_2 - p^2e_0\sin\beta' = 0, \end{aligned}\right\} \tag{30. 10}$$

where $a_1 = a\cos\beta'$ and $a_2 = a\sin\beta'$.

Let a_{10} and a_{20} be a_1 and a_2 in steady state ($\dot{a}_1 = \dot{a}_2 = 0$), respectively. From Eqs. (30.10), we can obtain the following equation for steady forced vibrations,

$$\{(p^2-\omega^2)^2 + 4n^2\omega^2\}a_0^2 - 2p^2(p^2-\omega^2)e_0a_0 + p^4e_0^2 = e_0^2\omega^4, \tag{30. 11}$$

where $a_0^2 = a_{10}^2 + a_{20}^2$, and a_0 is the amplitude of forced vibration. Introducing the dimensionless quantities v, ν, r and E, denoting them as follows:

$$v = \omega^2/p^2, \quad \nu^2 = 4n^2/p^2, \quad r = a_0/e_0, \quad E = e/e_0, \tag{30. 12}$$

we have

$$\{(1-v)^2 + \nu^2 v\}r^2 - 2(1-v)r + (1-E^2v^2) = 0. \tag{30. 13}$$

Eqs. (30.11) and (30.13) are the equations of the response curves (the amplitude —frequency curves).

We now discuss the criterion of stability of motion along the procedure[52)53)] by which A. Andronow and A. Witt, and the author employed in self-excited vibrations and in the generalized nonlinear systems, respectively. We replace a_1 and a_2 in Eqs. (30.10) with $a_{10}+\xi$ and $a_{20}+\eta$, where a_{10} and a_{20} are constants, and ξ and η are small deviations from a steady state, and then develope of Eqs. (30.10) in powers ξ and η, and reject all but the linear terms in ξ and η, obtaing:

$$\frac{d\eta}{d\xi} = \frac{A\xi + B\eta}{C\xi + D\eta}, \tag{30. 14}$$

where

$$\left.\begin{aligned} A &= \omega(p^2-\omega^2-2n^2) + p^2e_0\left\{-\frac{\omega}{a_0} + \frac{1}{a_0^3}(\omega a_{10}^2 - na_{10}a_{20})\right\}, \\ B &= -n(p^2+\omega^2) + p^2e_0\left\{\frac{n}{a_0} + \frac{1}{a_0^3}(\omega a_{10}a_{20} - na_{20}^2)\right\}, \\ C &= -n(p^2+\omega^2) + p^2e_0\left\{\frac{n}{a_0} - \frac{1}{a_0^3}(\omega a_{10}a_{20} + na_{10}^2)\right\}, \\ D &= -\omega(p^2-\omega^2-2n^2) + p^2e_0\left\{\frac{\omega}{a_0} - \frac{1}{a_0^3}(\omega a_{20}^2 + na_{10}a_{20})\right\}. \end{aligned}\right\} \tag{30. 15}$$

The motion is stable when $B+C<0$ and $AD-BC<0$ are held. From Eqs. (30. 15), we have

$$B+C=-2n(p^2+\omega^2)<0. \tag{30. 16}$$

Therefore in the present system the 1st stable condition $B+C<O$ is always held. Consequently we should examine only the 2nd condition $AD-BC\gtrless O$. The equation of the boundary lines between the stable and the unstable regions are given by $AD-BC=O$. From Eqs. (30. 15), we obtain the following equation of the boundary lines:

$$\{(p^2-\omega^2)^2+4n^2\omega^2\}a_0-p^2(p^2-\omega^2)e_0=0, \tag{30. 17}$$

or

$$\{(1-v)^2+\nu^2 v\}r-(1-v)=0. \tag{30. 17a}$$

It can be easily proved that the boundary lines represented by Eqs. (30. 13) and (30. 17a) are loci of the vertical tangents to the response curves. The boundary lines in $r-v$ plane are shown in Fig. 67. Obviously a_0 must be larger than e_0, *i.e.*, $r>1$, therefore, for example, the stable region for $\nu^2=0.05$ is the upper region from line $ABCD$, and the steady forced vibrations can not appear in the lower region.

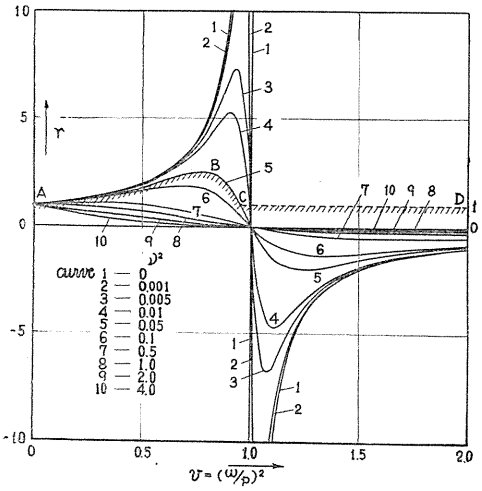

FIG. 67 (*left*). Boundary lines between stable and unstable regions.

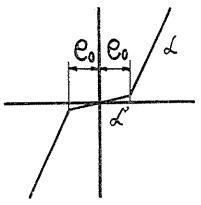

FIG. 68 (*right*). Characteristics of spring force.

If the restoring force is not zero and the spring constant is α' when the shaft ends lie within the radial elearances, *i.e.*, $r<1$, the characteristics of spring force is represented as shown in Fig. 68. For such cases, the equations of motion are rewritten as follows:

$$m\ddot{x}+c\dot{x}+\alpha x-\alpha e_0(1-\alpha'/\alpha)\frac{x}{\sqrt{x^2+y^2}}=me\omega^2\cos\omega t. \tag{30. 18}$$

Putting

$$e_0'=e_0(1-\alpha'/\alpha),\ E'=e/e_0',\ r'=a_0/e_0', \tag{30. 19}$$

and replacing e_0, E and r in Eqs. (30. 11), (30. 13), (30. 17) and (30. 17a) by e_0', E' and r', respectively, we can use these equations when α' is not zero.

31. Response curves

The response curves given by Eqs. (30.13) are shown in Figs. 69, 70 and 71 where $E = e/e_0$ is adopted as a parameter. Fig. 69 gives the response curves when the damping force is not present, *i.e.*, $\nu = 0$. In Figs. 69, 70 and 71, curve B is the boundary line between the stable and unstable regions given by Eqs. (30.17a), the full lines represent the stable motion and the dotted lines give the motion the appearance of a state which is actually impossible. We can observe that the response curves shown in these figures differ from those of the reciprocal vibrations on a straight line.

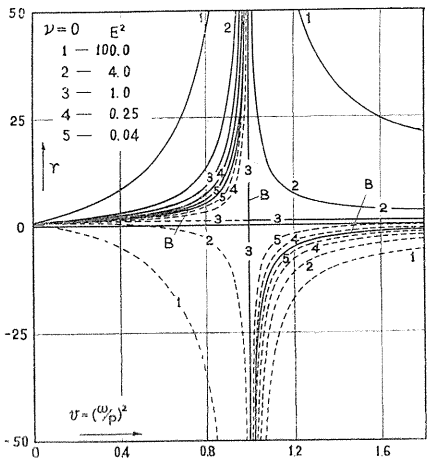

FIG. 69 (*left*). Response curves, ($\nu = 0.0$).

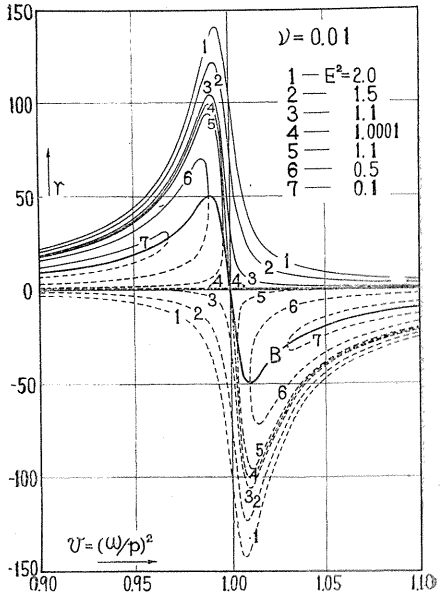

FIG. 70 (*right*). Response curves, ($\nu = 0.01$).

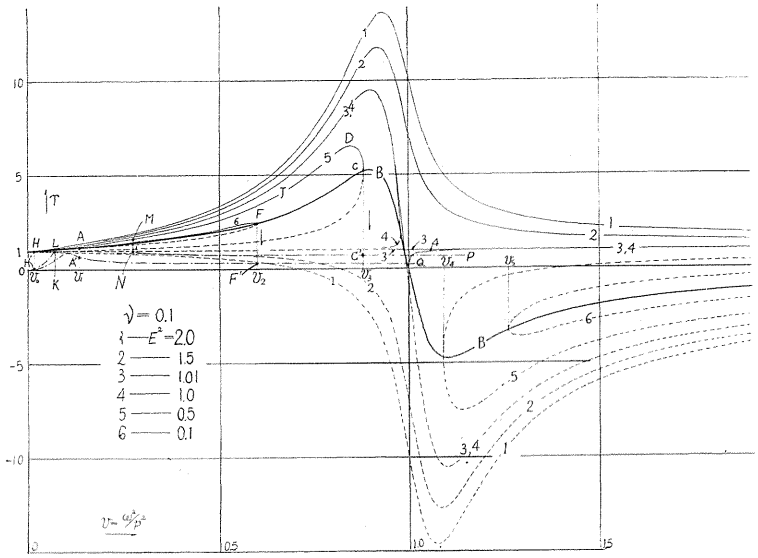

FIG. 71. Response curves, ($\nu = 0.1$).

Obviously amplitude r is a real quantity, therefore the discriminant of Eq. (30.13) should be positive, *i.e.*,

$$(1-v)^2-(1-E^2v^2)\{(1-v)^2+\nu^2v\}=E^2v[\{v(1-v)^2+\nu^2v^2\}-\nu^2/E^2]\geqq 0, \qquad (31.1)$$

or

$$A=v(1-v)^2+\nu^2v^2\geqq\nu^2/E^2. \qquad (31.1a)$$

$A-v$ curves are given in Fig. 72 where ν^2 is adopted as a parameter. In Curve 5 ($\nu=0.1$, $E^2=0.5$) of Fig. 71, ν^2/E^2 is 0.02. In Fig. 72, the points A, B and C are the intersecting points at which a straight line $\nu^2/E^2=0.02$ cuts $A-v$ curve of $\nu=0.1$ ($\nu^2=0.01$). Abscissa of points A, B and C are v_0, v_3 and v_4, respectively. Since the relation of Eq. (31.1) is satisfied only in the regions $v_0\leqq v\leqq v_3$ and $v_4\leqq v$, the response curves exist in these regions, and are not present in the regions $v\leqq v_0$ and $v_3\leqq v\leqq v_4$. As shown in Fig. 71, the response Curve 5 exist only in the regions $v_0\leqq v\leqq v_3$ and $v_4\leqq v$. Curves 6 of $E^2=0.1$ appear in regions $v_1\leqq v\leqq v_2$ and $v_5\leqq v$. When the damping force increases in Fig. 72 the straight line $\nu^2/E^2=$ constant is represented by $A_1B_1C_1$ and the regions increase in which the response curves cannot exist. Consequently when the damping force exists, there are two regions in which the response curves disappear, one in the neighborhood of $v=0$ and the other in the neighborhood of $v=1$. In these regions, d'Alambert's principle does not hold in the state in which the shaft ends move from A to A'

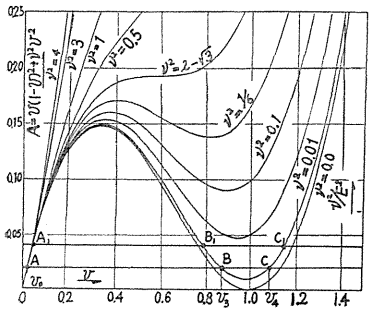

FIG. 72. $A-v$ diagrams.

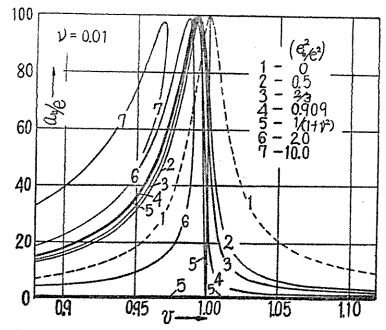

FIG. 73. Response curves, ($\nu=0.01$)

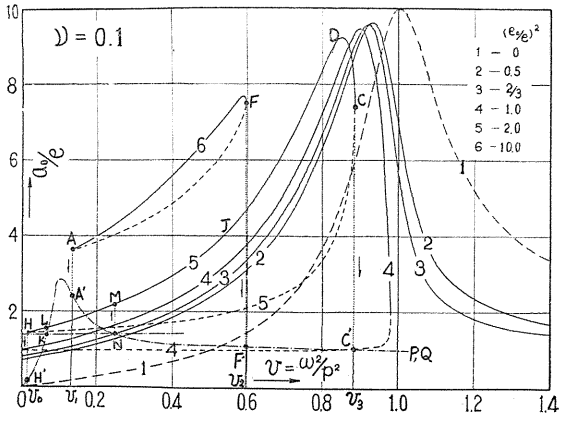

FIG. 74. Response curves, ($\nu=0.1$).

and from B to B' (see Fig. 66 a). Therefore the motion represented by Eqs. (30. 8) is impossible; an entirely different motion in which the shaft ends lie within the radial clearances takes place.

Figs. 73 and 74 represent the response curves when the eccentricity e is constant and the magnitudes of the backlashes e_0 take various values. We can see that the maximum amplitude decreases slightly as e_0 increases, and the peak of amplitude shifts to a lower angular velocity ω when e_0 increases.

Now we denote the angular velocity of the shaft ω at which the maximum amplitude appears as ω_{max}. Fig. 75 gives the $\gamma_{max} - (1 - v_{max})$ curves where $v_{max} = \left(\frac{\omega_{max}}{p}\right)^2$. Dotted line represents the curve when the backlash e_0 is zero. The shift of the peak of amplitude because of the backlash is observed in Fig. 75 and Fig. 76 includes diagrams $\gamma_{max} - v$.

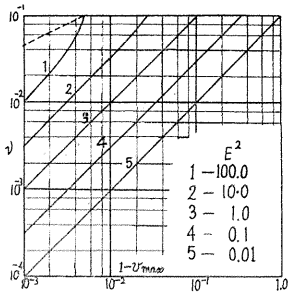

FIG. 75 (*left*). $v - (1 - v_{max})$ diagram.

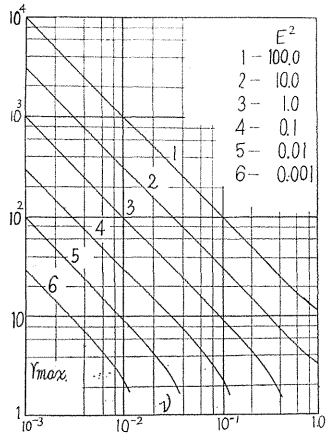

FIG. 76 (*right*). $\gamma_{max} - v$ diagram.

When the disc is not mounted at the middle point of the shaft ($a \neq b$) and τ does not exist, only the eccentricity e being present, the rseponse curves are as given in the following equation.

$$\left.\begin{aligned}&\left[\left[(\alpha - m\omega^2)\{\delta + (I_p - I)\omega^2\} - \gamma^2\right]^2 + c^2\omega^2\{\delta + (I_p - I)\omega^2\}^2\right]a_0^2\\&+ 2\left[(\alpha - m\omega^2)\{\delta + (I_p - I)\omega^2\} - \gamma^2\right]\left[(\gamma^2 e_0 + \gamma\delta\tau_0) - (\alpha e_0 + \gamma\tau_0)\{\delta + (I_p - I)\omega^2\}\right]a_0\\&+ \left[(\gamma^2 e_0 + \gamma\delta\tau_0) - (\alpha e_0 + \gamma\tau_0)\{\delta + (I_p - I)\omega^2\}\right]^2 = m^2 e^2\omega^4\{\delta + (I_p - I)\omega^2\}^2\end{aligned}\right\} \quad (31.\ 2)$$

In the above equation τ_0 is the inclination angle of the disc when both ends of the shaft move to A' and B' (Fig. 66) and the elastic deflection does not exist. The nature of the curve given by Eqs. (31. 2) resembles that of Eqs. (30. 11).

32. Jump phenomena

When the shaft end lies within the radial clearance, the motion is represented by

$$m\ddot{x} + c\dot{x} + \alpha' x = me\omega^2 \cos \omega t, \quad (32.\ 1)$$

where α' $(\alpha' < \alpha)$ is the spring constant when amplitude a_0 is smaller than e_0 (see Fig. 68). The amplitude of forced vibration is

$$r^2 = \frac{E^2 v^2}{(v - v')^2 + \nu^2 v}, \tag{32. 2}$$

in which $v' = \alpha'/\alpha$. Obviously Eqs. (32.1) and (32.2) are valid, provided $a_0 \leqq e_0$ and $r \leqq 1$. In the region where the response curves given by Eqs. (30.13) disappear, the following relation is held: (see Eq. (31.1a))

$$v(1 - v)^2 + \nu^2 v^2 \leqq \nu^2 / E'^2, \tag{32. 3}$$

Considering $E' = E(1 - v')^{-1}$, then Eq. (32. 3) is rewritten as follows:

$$\begin{aligned} E^2 v^2 &\leqq \nu^2 v (1 - v')^2 \{(1 - v)^2 + \nu^2 v\}^{-1} \\ &= -\{(1 - v)(v - v') - \nu^2 v\}^2 \{(1 - v)^2 + \nu^2 v\}^{-1} + \{(v - v')^2 + \nu^2 v\}. \end{aligned}$$

Then we have

$$\{(v - v')^2 + \nu^2 v\} - E^2 v^2 \geqq \{(1 - v)(v - v') - \nu^2 v\}^2 \{(1 - v)^2 + \nu^2 v\}^{-1} \geqq 0.$$

From the above equation we can see that the numerator in Eq. (32.2) is smaller than the denominator. Therefore in the regions where the response curves disappear and the relation of Eq. (32.3) holds, the amplitudes r given by Eqs. (32.1) and (32.2) are always smaller than unity and the motion governed by Eq. (32.1) is a possible motion. Consequently we can conclude that for all values of v, either the motion given by Eq. (30.13) or Eq. (32.1) is a possible one. When both kinds of motions can appear, the types of motion are decided by the initial conditions.

For $\alpha'/\alpha = v' = 0.1$, $E^2 = 0.5$ and $\nu = 0.1$, the response curves given by Eq. (32.2) are represented by the chain lines $OH'K$ and $NC'P$ in Fig. 71. For $\alpha'/\alpha = v' = 0.1$, $E^2 = 0.1$ and $\nu = 0.1$, these curves are given by the chain line $OA'F'Q$ in Fig. 71. Such response curves in both cases of $E^2 = 0.5$ and $E^2 = 0.1$ become one curve $OH'KLA'NF'C'P$ in Fig. 74.

Now we consider the motion for $E^2 = 0.5$. In Fig. 71 or Fig. 74, as the rotating speed of the shaft v increases, the amplitude moves along curve $OH'K$ and reaches K where $r = 1$, and where the jump phenomena from K to L take place, then amplitude passes through M, J, D and C, and jumps from C to $C'(v = v_3)$ and reaches P. When v is retarded, the amplitude moves along P, C', N, M, L. H, H' and O, and the jump phenomena takes place at $\overrightarrow{NM}$ and $\overrightarrow{HH'}(v = v_0)$. Eor $E^2 = 0.1$, $\nu = 0{,}1$, the response curve given by Eq. (32.2) is always smaller than unity for all values of v, therefore the amplitude moves along curve $OA'F'Q$ in Fig. 71 or Fig. 74 and the jump phenomena do not appear. When the motion removes from curve $OA'F'Q$ to curve 6 (curve AF) by disturbance, the amplitude moves along AF as v increases, and the jump phenomena $\overrightarrow{FF'}(v = v_2)$ occur, then amplitude reaches Q. In retardation, the amplitude moves along $QF'A'O$ and the jump phenomena is not present.

33. Experimental results

The results obtained by our experiments of the shaft and disc system will be shown.

As shown in Fig. 77, even if the radial clearance is present, the jump phenomena do not occur when the eccentricity e is comparatively large. In Fig. 77 the full lines and the marks □ and ■ represent the amplitudes of the major critical speed where the radial clearance is zero, and the dotted lines and the marks ○ and ● show the amplitudes when the small radial clearance is present. In this case, the magnitude of radial cleance between the outer ring and the bearing box is several micra. If the radial clearance exists, the resonance curve shifts slightly to a lower ravolution as shown in Fig. 77. In Fig. 78, the eccentricity e is very

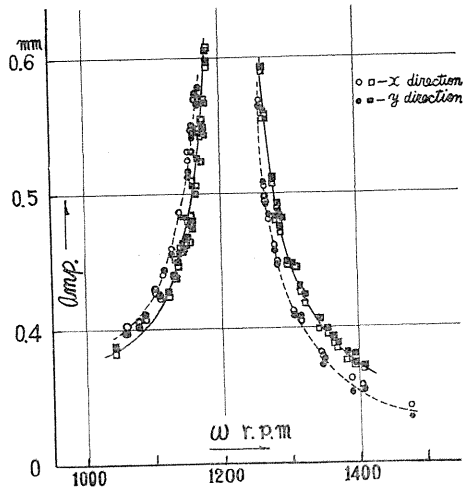

FIG. 77. Response curves (large eccentricity).

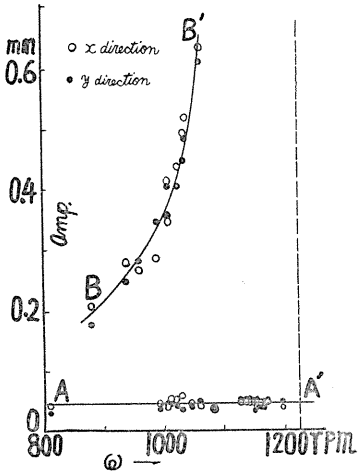

FIG. 79. Response curves (large radial clearance).

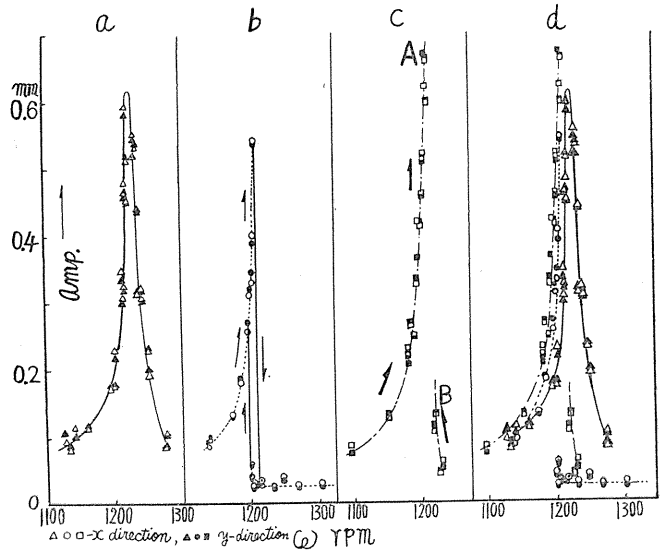

FIG. 78. Response curves (small eccentricity).

small. When e is small and the radial clearance does not exist, the continuous response curves are obtained as shown in Fig. 78 *a*. The magnitude of radial clearance in Figs. 78 *b* and 78 *c* is the same as that indicated by dotted lines in Fig. 77 and this value is several micra, as above mentioned. In the experiment shown in Fig. 78 *b* in which the small eccentricity e is the same as in Fig. 78 *a* and the radial clearance also exists, the jump phenomena take place. When a small radial clearance exists and e is somewhat larger than in Fig. 78 *a* and Fig. 78 *b*, the response curves are as shown in Fig. 78 *c*, Superposing Figs. 78 *a*, 78 *b*, and 78 *c* we obtain Fig. 78 *d*. Fig. 78 *d* also shows that the response curves shift slightly to a lower revolution due to the radial clearance. When the radial clearance between the outer ring and the bearing box increases to about 0.05 mm, the response curves are as shown in Fig. 79. In this figure, since the vertical dotted line shows the major critical speed when the clearance does not exist ($p=1225$ r.p.m.), the considerable displacement of the response curve to a lower speed is clearly seen. In this experiment, by cutting the spring coupling S and retarding the revolution of shaft, the shaft passes through the major critical speed ω_c, but the beat phenomena due to retardation[28)40)41)42)] do not appear and the amplitudes vary along the line AA' shown in Fig. 79. Plotted marks on the line AA' in Fig. 79, however, are obtained by experiments in constant angular velocity. In Figs. 77, 78 and 79, Disc No. 2 and Shaft No. 3 ($a:b=3:7$) are used.

The experimental results shown in Figs. 77, 78 and 79 prove that the theoretical results discussed in Sections 30, 31 and 32 are held. The response curves represented by dotted lines in Fig. 77 correspond to curve I in Fig. 70. The response curves in Fig. 78 *b* and Fig. 78 *c* correspond to curves 6 and 5 in Fig. 70, respectively, and the curves in Fig. 79 to curve 6 in Fig. 71 or Fig. 74.

The magnitude of $\nu=\dfrac{2n}{p}$ obtained by experiments of free vibrations is about $0.01\sim0.002$.

34. The effects of friction in bearing

Let the coefficients of friction in the upper and the lower bearings be μ_1 and μ_2, respectively. When the damping force exists on the disc, both the bending moment and the twisting moment apply on the shaft. The deflection curve of the shaft, howeyer, is a curve lying on a plane, provided that $\mu_1=\mu_2$ and $e_1=e_2$. The direction of elastic force at bearing does not coincide with the radial direction and therefore the angle between the direction of elastic force and the radial direction is $\tan\mu_1\fallingdotseq\mu_1=\mu_2$. The points O, S_0 and S do not lie on a straight line and the angle between OS_0 and SS_0 is $\mu=\mu_1$, provided $a=b$. This state is represented by Fig. 80. The response curves and the boundary lines between the stable and the unstable regions are

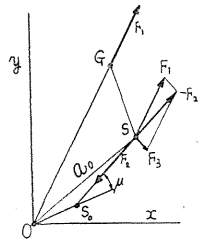

FIG. 80

$$[\{(1-v)^2+\nu^2v\}r^2-2(1-v)r+(1-E^2v^2)]r$$
$$+\{\mu^2(r-1)^2(1-v)+2\mu\nu\sqrt{v}\,r(r-1)\}=0, \qquad (34.1)$$
$$2[\{1-v)^2+\nu^2v\}r-(1-v)]r^2+\mu^2(1-v)(r^2-1)+2\mu\nu r^2\sqrt{v}=0, \qquad (34.2)$$

in which $a_0=SO$ as shown in Fig. 80. The teams in [ ] of Eqs. (34.1) and (34.2)

are the same as the left-hand sides of Eqs. (30.13) and (30.17a), respectively; the other terms are of the small order μ^2 and $\mu\nu$. Consequently the curves given by Eqs. (34.1) and (34.2) are almost the same as those of Eqs. (30.13) and (30.17a). When $a \neq b$ or $e_1 \neq e_2$ or $\mu_1 \neq \mu_2$ or $\tau \neq 0$, the disc not only rotates about the axis of F_3-direction in Fig. 80 but also about SS_0 axis, therefore the angle between OS_0 and SS_0 is not equal to $\mu = \mu_1 = \mu_2$, but is given by a complicated form. This angle, however, is the same order as μ, so that the effects of friction in bearing are also negligible small.

Summarizing, the response curves of the shaft supported by bearings with radial clearance are obtained and the stability criteria and jump phenomena are cleared up. We can conclude that the effects of the friction in bearing are very small.

35. Balancing in the major critical speed (Appendix)

In this section we point out that we should modify the conditions of balancing according to the arrangement of the shaft, *i.e.*, the vertical shaft or the horizontal shaft. If we do not consider this point, serious accidents under some circumstances are sure to occur.

For the vertical shaft, we should consider the potential energy due to the gravity, then the potential energy of the system is

$$V = \frac{1}{2}\alpha(x^2+y_2) + \gamma(x\theta_x + y\theta_y) + \frac{1}{2}\delta(\theta_x^2+\theta_x^2) - \{\theta_x \sin(\beta-\Theta) + \theta_y \cos(\beta-\Theta)\}mge, \tag{35.1}$$

in which g is gravitational acceleration. Then the differential equations of motion become

$$\left.\begin{aligned} &m\ddot{x} + \alpha x + \gamma\theta_x = me\omega^2 \cos\omega t,\\ &m\ddot{y} + \alpha y + \gamma\theta_y = me\omega^2 \sin\omega t,\\ &I\ddot{\theta}_x + I_p\omega\dot{\theta}_y + \gamma x + \delta\theta_x = (I_p - I)\tau\omega^2\cos(\omega t+\beta) + mge\cos\omega t,\\ &I\ddot{\theta}_y - I_p\omega\dot{\theta}_x + \gamma y + \delta\theta_y = (I_p - I)\tau\omega^2\sin(\omega t+\beta) + mge\sin\omega t. \end{aligned}\right\} \tag{35.2}$$

Comparing these with Eq. (3.27), we see that the terms of $mge\cos\omega t$ and $mge\sin\omega t$ are added respectively to the right-hand side of the 3rd and 4th equations of Eqs. (35.2). Therefore the condition of balancing is obviously different than that of the horizontal shaft with a motion as represented by Eqs. (3.27).

Chater V. Vibarations of the Shaft Carrying Two Discs

36. Behavior of vibrations

The behavior of vibrations of shaft mounting two discs is not substantially different from that of shaft carrying one disc. Results of such experiments are shown in Fig. 81. The arrangement of apparatus is shown in Fig. 82 and $a : b : c \fallingdotseq 3 : 4.5 : 2.5$. As shown in Fig. 81, two peaks of major critical speeds of $[+\omega]$ appear. In general, since the degrees of freedom system increase, there are many peaks of vibrations. In the experiment shown in Fig. 81, self-aligning double-row ball bearings are used.

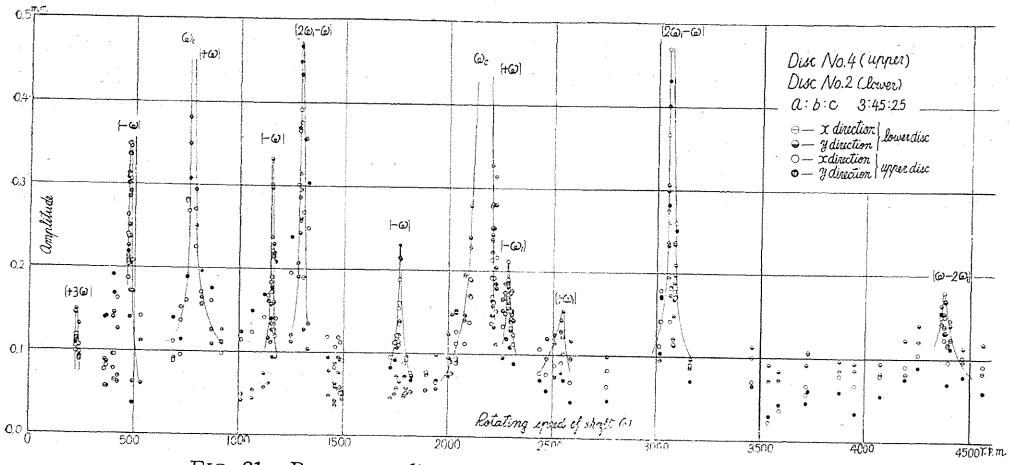

FIG. 81. Resonance diagram of the shaft carrying two discs.

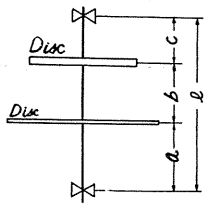

FIG. 82 (*left*). Test shaft carrying two discs.

FIG. 84 (*right*). Oscillographic paper of vibrations of $[2\omega_1 - \omega]$, (Disc No. 2 and Disc No. 4).

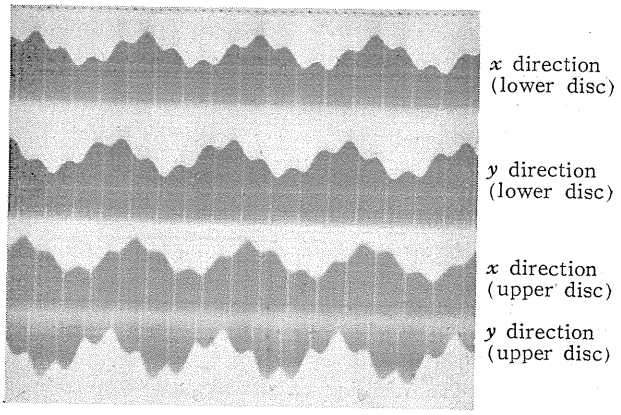

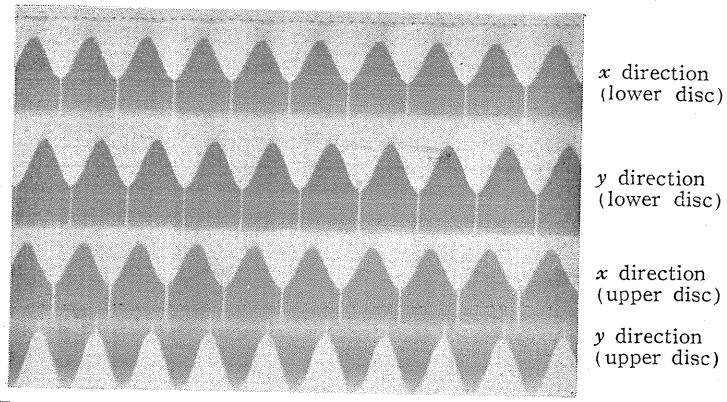

FIG. 83. Oscillographic paper of vibration of $[+\omega]$, (Disc No. 2 and Disc No. 4).

Summary

In this paper we have proved by the comparatively simple apparatus shown in Figs. 1 and 2 that various kinds of vibrations can take place in the shaft. Most of these vibrations occur because of irregularities in ball bearings and the flexibility of bearing pedestals.

Consequently, with perfect ball bearings and rigid pedestals, smooth operation will result. Some vibrations remain unexplained. These vibrations are left for future researches.

Acknowledgement

The author expresses his appreciation to Prof. Dr. K. Shogenji for his encouragements, to Prof. Dr. Y. Shimoyama for his guidance and valuable advice, and thanks Ass't. Prof. Y. Furuya and Lect. M. Murakami for their frank criticism. He also thanks Mr. H. Todorki for his assistance in the experiments. This research is indebted to Hydraulic Laboratory, Department of Mechanical Engineering, Nagoya University for laboratory use.

Notes and References

1) In this paper, "critical speed" means the angular velocity of shaft in which amplitudes of vibrations increase and the peaks of amplitudes are formed.
2) A. Stodola, Steam and Gas Turbines. Vol. **1**, Vol. **2**.
3) E. Schwerin "Die Stabilität rotierender achsial belasteter Wellen," Z. f. Angew. Math. u. Mech., **5** (1925), 101.
4) S. Timosheoko, Vibration Problems in Engineering, (1937).
5) J. P. Den Hartog, Mechanical Vibration, (1934).
6) H. H. Jeffcott, "The Lateral Vibration of Loaded Shafts in the Neighborhood of a Whirling Seeed: The Effect of Want of Balance," Phil. Mag., Vol. **37** (1919), 304.
7) S. Lees, "The Whirling of an Eccentrically-loaded Overhung Shaft," Phil. Mag., Vol. **37** (1919), 515.
8) S. Lees, "The Whirling of an Overhung Eccentrically-loaded Shaft," Phil. Mag., Vol. **45** (1923), 665.
9) K. Sezawa, Shindogaku, (1932).
10) T. Udoguchi, "A Consideration on the Relation between the Whirling and the Lateral Vibration of a Rotating Shaft," Trans. of Soc. of Mech. Engrs. (Japan), Vol. **14**, No. 42, (1948), 1-75.
11) A. Watari, "On the Motion of Rotating Shafts," Report of the Institute of Industrial Science, University of Tokyo, Vol. **2**. No, 4 (1952).
12) K. Karas, "Die kritischen Drehzahlen der fliegenden Welle mit Längsbelastung und Kreiselwirkung," Ing. Arch., **1** (1930), 84.
13) K. Karas, "Kritische Drezahlen stetig mit Masse belegter Wellen mit Längsbelastung und Kreiselwirkung," Ing. Arch. **1** (1930), 158.
14) K. Karas, Die kritischen Drehzahlen wichtiger Rotorformen, (1935).
15) M. Prohl, "A General Method for Calulating Critical Speeds of Flexible Rotors," A.S.M.E., Trans., Vol. **67** (1945), 142.
16) M. Smith, "The Motion of a Rotor carried by a Flexible Shaft in Flexible Bearings," Roy. Soc. London, Proc., Ser. A, Vol. **142** (1933), 92.
17) W. R. Foote, H. Poritsky and J. J. Slade. "Critical Speeds of a Rotor With Unequal Shaft Flexibilities, Mounted in Bearings of Unequal Flexibiliy," A.S.M.E., Trans., Vol. **65** (1943), A-77.

18) D. E. Miller, "Forced Lateral Vibration of Beams on Damped Flexible End Supports," Appl. Mech., J., Vol. **20** (1953), 167.
19) I. Oki, "The Lower Critical Speed of Horizontal Shaft," Jour. of Soc. of Mech. Engrs., (Japan), Vol. **21**, No. 52 (1918), 17.
20) O. Föpple, "Kritische Drehzahlen rasch umlaufender Welle," V.D.I., **63** (1919), 866.
21) H. Loernz. "Kritische Drehzahlen rasch umlaufender Welle," V.D.I., **63** ,(1919), 243.
22) F. Nakanishi, "The Secondary Vibration of Revolving Shafts," Jour. of Soc. of Mech. Engrs., (Japan), Vol. **35**, No. 188 (1932), 1170.
23) H. D. Taylor, "Critieal-Speed Behavior of Unsymmefrical Shaft," A.S.M.E., Trans., Vol. **62** (1940), A-71.
24) W. H. Hoppmann, "Forced Lateral Vibration of Beam Carrying a Concentrated Mass," Appl. Mech., J., Vol. **19** (1952), 301.
25) G. Sawaragi, "On the 'Shaft Whipping' excited by Dry Friction of Bearings," Trans. of Soc. of Mech. Engrs., (Japan), Vol. **17**, No. 57 (1951), 61.
26) B. L. Newkirk, "Shaft Whipping," General Electric Review, Vol. **27**, No. 3, (1924), 169.
27) A. L. Kimball, "Internal Friction Theory of Shaft Whipping," General Electric Review, Vol. **27**, No. 4, (1924), 224.
28) Y. Shimoyama and T. Yamamoto, "Vibrations generated on a Rotating Shaft by Passing through its Critical Speed with Some Angular Acceleration," Trans. of Soc. of Mech. Engrs. (Japan), Vol. **15**, No. 50 (1949), 113.
29) Spring coupling S prevents disturbing forces from driving belt, see S. Doi and others, "On the Vibration of the Grinding Wheel of Grindiog Machine," Trans. of Soc. of Mech. Engrs. (Japan), Vol. **7**, No. 29 (1936), IV-18.
30) Even if I is slighfly different in all directions, its effects do not appear in vibrations treated in this paper.
31) Y. Shimoyama and T. Yamamoto, "On the Critical Speed of a Shaft due to the Deflections of Bearing Pedestals," Trans. of Soc. of Mech. Engrs. (Japan), Vol. **20**, No. 91 (1954), 215.
32) Timoshenko. Applied Elasticity.
33) T. Yamamoto, "On the Critical Speed of a Shaft supported in Ball Bearing, (Part 1)," Trans. of Soc. of Mech. Engrs. (Japan), Vol. **20**, No. 99, (1954), 750.
34) T. Sasaki and others, "On the Planetary Motion of the Roller in the Roller Bearing," Trans. of Soc. of Mech. Engrs. (Japan), Vol. 8, No. 31, (1932), 64.
35) T. Yamamoto, "On the Critical Speed of a Shaft supported in Ball Bearing (Part 2)", Trans. of Soc. of Mech. Engrs. (Japan), Vol. **20**, No. 99, (1954), 755.
36) E. Schneider, Mathematishche Schwingungslehre, (1924).
37) In this case we may also take into consideration the unequal shaft flexihilities.
38) J. P. Den Hartog and R. M. Heiles, "Forced Vibration in Nonlinear System with Various Combinations of Linear Spring," A.S.M.E., Trans., Vol. **58** (1936), A-127.
39) S. Fujii, Science of Machine, Vol. **5**, No. 5 (1953), 302.
40) Takabayashi, Hitachi Review, No. 7 (1949-9), 102.
41) K. Klotter, Technische Schwingungslehre, (1951), 382.
42) Y. Furuya, Trans. of Soc. of Mech. Engrs. (Japan), Vol. **17**, No. 57 (1951), 67.
43) K. Yamanouchi, Ippan Rikihaku, 151.
44) A some detailed discussion is carried out in the following paper which is scheduled to be published in Trans. of Soc. of Mech. Engrs. (Japan), Vol. **21**, No. 103 (1955).
T. Yamamoto, "On the Vibrations of a Shaft supported by Bearings having Radial Clearances."
45) K. Nishino, "On the Vibratory Characteristics in the System with a small Clearance (1)," Journal of the Japan Society for Applied Mechanics, Vol. **3**, No. 19 (1950-1), 145; K. Nishino and M. Iwamoto, (2), Vol. **4**, No. 24 (1951-10), 81; K. Nishino and G. Watanabe, (3), Vol. **5**, No. 28 (1952-6), 49.
46) K. Tsuda, "On the Vibration of a Power-transmission System having Angular Clearances, (1), (2)," Trans. of Soc. of Mech. Engrs. (Japan) Vol. **18**, No, 75 (1952), 105, 112.

47) K. Futami, Shindo, (1946), 75.
48) S. Watanabe, "Vibration of a System with Backlash and Friction (1)," Trans. of Soc. of Mech. Engrs. (Japan), Vol. **20**, No. 91 (1954), 222.
49) T. Yamamoto, Science of Machine, Vol. **6**, No. 11 (1954), 927.
50) The effects of the deviational angle τ were pointed out by Prof. Dr. Y. Shimoyama, to whom the author is indebted.
51) We assume that the damping forces exert at the pcint S. The effects of the damping force are approximately the same as those exerted at the point G.
52) J. J. Stoker, Nonlinear Vibrations, (1950).
53) T. Yamamoto, "Contribution to the Stability Criterion for Forced Vibrations in Nonlinear Systems," Trans. of Soc. of Mech. Engrs. (Japan). Vol. **20**, No. 95 (1954), 501.